

Changes of air pollutant emissions in China during two clean air action periods derived from the newly developed Inversed Emission Inventory for Chinese Air Quality (CAQIEI)

Lei Kong^{1,3}, Xiao Tang^{*1,3}, Zifa Wang^{*1,3,4}, Jiang Zhu^{1,2}, Jianjun Li⁵, Huangjian Wu^{1,3}, Qizhong Wu⁶, Huansheng Chen^{1,3}, Lili Zhu⁵, Wei Wang⁵, Bing Liu⁵, Qian Wang⁷, Duohong Chen⁸, Yuepeng Pan^{1,3}, Jie Li^{1,3}, Lin Wu^{1,3}, and Gregory R. Carmichael⁹

¹State Key Laboratory of Atmospheric Boundary Layer Physics and Atmospheric Chemistry (LAPC), Institute of Atmospheric Physics, Chinese Academy of Sciences, Beijing 100029, China

²CAS-TWAS Center of Excellence for Climate and Environment Sciences (ICCES), Institute of Atmospheric Physics, Chinese Academy of Sciences, Beijing 100029, China

³College of Earth and Planetary Sciences, University of Chinese Academy of Sciences, Beijing 100049, China

⁴Center for Excellence in Regional Atmospheric Environment, Institute of Urban Environment, Chinese Academy of Sciences, Xiamen 361021, China

⁵China National Environmental Monitoring Centre, Beijing, 100012, China

⁶College of Global Change and Earth System Science, Faculty of Geographical Science, Beijing Normal University, Beijing 100875, China

⁷Shanghai Environmental Monitoring Centre, Shanghai, 200030, China

⁸Guangdong Ecological Environment Monitoring Centre, National Key Laboratory of Regional Air Quality Monitoring for Environmental Protection, Guangzhou 510308, China

⁹Center for Global and Regional Environmental Research, University of Iowa, Iowa City, IA 52242, USA

Correspondence to: Xiao Tang (tangxiao@mail.iap.ac.cn) and Zifa Wang (zifawang@mail.iap.ac.cn)

Abstract

A new long-term emission inventory called the Inversed Emission Inventory for Chinese Air Quality (CAQIEI) was developed in this study by assimilating surface observations from the China National Environmental Monitoring Centre (CNEMC) using the ensemble Kalman filter (~~EnKF~~) and the Nested Air Quality Prediction Modeling System (~~NAQPMS~~). This inventory contains the constrained monthly emissions of NO_x, SO₂, CO, primary PM_{2.5}, primary PM₁₀, and NMVOCs in China from 2013 to 2020, with a horizontal resolution of 15 km × 15 km. This paper documents detailed descriptions of the assimilation system and the evaluation results for the emission inventory. The results suggest that CAQIEI can effectively reduce the biases in the *a priori* emission inventory, with the normalized mean biases ranging from -9.1% to 9.5% in the *a posteriori* simulation, which are significantly reduced from the biases in the *a priori* simulations (-45.6% to 93.8%). The calculated RMSEs (0.3 mg/m³ for CO and 9.4–21.1 μg/m³ for other species, on the monthly scale) and correlation coefficients (0.76–0.94) were also improved from the *a priori* simulations, ~~demonstrating the good performance of the data assimilation systems suggesting that CAQIEI can reasonably reproduce the magnitude and variation of emissions of different air pollutants in China.~~ Based on CAQIEI, we estimated China's total emissions (including both natural and anthropogenic emissions) of the 6 species in 2015 to be as follows: 25.2 Tg of NO_x, 17.8 Tg of SO₂, 465.4 Tg of CO, 15.0 Tg of PM_{2.5}, 40.1 Tg of PM₁₀, and 46.0 Tg of NMVOCs. From 2015 to 2020, the total emissions reduced by 54.1% for SO₂, 44.4% for PM_{2.5}, 33.6% for PM₁₀, 35.7% for CO, and 15.1% for NO_x, but increased by 21.0% for NMVOCs. ~~It is also estimated that the Larger~~ emission reductions were ~~achieved~~ larger during ~~the~~ 2018–2020 ~~(from -26.6% to -4.5%)~~ action plan than during ~~the~~ 2015–2017 ~~(from -23.8% to 27.6%)~~ action plan for most species. ~~In P~~particularly, ~~the total Chinese NO_x and NMVOC emissions were shown to increase during the 2015–2017,~~ ~~action pla~~ especially over the ~~in,~~ and there were obvious emission increases in the Fengwei Plain area (FW) where the emissions of particulate matter (PM) also increased over the Central China region. The situation changed during 2018–2020 when the upward trends were contained and reversed to a downward trends for both the total emissions of NO_x and NMVOC, and the PM emissions over FW. However, NO_x and NMVOC emissions declined during the 2018–2020 action plan, and the emissions over the Fengwei Plain area also decreased. This suggests that the emission control policies ~~may bewere~~ improved

45 in the 2018–2020 action plan. We also compared ~~the~~ CAQIEI with ~~previous other air pollutant emission inventories in China,~~
46 which verified our inversion results in terms of total emissions of NO_x, SO₂ and NMVOCs, and more importantly identified
47 the potential uncertainties in ~~our current understanding of China's air pollutant emission inventories.~~ Firstly, ~~the CAQIEI~~
48 ~~suggested higher~~ CO emissions in China ~~may be substantially underestimated by current inventories,~~ with ~~the~~ CO emissions
49 estimated by CAQIEI (426.8 Tg) being more than twice the amount in previous inventories (120.7–237.7 Tg). ~~Significantly~~
50 ~~higher emissions were also suggested~~ ~~Significant underestimations for other air pollutant emissions may also exist over the~~
51 western and northeastern China ~~for other air pollutants.~~ ~~Secondly~~~~In addition,~~ ~~the CAQIEI suggested higher the~~ NMVOC
52 emissions ~~than previous emission inventories by about 30.4–81.4% over the NCP region were shown to be substantially~~
53 ~~underestimated over northern China but suggested lower NMVOC emissions by about 27.6–0.0% but overestimated in over~~
54 ~~the SE regionsouthern China.~~ ~~Thirdly~~~~Secondly,~~ ~~the CAQIEI suggested smaller the~~ emission reduction rates ~~during 2015–2018~~
55 ~~during 2015–2018 estimated by CAQIEI are generally smaller than those estimated by previousprevious emission inventories~~
56 ~~for most species except of CO₂, especially for NO_x, PM₁₀ and NMVOCs, suggesting that the mitigation effects of the air~~
57 ~~pollution control may be overestimated currently.~~ ~~In P~~~~particularl~~y, China's NMVOC emissions were shown to have increased
58 by 26.6% from 2015 to 2018, especially over the ~~NCPNorth China Plain~~ (by 38.0%), ~~n~~North China (by 38.3%), and
59 ~~c~~Central China (60.0%). ~~In contrast, the emissions reduction rate of CO may be underestimated.~~ ~~These results provide us with~~
60 ~~Overall, our emissions inventory sheds new light insight intoon~~ the complex variations of air pollutant emissions in China
61 during its two recent clean air action ~~periods,~~ which ~~has the potential toeould significantly~~ improve our understanding of air
62 pollutant emissions ~~in China~~ -and ~~related changes~~~~their impacts on-in~~ air quality ~~in China~~. The ~~whole~~ datasets are available at
63 <https://doi.org/10.57760/sciencedb.13151> (Kong et al., 2023).

64 1 Introduction

65 Air pollution is a serious environmental issue owing to its substantial impacts on human health, ecosystems, and climate
66 change (Von Schneidmesser et al., 2015; Cohen et al., 2017; Bobbink et al., 1998). According to the World Health
67 Organization, air pollution-induced strokes, lung cancer, and heart disease are causing millions of premature deaths worldwide
68 every year (WHO, 2016). The fine particulate matter (PM_{2.5}) in the atmosphere not only degrades visibility but also affects the
69 radiative forcing of the climate, both directly and indirectly (Martin et al., 2004). After removal from the atmosphere through
70 dry and wet deposition, air pollutants such as sulfur, nitrate, and ammonium contribute significantly to soil acidification,
71 eutrophication, and even biodiversity reduction (Krupa, 2003; Hernández et al., 2016).

72 China has experienced severe PM_{2.5} pollution in recent decades, due to its large emissions of air pollutants associated
73 with rapid urbanization and high consumption of fossil fuels (Kan et al., 2012; Song et al., 2017). The annual concentrations
74 of PM_{2.5} in 2013 reached 106, 67 and 47 µg/m³ over the Beijing–Tianjin–Hebei, Yangtze River Delta, and Peral River Delta
75 region, respectively, which were all higher than China's national standard (35 µg/m³), and 5–10 times higher than that of the
76 World Health Organization (10 µg/m³). To tackle this problem, strict emission control policies (so-called “clean air action
77 plans”) have been proposed by China's government, including the “Action Plan on the Prevention and Control of Air Pollution”
78 from 2013 to 2017 (hereinafter called the “2013–2017 ~~a~~Action ~~p~~Plan”), and the “Three-year Action Plan for Winning the Bule
79 Sky War” from 2018–2020 (hereinafter called the “2018–2020 ~~a~~Action ~~p~~Plan”). With the successful implementation of these
80 two action plans, the air quality was substantially improved in China, as evidenced in both observational and reanalysis datasets
81 (Li et al., 2020b; Zheng et al., 2017; Krotkov et al., 2016; Zhong et al., 2021; Li et al., 2017a; Kong et al., 2021). However,
82 with the deepening of air pollution control, unexpected changes have occurred in China, bringing about new challenges for the
83 mitigation of air pollution in the future. On the one hand, despite a significant decline in PM_{2.5} concentrations in China, severe
84 haze still occasionally occurs during the wintertime (Zhou et al., 2022b; Li et al., 2017c). In addition, field measurements in
85 cities over different regions of China consistently show different responses of aerosol chemical compositions to the emission

86 control policies (Tang et al., 2021; Zhou et al., 2019; Wang et al., 2022; Zhang et al., 2020; Li et al., 2019a; Xu et al., 2019b;
87 Lei et al., 2021; Zhou et al., 2022a). Compared with other aerosol species that show~~ed~~ substantial decreases during the clean
88 air action plans, nitrate has shown a weaker response to the control measures, remaining at high levels and in some cases
89 having even increased slightly. As a result, nitrate is playing an increasingly important role in heavy haze episodes in winter,
90 and dominates the chemical composition of PM_{2.5} (Fu et al., 2020; Xu et al., 2019a), leading to a rapid transition from sulphate-
91 to nitrate-driven aerosol pollution (Li et al., 2019a; Wang et al., 2019b). On the other hand, photochemical pollution has
92 deteriorated in China, with ozone (O₃) concentrations having increased substantially in eastern China during 2013–2017 (Li et
93 al., 2019b; Lu et al., 2018; Lu et al., 2020; Wang et al., 2020b).

94 These unexpected changes have raised considerable concern among the scientific community and policymakers regarding
95 the overall effects of the clean air action plans, and how to coordinate the control of PM_{2.5} and O₃ pollution. Addressing this
96 problem requires a comprehensive understanding of the effects of the clean air action plans on the emissions of different
97 chemical species. In this respect, previous studies have compiled several long-term air pollutant emission inventories in China
98 using the bottom-up approach – for example, the Multi-resolution Emission Inventory for China (MEIC) developed by
99 Tsinghua University for 2010–2020 (Zheng et al., 2018); the Air Benefit and Cost and Attainment Assessment System-
100 Emission Inventory version 2.0 (ABaCAS-EI v2.0) developed by Tsinghua University for 2005–2021 (Li et al., 2023); the
101 Regional Emission Inventory in Asia (REAS) for 1950–2015 developed Kurokawa and Ohara (2020); the Emissions Database
102 for Global Atmospheric Research (EDGAR) for 1970–2018 developed by Jalkanen et al. (2012); the Hemispheric Transport
103 of Air Pollution (HTAP) Inventory for 2000–2018 developed by Crippa et al. (2023); and the Community Emissions Data
104 System (CEDS) Inventory for 1970–2019 developed by McDuffie et al. (2020). These emission inventories have provided the
105 community with important insights into the long-term changes in the emissions of different air pollutants in China, thus playing
106 an indispensable role in our understanding of the effects of the country’s clean air action plans on emissions and air quality.
107 However, due to the lack of accurate activity data and emission factors, bottom-up emission inventories are~~still~~ subject to
108 large uncertainties, particularly during the clean air action periods when the activity data and emission factors changed
109 considerably and were difficult to track. Consequently, the estimated emission rates from different bottom-up emission
110 inventories could differ by more than a factor of 2 (Elguindi et al., 2020). For example, the estimated emissions for the year
111 2010 from different bottom-up inventories were 104.9–194.5 Tg for carbon monoxide (CO), 15.6–25.4 Tg for nitrogen oxides
112 (NO_x), 22.9–27.0 Tg for non-methane volatile organic compounds (NMVOCs), 15.7–35.5 Tg for sulfur dioxide (SO₂), 1.28–
113 2.34 Tg for black carbon (BC), and 2.78–4.66 Tg for organic carbon (OC), reflecting the large uncertainty in current bottom-
114 up estimates of air pollutant emissions in China, which hinders the proper assessment of the effects of the clean air action
115 plans.

116 Inverse modeling of multiple air pollutant emissions (i.e., a top-down approach) provides an attractive way to constrain
117 bottom-up emissions by reducing the discrepancy between the model and observation through the use of data assimilation.
118 Numerous studies have confirmed the effectiveness of such a top-down method in verifying bottom-up emission estimates and
119 reducing their uncertainties (e.g., Elbern et al., 2007; Henze et al., 2009; Miyazaki and Eskes, 2013; Tang et al., 2013; Koohkan
120 et al., 2013; Koukouli et al., 2018; Jiang et al., 2017; Muller et al., 2018; Paulot et al., 2014; Qu et al., 2017. Based on long-
121 term satellite observations, the top-down method has also been used to track the long-term variations of emissions. For example,
122 Zheng et al. (2019) estimated the global emissions of CO for the period 2000–2017 based on a multi-species atmospheric
123 Bayesian inversion approach; Qu et al. (2019) constrained global SO₂ emissions for the period 2005–2017 by assimilating
124 satellite retrievals of SO₂ columns using a hybrid 4DVar/mass balance emission inversion method; by assimilating satellite
125 observations of multiple species, Miyazaki et al. (2020b) simultaneously estimated global emissions of CO, NO_x, and SO₂ for
126 the period 2005–2018; and, most recently, a regional top-down estimation of PM_{2.5} emissions in China during 2016–2020 was
127 carried out by Peng et al. (2023) by assimilating surface observations. These studies provide us with valuable clues for
128 evaluating bottom-up emissions and improving our knowledge on the changes in emissions of different species in China during

129 the clean air action plans. However, most of these studies focused on emission trends at the global scale, which involved the
130 use of coarse model resolutions ($>1^\circ$) that may be insufficient to capture the spatial variability of emission variations at the
131 regional scale. Meanwhile, current long-term, top-down estimates mainly focus on single species and do not fully cover the
132 two clean air action periods in China. Indeed, to date, there are still no long-term, top-down estimates of major air pollutant
133 emissions in China that fully cover the two clean air action periods.

134 In a previous study performed by our group, we developed a high-resolution air quality reanalysis dataset over China
135 (CAQRA) for the period 2013–2020 to track the air quality trends in China during the clean air action periods (Kong et al.,
136 2021). In the present study, as a follow up to this work, we constrained the long-term emission trends of major air pollutants
137 in China for 2013–2020 (which will be extended in the future on a yearly basis) by assimilating surface observations of air
138 pollutants from the China National Environmental Monitoring Centre (CNEMC) using an ensemble Kalman filter and the
139 Nested Air Quality Prediction and Forecasting System (NAQPMS). In the following sections, we present detailed descriptions
140 of the chemical data assimilation, the evaluation results of the inversed emissions inventory, and the estimated emission trends
141 of different air pollutants in China during the clean air action periods.

142 2 The chemical data assimilation system

143 We used the chemical data assimilation system (ChemDAS) developed by the Institute of Atmospheric Physics, Chinese
144 Academy of Sciences, to constrain the long-term emission trends of different air pollutants in China, which was used in the
145 development of CAQRA in our previous work (Kong et al., 2021). Since the chemical transport model (CTM) and the
146 observations used in the top-down estimation were the same as those used in CAQRA, we only briefly describe these two
147 components in the following two subsections, instead concentrating on providing a fuller description (in the third subsection)
148 of the inversion scheme in ChemDAS.

149 2.1 Chemical transport model

150 The NAQPMS model was used as the forecast model to represent the atmospheric chemistry in this study, and the Weather
151 Research and Forecasting (WRF) model was used as the meteorological model to provide the meteorological input data.
152 NAQPMS contains comprehensive modules for the emission, diffusion, transportation, deposition, and chemistry processes in
153 the atmosphere, and has been used in previous inversion studies (Tang et al., 2013; Kong et al., 2019; Wu et al., 2020a; Kong
154 et al., 2023). Detailed configurations of the different modules used in NAQPMS are available in these publications.

155 Figure 1 shows the domain of the inverse model, which is the same as that used in CAQRA, with a fine-scale horizontal
156 resolution of 15 km. The *a priori* emissions inventory includes the anthropogenic emissions obtained from the HTAP v2.2
157 emissions inventory that provides the emissions from energy, industry, transport, residential, agriculture, air and ship sectors,
158 with a base year of 2010 (Janssens-Maenhout et al., 2015); biogenic emissions obtained from the Monitoring Atmospheric
159 Composition and Climate (MACC) project (Sindelarova et al., 2014); biomass burning emissions obtained from the Global
160 Fire Emissions Database (GFED), version 4 (Van Der Werf et al., 2010; Randerson et al., 2017); soil and lightning NO_x
161 emissions obtained from Yan et al. (2003) and Price et al. (1997); and marine volatile organic compound emissions obtained
162 from the POET database (Granier et al., 2005). The dust emissions were calculated online in NAQPMS as a function of the
163 relative humidity, frictional velocity, mineral particle size distribution, and the surface roughness (Li et al., 2012), while the
164 sea salt emissions were calculated using the scheme of Athanasopoulou et al. (2008). Note that we did not consider the temporal
165 variation in the *a priori* emission inventory, so that the top-down estimated emission trends were only derived from the surface
166 observations. In addition, we used the constant diurnal variation of the emissions in this study due to the lack of information
167 on the diurnal variation of the emissions from different sectors, which is a potential limitation in our current work. However,
168 since the emission inversion was performed on the daily basis (Sect. 2.3.3), the diurnal variations of the emission may not

169 significantly influence the simulation results of the daily mean concentrations of air pollutants (less than 1 ppbv for SO₂, NO₂
170 and O₃) according to the sensitivity experiments conducted by Wang et al. (2010). The initial condition was treated as clean
171 air in NAQPMS, with a 2-week spin-up time. Top and boundary conditions were provided by the Model for Ozone and Related
172 Chemical Tracers (MOZART) (Brasseur et al., 1998; Hauglustaine et al., 1998) data products provided by National Center for
173 Atmospheric Research (NCAR). Note that since the MOZART data products were not available for years after 2018, the multi-
174 year average results from 2013 to 2017 were used for the simulations after 2018. Because most of the model boundaries were
175 set in the clean areas and are located at distance from China, we assumed that the differences in boundary conditions would
176 not significantly affect the modeling results over the China. To improve the performance of meteorological simulation, a 36-
177 h free run of the WRF model was conducted for each day by using the NCAR/NCEP 1°×1° reanalysis data. The simulation
178 results of the first 12 h were treated as the spin-up run, and the remaining 24 h were used to provide the meteorological inputs
179 for the NAQPMS model.

180 **2.2 Assimilated observations**

181 The assimilated observational dataset in this study was the same as that used in CAQRA, which includes surface
182 concentrations of PM_{2.5}, PM₁₀ (coarse particulate matter), SO₂, NO₂ (nitrogen dioxide), CO, and O₃, from 2013 to 2020,
183 obtained from CNEMC (Fig. 1). Before the assimilation, outliers of the observations were filtered out by using an automatic
184 quality control method developed by Wu et al. (2018). Four types of outliers characterized by temporal and spatial
185 inconsistencies, instrument-induced low variances, periodic calibration exceptions, and lower PM₁₀ concentrations than those
186 of PM_{2.5}, were filtered out to prevent adverse impacts on the inversion process. As estimated in Kong et al. (2021), about 1.5%
187 of observational data were filtered out after quality control, but further assessment showed that it had few effects on the average
188 concentrations of different species, which were estimated to be less than 1 µg/m³ for the gaseous air pollutants and less than
189 5 µg/m³ for the particulate matter. Estimation of observation error is also important to the inversion of emissions since the
190 observational error and background errors determine the degree of adjustment to the emissions. The observational error
191 comprises the measurement error and the representativeness error induced by the different spatial scales that the model and
192 observations represent. The estimations of these two components of observational error were the same as those used in CAQRA,
193 detailed descriptions of which are available in Kong et al. (2021).

194 It should be noted that the number of observation sites were not constant throughout the whole inversion period, being
195 approximately 510 in 2013 and then increasing to 1436 in 2015. According to Fig. S1, the observation sites were mainly
196 concentrated in the megacity clusters in China (e.g., North China Plain, Yangtze River Delta and Pearl River Delta) and the
197 capital cities of each province in 2013. The number of observation sites continued to increase across the China in 2014 and
198 2015. In particular, many areas that were previously unobserved in 2013 have added monitoring stations, which significantly
199 increased the observation coverage in China and,~~which~~ could lead to spurious trends in the top-down estimated emissions. To
200 investigate the potential impacts of this on the top-down estimations, the changes in the coverage of observations over different
201 regions of China from 2013 to 2020 were firstly calculated by the ratio of areas that were influenced by observations to the
202 total area of each region (Fig. 2). It can be clearly seen that the observational coverage increased from 2013 to 2015 with the
203 expansion of the air quality monitoring network in China, and became stable after 2015. However, the influence of the variation
204 in the number of observation sites varied among different regions. Over the North China Plain (NCP) region, the observational
205 coverage was approximately 90% in 2013, and reached 100% in 2014, suggesting that the variation in the observation sites
206 may have little influence on the estimated changes in emissions there. A similar conclusion can be drawn for the Southeast
207 China (SE) region, where the observational coverage was about 75% in 2013 and reached 100% in 2015. Elsewhere, in the
208 other four regions, the influence of the variation in observation sites is expected to be larger because of the low observational
209 coverage in both 2013 and 2014. For example, the observational coverage over the Northwest China (NW) region was less
210 than 10% in 2013, but increased to about 60% in 2015. To better illustrate the impact of changes in observation coverage on

211 the inversions, the sensitivity analysis of the emission increments with the fixed observation sites or varying observation sites
 212 is performed in this study. Such large changes in observational coverage are believed to significantly influence the estimated
 213 changes in emissions over these regions (Text S1 and Fig. S2). It shows that the additional emission increments caused by the
 214 increases of observation sites would weaken the decreasing trends estimated in the fixed-site scenario for the emissions of
 215 PM_{2.5}, NO_x and NMVOC and even lead to increasing trends for the emissions of PM₁₀ and CO. In contrast, the increases of
 216 observation sites would enhance the decreasing trends of SO₂ estimated in the fixed-site scenario. Such different behaviors are
 217 mainly related to the different sign of the emission increment of different species as we illustrated in Text S1. These results
 218 highlighted the significant influences of the site differences on the estimated emissions and their trends, which should be noted
 219 by the potential users. Therefore, in order to reduce this influence on the estimated emission trends, in our following analysis
 220 we mainly present the emission trends after 2015, when the observational coverage had stabilized in all regions.

221 2.3 Data assimilation algorithm

222 We used the modified EnKF coupled with state augmentation method to constrain the long-term emissions of different
 223 air pollutants. EnKF is an advanced data assimilation method originally proposed by Evensen (1994) that features representing
 224 the background error covariance matrix with a stochastic ensemble of model realizations. Through the use of ensemble
 225 simulations, it has the ability to consider the indirect relationship between the emissions and chemical concentrations caused
 226 by the complex physical and chemical processes in the atmosphere. It also allows for the estimation of flow-dependent
 227 emission–concentration relationships that vary in time and space depending on the atmospheric conditions. The modified
 228 EnKF is an offline application of the EnKF method that works by decoupling the analysis step from the ensemble simulation,
 229 which has benefits in the reuse of costly ensemble simulations and makes high-resolution long-term inversion affordable (Wu
 230 et al., 2020a). In this method, the ensemble simulation was performed firstly with the perturbed emissions, and then the
 231 observations were assimilated to constrain the emissions (Wu et al., 2020a). The state augmentation method is a commonly
 232 used parameter estimation method (Tandeo et al., 2020) in which the air pollutant emissions are taken as the state variable and
 233 are updated according to the error covariance between the emissions and the concentrations of related species.

234 2.3.1 State variable and ensemble generations

235 The state variable used in this study was chosen following our previous multi-species inversion study (Kong et al., 2023),
 236 which included the scaling factors for the emissions of fine-mode unspiciated aerosol (PMF), coarse-mode unspiciated aerosol
 237 (PMC), BC, OC, NO_x, SO₂, CO, and NMVOCs, as well as the chemical concentrations of PM_{2.5}, PM_{10-2.5} (PM₁₀ minus PM_{2.5}),
 238 NO₂, SO₂, CO, and daily maximum 8-h O₃ (MDA8h O₃), which are formulated as follows:

$$239 \mathbf{x} = [\mathbf{c}, \boldsymbol{\beta}]^T, \quad (1)$$

$$240 \mathbf{c} = [\text{PM}_{2.5}, \text{PM}_{10-2.5}, \text{NO}_2, \text{SO}_2, \text{CO}, \text{MDA8h O}_3], \quad (2)$$

$$241 \boldsymbol{\beta} = [\beta_{\text{PMF}}, \beta_{\text{PMC}}, \beta_{\text{BC}}, \beta_{\text{OC}}, \beta_{\text{NO}_x}, \beta_{\text{SO}_2}, \beta_{\text{CO}}, \beta_{\text{NMVOC}}],$$

$$242 \text{—————} (3)$$

243 where \mathbf{x} denotes the vector of the state variable, \mathbf{c} denotes the vector of the chemical concentrations of different species, and
 244 $\boldsymbol{\beta}$ denotes the vector of the scaling factors for the emissions of different species. Note that although the chemical concentration
 245 variables are included in the state variable, they are not optimized simultaneously with the emission in the analysis step and
 246 are only used to estimate the covariance between the emission and concentrations. Detailed descriptions of the state variables
 247 are available in Table 1.

248 The ensemble of the scaling factors was generated using the same method of Kong et al. (2021), which has a medium size
 249 of 50 and considers the uncertainties of major air pollutant emissions in China, including SO₂, NO_x, CO, NMVOCs, ammonia,
 250 PM₁₀, PM_{2.5}, BC, and OC. The uncertainties of these species were considered to be 12%, 31%, 70%, 68%, 53%, 132%, 130%,
 251 208% and 258%, respectively according to the estimates of Li et al. (2017b) and Streets et al. (2003). The ensemble of the

252 chemical concentrations was generated through an ensemble simulation based on NAQPMS and the perturbed emissions
 253 calculated by multiplying the *a priori* emissions by the ensemble of the scaling factors. This treatment implicitly assumes that
 254 the uncertainty in the chemical concentration is mainly caused by the emission uncertainty. This makes sense on a monthly or
 255 yearly basis, considering that substantial changes in emissions are expected to have taken place during the clean air action
 256 plans, which are subject to large uncertainty. However, the lack of consideration of other error sources, such as those of the
 257 meteorological simulation and the model itself, may lead to underestimation of the background error covariance and
 258 overcorrection of the emissions, which is a potential limitation of this study. In addition, the dust and sea salt emissions were
 259 not perturbed and constrained in this study, and thus the errors in the simulated fine and coarse dust emissions would influence
 260 the inversion of PM_{2.5} and PM₁₀ emissions. As a result, the top-down estimated PM_{2.5} and PM₁₀ emissions will contain errors
 261 in the simulated dust and sea salt emissions. Particularly, we did not consider the emission of coarse dust during the inversion
 262 process since we found large errors in the simulated coarse dust concentration that could have significantly influenced the
 263 inversion of PM₁₀ emissions. Consequently, the top-down estimated PM₁₀ emissions in this study comprise all coarse dust
 264 emissions. A detailed description of the ensemble generation is available in Kong et al. (2021).

265 2.3.2 Inversion algorithm

266 We used a deterministic form of EnKF (DEnKF) proposed by Sakov and Oke (2008) to update the scaling factors of the
 267 emissions of different species, which is formulated as follows:

$$268 \bar{\mathbf{x}}^a = \bar{\mathbf{x}}^b + \mathbf{K} \lambda \mathbf{B}_e^b \mathbf{H}^T (\mathbf{H} \lambda \mathbf{B}_e^b \mathbf{H}^T + \mathbf{R})^{-1} (\mathbf{y}^o - \mathbf{H} \bar{\mathbf{x}}^b),$$

269 _____ (42)

$$270 \mathbf{X}^a = \mathbf{X}^b - \frac{1}{2} \mathbf{K} \mathbf{H} \mathbf{X}^b \quad (5)$$

$$271 \mathbf{K} = \lambda \mathbf{B}_e^b \mathbf{H}^T (\mathbf{H} \lambda \mathbf{B}_e^b \mathbf{H}^T + \mathbf{R})^{-1}, \quad (6)$$

$$272 \bar{\mathbf{x}}^b = \frac{1}{N} \sum_{i=1}^N \mathbf{x}_i^b; \mathbf{X}_i^b = \mathbf{x}_i^b - \bar{\mathbf{x}}^b, \quad (3)$$

$$273 \mathbf{B}_e^b = \frac{1}{N-1} \sum_{i=1}^N \mathbf{X}_i^b (\mathbf{X}_i^b)^T, \quad (74)$$

$$274 \bar{\mathbf{x}}^b = \frac{1}{N} \sum_{i=1}^N \mathbf{x}_i^b; \mathbf{X}_i^b = \mathbf{x}_i^b - \bar{\mathbf{x}}^b, \quad (8)$$

275
 276 where $\bar{\mathbf{x}}$ denotes the ensemble mean of the state variable; the superscript **b** and **a** respectively denote the *a priori* and *a*
 277 *posteriori* estimate; \mathbf{X}^a is the analysed anomalies that can be used to calculate the uncertainty of the *a posteriori* emissions. **K**
 278 is the Kalman gain matrix; \mathbf{B}_e^b is the background error covariance matrix calculated by the background perturbation \mathbf{X}^b ; \mathbf{y}^o is
 279 the vector of the observation and **R** is the observation error covariance matrix; **H** is the linear observation operator, which
 280 maps the model space to the observation space; λ is the inflation factor used to compensate for the underestimation of the
 281 background error caused by the limited ensemble size and unaccounted error sources, which is calculated using the method of
 282 Wang and Bishop (2003),

$$283 \lambda = \frac{(\mathbf{R}^{-1/2} \mathbf{d})^T \mathbf{R}^{-1/2} \mathbf{d} - p}{\text{trace}\{\mathbf{R}^{-1/2} \mathbf{H} \mathbf{B}_e^b (\mathbf{R}^{-1/2} \mathbf{H})^T\}} \quad (95)$$

$$284 \mathbf{d} = \mathbf{y}^o - \mathbf{H} \bar{\mathbf{x}}^b \quad (106)$$

285 where **d** is the observation innovation and **p** is the number of observations. Table S1 summarized the calculated average value
 286 (standard deviation) of the used inflation factor for different species. It shows that the inflation factor over the east China
 287 (including NCP and SE region) was generally round 1.0, suggesting that the original ensemble can well represent the simulation
 288 errors of the different air pollutants over these regions. The inflation factor is larger over the western China (including SW,
 289 NW and Central regions), especially for PM₁₀ (36.0–78.1) and SO₂ (7.8–176.1), suggesting that the original ensemble may
 290 underestimate the simulation errors of the air pollutants. This is associated with the large biases in the simulated air pollutant

291 concentrations over there and reflect that the emission uncertainties assumed in our studies may be underestimated over these
292 regions. This also highlighted the importance of the use of inflation method during the inversion, otherwise it would lead to
293 filter divergency caused by the underestimations of the background error covariance.

294 In order to reduce the influence of the spurious correlations on the performance of data assimilation, the EnKF was
295 performed locally in this study in that the analysis was calculated grid by grid with the assumption that only measurements
296 located within a certain distance (cutoff radius) from a grid point would influence the analysis results of this grid. The use of
297 this local analysis method also allowed the inflation factor to be calculated locally and to vary in time and space, which can
298 help characterize the spatiotemporal variations of errors as we illustrated above. Similar to in Kong et al. (2021) and Kong et
299 al. (2023), the cutoff radius was chosen as 180 km for each species based on the wind speed and the lifespan of the species
300 (Feng et al., 2020), and The same local scheme with a buffer area was also employed during the inversion to alleviate the
301 discontinuities in the updated state caused by the cut-off radius. A detailed description of the local analysis scheme is available
302 in Kong et al. (2021).

303 Table 1 ~~then~~ summarizes the corresponding relationships between the emissions and chemical concentrations. Similar to
304 in Ma et al. (2019) and Miyazaki et al. (2012), we did not consider the inter-species correlation during the assimilation, to
305 prevent the spurious correlations between non- or weakly related variables. In most cases, observations of one particular species
306 were only allowed to adjust the emissions of the same species. The assimilation of PM_{2.5} mass observation was more
307 complicated ~~than that of other species~~ as there are multiple error sources in the simulated mass concentrations of PM_{2.5}, not
308 only from primary emission, but also from secondary production. In this study, the PM_{2.5} mass observation was used to
309 constrain the emissions of PMF, BC and OC but not used to constrain the emissions of its precursors to avoid the spurious
310 correlations and nonlinear chemistry effects, which is similar to the scheme used in Ma et al. (2019). This is feasible since the
311 emissions of primary PM_{2.5} (i.e., PMF, BC and OC) and the emissions of PM_{2.5} precursors (e.g., SO₂, NO₂) were perturbed
312 independently in our method, thus the contributions of primary PM_{2.5} emission and the secondary PM_{2.5} productions to the
313 PM_{2.5} mass could be isolated through the use of ensemble simulations. Meanwhile, the use of iteration inversion method (which
314 will be introduced later) can further reduce the influence of the errors in the precursors' emissions on the inversion of primary
315 PM_{2.5} emission, since the precursors' emission would be constrained by their own observations during the iterations. However,
316 the lack of assimilation of speciated PM_{2.5} observations may lead to uncertainties in the estimated emissions of PMF, BC and
317 OC, which is a potential limitation in current work. For example, if the a priori simulated PM_{2.5} equals the observations, the
318 emissions of PMF, BC and OC would not be adjusted by using the current method. However, in such cases, there may still be
319 discrepancies in the proportions of the emissions of different PM_{2.5} components. To adjust the emissions of PMC, we used the
320 observations of PM_{10-2.5} to avoid the potential cross-correlations between PM_{2.5} and PM₁₀ (Peng et al., 2018; Ma et al., 2019).
321 For the NO_x emissions Meanwhile, although the O₃ concentration are chemically related to the NO_x emissions, we did not use
322 the O₃ concentrations to constrain the NO_x emission in this study since there is nonlinear relationship between the O₃
323 concentration and NO_x emission which would lead to wrong adjustment of NO_x emissions (Tang et al., 2016).

324 The inversion of NMVOC emission is more difficult than other species dDue to the lack of long-term nationwide NMVOC
325 observations and the strong chemical activity. Previous studies usually assimilated the satellite observations of formaldehyde
326 and glyoxal to constrain the NMVOC emissions, such as Cao et al. (2018) and Stavrou et al. (2015). However, these
327 inversion studies are hindered by the NO_x-VOC-O₃ chemistry and the inherent uncertainty in the satellite observations of
328 formaldehyde and glyoxal. Considering the strong chemical relationship between the O₃ and NMVOC, some pioneer studies
329 have also explored the method of assimilating ground-level O₃ concentrations to constrain the NMVOC emissions (Ma et al.,
330 2019; Xing et al., 2020), and demonstrated the effectiveness of this approach. For example, Ma et al. (2019) found that the
331 assimilation of O₃ concentration could adjust the NMVOC emissions in the direction resembling the bottom-up inventories,
332 and the forecast skill of O₃ concentrations were also improved, indicating that the constrained NMVOC emissions are improved
333 relative to their a priori. Inspired by these studies, we have made an attempt to constrain the NMVOC emissions based on ,the

334 MDA8h O₃ was used to constrain the NMVOC emissions considering its strong chemical relationship with the NMVOC
 335 emissions. Meanwhile, the use of MDA8h O₃ rather than the daily mean O₃ concentration is to avoid the effects of the
 336 nighttime O₃ chemistry. An important issue that should be noted when using the MDA8h O₃ to constrain the NMVOC emission
 337 is the nonlinear interactions among NO_x, NMVOC and O₃. On the one hand, the O₃ concentrations are dependent not only on
 338 the NMVOC emissions but also on the NO_x emissions. The errors in the a priori emissions of NO_x would also contribute to the
 339 simulation errors of O₃, and deteriorate the inversion of NMVOC. Another important issue that should be noted when using
 340 the MDA8h O₃ to constrain the NMVOC emission is that the errors in the simulation results of MDA8h O₃ are also caused by
 341 the errors in NO_x emissions. The iteration inversion scheme could help deal with this issue as the errors in the NO_x emissions
 342 will be constrained by the NO₂ observations in the next iteration, which can reduce the influences of errors in the NO_x emission
 343 on the inversion of NMVOC emission based on the MDA8h O₃ concentrations. This is in fact similar to the approach used by
 344 Xing et al. (2020) who firstly constrained the NO_x emissions based on observations of NO₂, and then constrained the NMVOC
 345 emissions based on O₃ concentrations. Also, in Feng et al. (2024), the NO₂ observations were simultaneously assimilated to
 346 constrain the NO_x emissions to account for the influences of errors in NO_x emissions on the NMVOC emissions, suggesting
 347 that the iteratively nonlinear joint inversion of NO_x and NMVOCs is an effective way to address the intricate relationship
 348 among VOC-NO_x-O₃ (Feng et al., 2024). On the other hand, the emission adjustments of NMVOC may exhibit bidirectionality
 349 dependent on the VOC-limited or NO_x-limited regimes. According to Fig. 3, the NMVOC emissions were adjusted in
 350 alignment with the direction of the O₃ errors, suggesting a VOC-limited regime over urban areas in China, given that the O₃
 351 observation sites are predominantly situated in the urban areas. This agrees with Ren et al. (2022) who diagnosed the NO_x-
 352 VOC-O₃ sensitivity based on the satellite retrievals and found that the VOC-limited regimes are mainly located in the urban
 353 areas in China. This suggests that the relationship between the O₃ concentrations and VOC emissions could be reasonably
 354 reflected by our inversion system, providing the feasibility in utilizing the O₃ observations to constrain the VOC emissions.
 355 Note that due to the lack observations of the VOC components, we only optimize the gross emissions of the VOC during the
 356 assimilation. Meanwhile, although the O₃ concentration are chemically related to the NO_x emissions, we did not use the O₃
 357 concentrations to constrain the NO_x emission in this study since there is nonlinear relationship between the O₃ concentration
 358 and NO_x emission which would lead to wrong adjustment of NO_x emissions (Tang et al., 2016).

359 As we illustrated before, there exists nonlinear effects in the atmospheric chemistry which could influence the inversion
 360 results of different species. In addition, since we did not consider the temporal variations in the a priori emissions, it was
 361 expected that there would be significant biases in the a priori emissions for the years after 2013, as substantial changes in
 362 emissions were expected owing to the implementation of strict emission control measures. Such bias in the a priori emissions
 363 does not conform to the assumption of the EnKF that the a priori estimate is unbiased, which could thus lead to incomplete
 364 adjustments of the a priori emissions and degrade the performance of the data assimilation (Dee and Da Silva, 1998). To
 365 address these issues, an iteration inversion scheme was employed in this study, which has been used previously in Kong et al.
 366 (2023). The main idea of the iteration inversion scheme is to preserve the background perturbation \mathbf{X}^b but to update the
 367 ensemble mean of the state variable $\bar{\mathbf{x}}^b$ based on the inversion results of the k th iteration and corresponding model simulation.
 368 According to this, a new single model simulation is required to be conducted by using the a posteriori emission from the
 369 previous iteration as the input to update the ensemble mean of the original ensemble. This enables the observational information
 370 and the adjusted emissions to be promptly incorporated into the model, thereby providing feedback for the adjustments of
 371 emission in the next iteration. However, we did not reassemble the ensemble simulation for each iteration due to the expensive
 372 computational cost of the ensemble simulation. Therefore, in each iteration calculation, the ensemble perturbation that were
 373 used to calculate the background error covariance matrix remains the same with only the ensemble mean being updated based
 374 on the inversion results of the previous iteration. The state variable used in the $(k + 1)$ th inversions is then formulated as
 375 follows:

$$376 \mathbf{x}_i^{b,k+1} = [\mathbf{c}^k + \mathbf{c}_i^e - \bar{\mathbf{c}}^e, \boldsymbol{\beta}^k + \boldsymbol{\beta}_i^e - \bar{\boldsymbol{\beta}}^e]^T, \quad (117)$$

377 where \mathbf{c}^k represents the model simulations using the inversed emissions of the k th iteration, \mathbf{c}_i^e represents the i th member of
378 ensemble simulations with an ensemble mean of $\bar{\mathbf{c}}^e$, β^k represents the updated scaling factors at the k th iteration, and
379 β_i^e represents the i th member of the ensemble of scaling factors with a mean value of $\bar{\beta}^e$. Two rounds of iteration were
380 conducted in this study based on our previous inversion study to maintain a balance between the inversion performance and
381 the computational cost of the long-term inversions (Kong et al., 2023), which is enough for reducing the biases in the *a priori*
382 emissions.

383 2.3.3 Setup of inversion estimation

384 Based on this inversion scheme, we firstly constrained the daily emissions of PMF, PMC, BC, OC, NO_x, SO₂, CO, and
385 NMVOCs, from 2013 to 2020, based on the daily averaged observations of PM_{2.5}, PM_{10-2.5}, NO₂, CO, and MDA8h O₃.
386 However, similar to in Kong et al. (2023), we only provide the emissions of PM_{2.5} (PMF+BC+OC) and PM₁₀ (PM_{2.5}+PMF)
387 for the aerosol species since the lack of speciated PM_{2.5} observations would lead to uncertainties in the estimated emissions of
388 PMF, BC, and OC as we mentioned before. Meanwhile, as mentioned in subsection 2.3.1, the meteorological and model
389 uncertainty were not considered in the ensemble simulation. Thus, the errors in the meteorological simulation would cause
390 fluctuations in the daily emissions that could contaminate the inversion results and are, which would be difficult to isolate
391 from the inherent variations of emissions (Tang et al., 2013). Considering this, the daily emissions were averaged to monthly
392 values to reduce the influences of random model errors after the assimilation.

393 3 Performance of the chemical data assimilation system

394 3.1 Analysis of OmF and emission increment

395 The observation-minus-forecast (OmF) and emission increment (*a posteriori* emission minus *a priori* emission) were
396 firstly analyzed to demonstrate the performance of the data assimilation. As shown in Fig. 3, the *a priori* simulation generally
397 underestimated the PM_{2.5} concentrations over the NCP, SE and SW regions (positive OmF values) during 2013–2014, but
398 overestimated the PM_{2.5} concentrations from 2016, reflecting the effects of the emission control measures during these years.
399 In the NE, NW and central China (hereafter, “Central”) regions, obvious underestimation of the PM_{2.5} concentration was found
400 (positive OmF values) throughout almost the entire assimilation period. Similarly, the OmF values of PM₁₀ were positive
401 throughout the whole assimilation period over all regions of China. In contrast, the OmF values for SO₂ were negative for most
402 regions, and the negative OmF values over the NCP region became larger as the years progressed, which reflects the effects
403 of the emission control measures. The OmF for NO₂ reveals a seasonal variation over the NCP and SE regions, with negative
404 values during summer and positive values during winter, while there were obvious positive OmF values over the NE, SW, NW
405 and Central regions. In terms of CO, large positive OmF values were found over all regions of China, and there were decreasing
406 trends in the OmF values of CO over different regions of China associated with the emission control policies during these
407 years. The OmF values for O₃ were positive over most regions of China, except the NW region. These results provide us with
408 valuable information on the potential deficiencies in the suggest that the *a priori* emissions may underestimate the emissions
409 of PM_{2.5}, PM₁₀, CO, NO₂ and NMVOCs in China, but overestimate the SO₂ emissions. However, since our inversion method
410 did not differentiate between anthropogenic and natural emissions, the biases in the model simulation may also be attributable
411 to the errors in natural emissions such as dust, especially over the major dust-source areas of China (e.g., the NW and Central
412 regions). In addition, the effects of emission control were not considered in the *a priori* emissions, which is another important
413 contributor to the errors in the model simulation for the later years. Thus, the emission increments calculated by the assimilation
414 should reflect the combined effects of errors in the anthropogenic and natural emissions, as well as the emission control.

415 The calculated emission increments were consistent with the OmF values for all species, which indicates that the data
416 assimilation method can probably constrain the emissions based on the observations. According to Fig. 3, the emission

417 increments were positive for PM_{2.5} over the NE, NW and Central regions, for NO₂ over the NE, SW, NW and Central regions,
418 and for PM₁₀, CO and NMVOC over almost all regions throughout the assimilation period. In contrast, the emission increments
419 were negative for the SO₂ emissions for most cases. Consistent with the OmF values, the emission increments were positive
420 for PM_{2.5} over the NCP, SE and SW regions during 2013–2014, but became negative from 2016 owing to the implementation
421 of strict emission control measures. The emission increments for NO_x also showed significant seasonal variation over the NCP
422 and SE regions, being positive during winter and negative during summer. The *a posteriori* biases for the model simulations
423 of different species were also plotted to assess the performance of the data assimilation. It can be clearly seen that the biases
424 were substantially reduced for all species, and the calculated root-mean-square error (RMSE) reduced by 23.2–52.8% for PM_{2.5},
425 19.9–37.8% for PM₁₀, 36.4–77.3% for SO₂, 18.3–25.2% for NO₂, 29.9–40.5% for CO, and 4.4–26.1% for O₃ over the different
426 regions of China, suggesting a good performance of the data assimilation system.

427 3.2 Evaluation of the inversion results

428 Table 2 shows the calculated evaluation statistics for the inversion at different temporal scales. It can be clearly seen that
429 the model simulation with the *a posteriori* emission inventory reproduced well the magnitude and temporal variations of the
430 different air pollutants in China, with calculated correlation coefficients of approximately 0.77, 0.72, 0.64, 0.67, 0.69 and 0.71,
431 and normalized mean biases of approximately 4.5%, –4.6%, –9.0%, –3.9%, –8.8% and 9.5%, for the hourly concentrations of
432 PM_{2.5}, PM₁₀, SO₂, NO₂, CO and O₃, respectively. Moreover, the *a posteriori* model simulation achieved comparable accuracy
433 with the air quality reanalysis data we developed in Kong et al. (2021) in terms of the RMSE, which was 32.4 µg·m⁻³, 53.1
434 µg·m⁻³, 24.9 µg·m⁻³, 19.9 µg·m⁻³, 0.56 mg·m⁻³ and 34.9 µg·m⁻³, respectively, for these species at the hourly scale. At the daily,
435 monthly and yearly scales, the constrained model simulation performed better, with RMSEs of about 9.1–20.0 µg·m⁻³ (PM_{2.5}),
436 18.5–31.6 µg·m⁻³ (PM₁₀), 11.5–16.0 µg·m⁻³ (SO₂), 8.1–12.8 µg·m⁻³ (NO₂), 0.28–0.39 mg·m⁻³ (CO), and 14.2–26.1 µg·m⁻³ (O₃),
437 which were respectively reduced by 56.7–67.3%, 49.2–52.1%, 68.8–72.8%, 36.3–39.8%, 47.0–58.0%, and 22.9–30.5%
438 compared to the RMSEs of the *a priori* simulations. These validation results confirm the good performance of the data
439 assimilation method and ~~suggest indicate~~ that the inversed emissions inventory has the capability to can reasonably represent
440 the magnitude and long-term trends of the air pollutant emissions in China during 2013–2020.

441 4 Results

442 Based on the top-down estimation, the gridded emissions for PM_{2.5}, PM₁₀, SO₂, CO, NO_x and NMVOCs over China from
443 2013 to 2020 were developed into what we have called the Inversed Emissions Inventory for Chinese Air Quality (CAQIEI).
444 In the following sections, we first analyze the magnitude and seasonality of the air pollutant emissions in China by taking 2015
445 as a reference year ~~for~~ when the number of observation sites became stable. After that, the changes in emissions of different
446 air pollutants from 2015 to 2020 are analyzed and compared between the two clean air action plans in China. Note that due to
447 the impacts of the changes in observation coverage, it is difficult to estimate the overall emission reduction rates during the
448 2013–2017 action plan by using our inversion results. The emission change rates during 2015–2017 were then sampled in this
449 study to assess the mitigation effects during the 2013–2017 action plan and to be compared with the emission change rates
450 during 2018–2020. Finally, CAQIEI is compared to the previous bottom-up and top-down emission inventories to validate our
451 top-down estimation and identify the potential uncertainties in the current understanding of China’s air pollutant emissions.

452 4.1 Top-down estimated Chinese air pollutant emissions in 2015

453 The top-down estimated emissions of different species in 2015 are as follows: 25.2 Tg of NO_x, 17.8 Tg of SO₂, 465.4 Tg
454 of CO, 15.0 Tg of PM_{2.5}, 40.1 Tg of PM₁₀, and 46.0 Tg of NMVOCs. Note that these values not only contain anthropogenic

emissions but also natural (e.g., dust and biogenic NMVOC) emissions. Thus, the top-down estimated emissions of PM and NMVOCs were higher than those estimated by previous studies, as we mention in the following sections. Emission maps of all species in 2015 are shown in Fig. 4, and the calculated emissions of different species over different regions are presented in Table 3. According to Fig. 4, higher air pollutant emissions are widely distributed in the megacity clusters (e.g., NCP, Yangtze River Delta and Pearl River Delta) and the developed cities in China, reflecting the influences of human activities. NCP ~~was~~ the region with the largest emission intensity of air pollutants in China, contributing 5.1 Tg of NO_x, 3.5 Tg of SO₂, 82.2 Tg of CO, 2.7 Tg of PM_{2.5}, 8.7 Tg of PM₁₀ and 9.0 Tg of NMVOCs to the total emissions in China. ~~There were also obvious emission hotspots distributed over the large cities of other regions, reflecting the influences of human activities. The inversion results also demonstrate the contribution of natural sources to the air pollutant emissions, such as the soil NO_x emissions and the biogenic NMVOC emission distributed in the Tibet Plateau region.~~ In general, the majority of air pollutant emissions were located in eastern China (including the NCP, NE and SE regions), where the economy is relatively well developed, which in total accounted for 66.0% of NO_x, 60.9% of SO₂, 57.5% of CO, 60.4% of PM_{2.5}, 60.5% of PM₁₀, and 67.8% of NMVOC emissions in China. However, although the GDP of western China (including the SW, NW and Central regions) is less than one third that of eastern China, the top-down estimation indicates that the air pollutant emissions in western China could have accounted for about 32.2–42.5% of the total emissions, which reflects the low emission control levels over these regions.

Figure 5 shows the monthly variations of air pollutant emissions in China for year 2015. The monthly profile of NO_x emissions was relatively flat among the six species. SO₂ and CO showed higher emissions during wintertime because of the enhanced residential emissions associated with higher coal consumption for heating during that time of year. Meanwhile, the emission factor for CO from vehicles in winter was also higher than in other seasons, due to additional emissions from the cold-start process (Kurokawa et al., 2013; Li et al., 2017b). PM_{2.5} and PM₁₀ had higher emissions during winter and spring, which, on the one hand was due to the enhanced emissions from the residential and industrial sectors during wintertime (Li et al., 2017b), whilst on the other hand was due to the enhanced dust emissions during the spring season (Fan et al., 2021). Emissions of NMVOCs exhibited strong monthly variations, with higher emissions mainly in summer because of the enhanced NMVOC emissions from biogenic sources.

4.2 Top-down estimated emission changes of different air pollutants

4.2.1 Emission changes of particular matter

Figure 6 shows the top-down estimated emission changes of PM_{2.5} and PM₁₀ over China during two clean air action periods. Both PM_{2.5} and PM₁₀ emissions decreased substantially, by 44.3% and 21.2% respectively, from 2013 to 2020. On the contrary, the top-down estimates showed increases of PM_{2.5} and PM₁₀ emissions in 2014 and 2015, but this would be likely to be a spurious trend caused by the changes of observation sites as we seen by the good correlation between the inversed PM_{2.5} emissions and the observational coverage over the NW region (Fig. 2 and Fig. S1) discussed in Text S1. Therefore, the emissions in 2013 and 2014 were discarded to prevent the spurious trends. According to Fig. 6, the PM_{2.5} emissions decreased by 14.5% from during the 20153 (15.0 Tg) to 2017 (12.8 Tg) clean air action period, from 15.0 Tg in 2015 to 12.8 Tg in 2017, and the reduction in emissions was roughly uniform throughout the period, which was about 8% compared to previous years. The PM₁₀ emissions showed a smaller reduction rate (−7.2%) than that of PM_{2.5}, decreasing from 40.1 Tg in 2015 to 37.2 Tg in 2017. Compared with the emission reduction rate during the 2015–20173–2017 action plan, both PM_{2.5} and PM₁₀ showed larger emission reduction rates during the 2018–2020 action period, estimated to be 27.2% and 25.5%, respectively, from 2018 to 2020. The emission reductions in each year were also larger, especially for PM₁₀. For example, PM_{2.5} and PM₁₀ emissions reduced by about 19.3% and 14.0% in 2019 compared to 2018. This may have been due to that in addition to the strict controls imposed on the industrial and power sectors during the 2013–2017 action period, along with the strengthened controls the on

496 residential emissions [have been strengthened](#) during the 2018–2020 action period. In particular, “coal-to-electricity” and “coal-
497 to-gas” strategies were vigorously implemented in northern China during [the 2018–2020 action](#) [wintertime](#) to reduce coal
498 consumption and related air pollutant emissions (Liu et al., 2016; Wang et al., 2020a). Thus, our inversion results confirm the
499 effectiveness of the controls on residential emissions in terms of reducing the emissions of PM_{2.5} and PM₁₀. In addition, the
500 control of non-point sources, such as blowing-dust emissions, was also strengthened during the 2018–2020 action period,
501 which is consistent with the faster reduction of PM₁₀ emissions during 2018–2020. The annual trends of PM_{2.5} and PM₁₀
502 emissions were also calculated in China using the Mann–Kendall trend test and the Theil–Sen trend estimation method, the
503 results of which are summarized in Table 4. The calculation of emission trends can help extend the existing emission datasets
504 forward in time to produce up-to-date products. The top-down estimated trends of PM_{2.5} and PM₁₀ emissions were –1.4 and
505 –2.6 Tg/year during 2015–2020, attributable to the strict emission control measures imposed during the two clean air action
506 plans. As mentioned, the decreasing trends were larger during [the 2018–2020 action plan](#) (–1.5 and –4.6 Tg/year) than during
507 [the 2013–2017 action plan](#) (–1.1 and –1.5 Tg/year).

508 On the regional scale (Fig. [S31](#)), it can be clearly seen that the PM_{2.5} emissions decreased consistently over all regions,
509 by 59.8% in NCP, 49.6% in SE, 39.5% in NE, 35.8% in SW, 33.2% in NW, and 41.0% in Central, from 2015 to 2020. The
510 NCP region showed the largest reduction in emissions among the six regions, with its emission reduction rate being almost
511 larger than 10% in each year. This is consistent with the strictest emission control policies having been imposed over the NCP
512 region. The SE region showed a similar reduction in emissions to the NCP region, with its emission reduction rate being larger
513 than 10% in most years. Obvious increases of PM_{2.5} emissions could be found over the NW region from 2013 to 2015 [possibly](#)
514 owing to the increase in the number of observation sites in those years. After 2015, PM_{2.5} emissions generally decreased over
515 the NW region, while there was a slight rebound in PM_{2.5} emissions in 2016 and 2018, possibly due to the influences of the
516 errors in fine dust emission. The Central region showed different characteristics of emission changes to the other regions
517 insofar as it showed little change in PM_{2.5} emissions during 2015–2018 but large reductions in 2019. This may be consistent
518 with the control of emissions over the Fengwei Plain area (the part of the Central region where the emission intensity is largest)
519 being weak during the 2013–2017 action plan but strengthened during the 2018–2020 action plan. In terms of the PM_{2.5}
520 emission trends over the different regions, the calculated PM_{2.5} emission trends were about –0.32 Tg/year in NCP, –0.32
521 Tg/year in SE, –0.24 Tg/year in NE, –0.21 Tg/year in SW, –0.09 Tg/year in NW, and –0.15 Tg/year in Central, from 2015 to
522 2020.

523 The changes of PM₁₀ emissions were generally similar to those of PM_{2.5}, i.e., with decreases in all regions from 2015 to
524 2020 (Fig. [S42](#)). The top-down estimated PM₁₀ emission reductions from 2015 to 2020 were about 3.5 Tg (40.0%) in NCP,
525 2.6 Tg (35.5%) in SE, 3.0 Tg (36.6%) in NE, 2.0 Tg (35.9%) in SW, 1.0 Tg (25.3%) in NW, and 1.3 Tg (21.6%) in Central;
526 and the calculated trends were about –0.64 Tg/yr, –0.52 Tg/yr, –0.51 Tg/yr, –0.40 Tg/yr, –0.20 Tg/yr, and –0.27 Tg/yr,
527 respectively. However, due to the influences of the changes in the number of observation sites, the PM₁₀ emissions over the
528 NE, SW and NW regions increased substantially from 2013 to 2015, while they decreased in almost all years after 2015.
529 Different from the other regions, the Central region showed increases in PM₁₀ emissions from 2015 to 2018, by about 0.92 Tg
530 (14.9%), but substantial decreases in 2019 and 2020. [The resultis](#) also shows that most PM₁₀ emission reductions were achieved
531 during the 2018–2020 action plan. According to CAQIEI, the PM₁₀ emissions decreased by 0.64–2.3 Tg (17.4–31.8%) from
532 2018 to 2020, which accounted for 48.4–169.0% of the total reduction in emissions from 2015 to 2020. This again emphasizes
533 the effectiveness of the control of blowing-dust emissions during the 2018–2020 action plan.

534 4.2.2 Emission changes of gaseous air pollutants

535 4.2.2.1 SO₂ and CO

536 Figure 7 shows the emission changes of different gaseous air pollutants in China from 2013 to 2020. Similar to the PM
537 emissions, SO₂ and CO emissions decreased continuously during the two action plan periods, with top-down estimated

538 emission reductions of about 9.6 Tg (54.1%) and 166.3 Tg (35.7%) for SO₂ and CO from 2015 to 2020, respectively.
539 Meanwhile, both SO₂ and CO showed a significant decreasing trend from 2015 to 2020, with estimated trends of approximately
540 -2.1 Tg/yr and -36.0 Tg/yr, respectively (Table 5). The reductions in SO₂ and CO emissions are closely consistent with the
541 strict emission control measures imposed during the action plan periods, such as the phasing out of outdated industrial capacity
542 and high-emitting factories, the strengthening of emission standards for industry and the power sector, the elimination of small
543 coal-fired industrial boilers, and the replacement of coal with cleaner energies, which reflects the effectiveness of the emission
544 control measures during the two action plan periods. Reductions of SO₂ emission were generally steady during the two action
545 plan periods, which were approximately 4.2 Tg (23.8%) from 2015 to 2017 and 2.5 Tg (23.5%) from 2018 to 2020. However,
546 CO showed a different emission reduction rate during the two action plan periods, with its emission reductions (67.1 Tg, 18.3%)
547 during ~~the 2018–2020 action plan~~ being larger than those (45.6 Tg, 9.8%) during ~~2015–2017~~~~the 2013–2017 action plan~~. This
548 contrast may reflects the different emission control policies during the two clean air action periods, as well as the different
549 emission distributions among the sectors between SO₂ and CO. According to the estimates of Zheng et al. (2018), the share of
550 emissions from the industrial and power sector for SO₂ (77%) is nearly double that for CO (39%). Thus, the smaller reduction
551 of CO emissions ~~during the 2013–2017 action plan~~ than that of SO₂ ~~during 2015–2017~~ provides evidence that the 2013–2017
552 action plan mainly focused on controlling the emissions from the industrial and power sectors. During the 2018–2020 action
553 plan, strict control measures targeted on the residential and transportation sectors were also implemented, which together
554 account for 61% of CO emissions but only 23% of SO₂ emissions. As a result, CO showed a larger emission reduction rate
555 during ~~the 2018–2020 action plan~~, while the emission reduction rate for SO₂ was similar to that ~~during in the 2015–2017~~
556 ~~action plan~~. The calculated trends of SO₂ and CO emissions during the two action plans are presented in Table 4, which are
557 -2.1 Tg/yr and -1.3 Tg/yr for SO₂, and -22.8 Tg/yr and -33.5 Tg/yr for CO, respectively.

558 The reduction of SO₂ and CO emissions was also evident on the regional scale (Fig. S53 and S64). According to the top-
559 down estimation, the reduction of SO₂ emissions ranged from 0.44 to 2.42 Tg (41.7–69.9%) from 2015 to 2020, with the NCP
560 region exhibiting the largest reductions. The calculated decreasing trend of SO₂ emissions was also significant over all regions,
561 ranging from -0.08 Tg/yr over the NW region to -0.57 Tg/yr over the NCP region (Table 5). With regards to the emission
562 reduction rate during the different action plans, the results suggest that the emission reduction rate of SO₂ was higher during
563 ~~the 2015–2017~~~~2013–2017 action plan~~ (by 20.8–39.8%) than that ~~during during the 2018–2020 action plan~~ (16.6–29.0%) over the
564 NCP, SE, NE and SW regions. This may have been because, after the strict emission controls imposed upon industry and
565 power plants during the 2013–2017 action plan, the room for further reductions in SO₂ emissions become smaller during the
566 2018–2020 action plan over these regions. Although residential and vehicle emissions were controlled more strictly during the
567 2018–2020 action plan, in total they account for ~20% of anthropogenic SO₂ emissions in China (Zheng et al., 2018). Thus,
568 the enhanced reductions in SO₂ emissions from the residential and transportation sectors may not have been able to fully
569 compensate for the weakened reductions from the industrial and power sectors, leading to a smaller SO₂ emission reduction
570 rate over these regions. In contrast, the SO₂ emission reduction rate during ~~g the 2018–2020 action plan~~ (31.1–34.8%) was
571 higher than that during ~~the 2015–2017~~~~2013–2017 action plan~~ (14.1–20.4%) over the NW and Central regions. This may have been due
572 to the fact that the emission controls over the NW and Central regions were relatively weak during the 2013–2017 action plan
573 (as also evidenced by the emission reduction rates of other species) owing to its less-developed economy. During the 2018–
574 2020 action plan, the emission controls over these two regions were strengthened, which led to their higher emission reduction
575 rates. Accordingly, the enhanced SO₂ emission reduction rates over the NW and Central regions compensated for the weakened
576 reduction rates over the other regions, leading to a steady SO₂ emission reduction rate on the national scale.

577 The reductions of CO emissions from 2015 to 2020 were approximately 14.9–42.3 Tg (21.6–51.4%) over the different
578 regions of China, with significant decreasing trends ranging from -3.0 to -8.7 Tg/yr (Fig. S63 and Table 5). Consistent with
579 the comparisons of national CO emission reduction rates between the two action plans, the emission reduction rates during ~~the~~
580 ~~2015–2017~~~~2013–2017 action plan~~ (4.4–24.6%) were estimated to be smaller than those during ~~the 2018–2020 action plan~~ (12.2–24.6%)

581 over all the different regions except the Central region, where the CO emission reduction rate was similar during the two action
582 plans (Fig. S64).

583 4.2.2.2 NO_x and NMVOCs

584 The top-down estimated NO_x and NMVOC emissions showed different changes to the other four species, by increasing
585 during ~~the 2013–2017 action plan~~ but declining during ~~the 2018–2020 action plan~~. Specifically, NO_x emissions increased
586 slightly by 5.9% from 2015 (25.2 Tg) to 2017 (26.6 Tg), with a non-significant increasing trend of 0.74 Tg/yr. Then, NO_x
587 emissions began to decrease in 2018, with a top-down estimated emission reduction and calculated trend of approximately 3.1
588 Tg (12.7%) and –1.6 Tg/yr, respectively, from 2018 to 2020. NMVOCs showed stronger emission increases than did NO_x,
589 with top-down estimated emission increases of approximately 12.7 Tg (27.6%) and a calculated emission trend of about 6.3
590 Tg/yr from 2015 to 2017. Similar to NO_x, NMVOC emissions began to decrease after 2018, with a top-down estimated
591 reduction of approximately 2.6 Tg (–4.4%) from 2018 to 2020, and a calculated trend of about –1.3 Tg/yr.

592 The increases of NO_x and NMVOC emissions ~~during 2015–2017 suggest indicate~~ that the 2013–2017 action plan may not
593 have achieved desirable mitigation effects on these two species. For NO_x emissions, the upward trend may have been associated
594 with the following ~~three~~ factors. ~~Firstly~~ On the one hand, vehicle exhaust is one of the most important sources of NO_x in China,
595 accounting for 31% of all NO_x emissions nationally (Zheng et al., 2018). From 2013 to 2017, the number of vehicles in China
596 continued to increase and reached 310 million in 2017, approximately 33.5% higher than in 2013 (MEE, 2017), which led to
597 increases of NO_x emissions from vehicles in China. ~~Secondly, as discussed, the control measures implemented during the~~
598 ~~2013–2017 action plan mainly focused on power plants and industrial sources. Controls on vehicle sources were relatively~~
599 ~~weak. In particular, vehicles with high NO_x emissions, such as heavy-duty diesel trucks, were not controlled strictly during the~~
600 ~~2013–2017 action plan. On the other hand~~ Thirdly, although the 2013–2017 action plan was effective in reducing the NO_x
601 emissions from coal-fired power plants by promoting denitrification facilities and an ultra-low emission standard, the
602 mitigation impacts on industrial NO_x emissions may have been relatively small. For example, Wang et al. (2019a) compiled a
603 unit-based emissions inventory for China's iron and steel industry from 2010 to 2015, based on detailed survey results of
604 approximately 4900 production facilities in mainland China. They found that there were almost no NO_x control measures in
605 China's iron and steel industry during 2010–2015, resulting in a 12.4% increase in China's NO_x emissions from the iron and
606 steel industry in 2015 compared to 2010. In addition, although the penetration rate of denitrification facilities in China's cement
607 industry reached 92% in 2015, the actual operating rate of denitrification facilities in the cement industry was not desirable,
608 due to the lack of online emission monitoring systems. According to the research results of the Ministry of Ecology and
609 Environment, 800, 1300, and 1400 cement production kilns were equipped with selective non-catalytic denitrification facilities
610 from 2013 to 2015, but the actual operating rates were only 51%, 54% and 73%, respectively (Liu et al., 2021). In addition,
611 the new precalciner kilns used in the cement industry have a higher NO_x emission factor, such that the shift from traditional
612 vertical kilns to precalciner kilns has to some extent increased the cement industry's emissions of NO_x (Liu et al., 2021). Thus,
613 there is evidence that the mitigation effects of the industrial control measures on NO_x emissions may not be as significant as
614 expected. Overall, the increased number of vehicles may have offset the emission mitigation effects brought about by the
615 control of power plants, ~~and~~. ~~Meanwhile~~, the mitigation effects of controlling ~~vehicle and~~ industrial NO_x emissions were also
616 undesirable. Consequently, NO_x emissions in China may not have decreased, and even increased slightly, during the 2013–
617 2017 action plan. Figure S75 further shows the changes in NO_x emissions over different regions of China, revealing that NO_x
618 emissions over the NCP, SE, NE and SW regions were roughly unchanged (by less than 5%) from 2015 to 2017, while they
619 increased over NW (18.6%) and Central (17.5%). This is consistent with previous results and indicates that NO_x emissions
620 may have increased over the NW and Central regions, possibly due to their increased human activities and weak emission
621 controls.

622 In terms of NMVOC emissions, since the inversion results did not differentiate between anthropogenic and biogenic
623 sources, the changes in NMVOC emissions may have been related to both anthropogenic and biogenic emissions. With respect
624 to anthropogenic emissions, previous bottom-up studies have suggested that China's NMVOC emissions did not decline during
625 the 2013–2017 action plan, due to the lack of effective control measures on the chemical industry and solvent use (Zheng et
626 al., 2018; Li et al., 2019c). According to the estimates of Li et al. (2019c), China's NMVOC emissions from solvent use
627 increased by 11.1% in 2017 compared to those in 2015. Meanwhile, the increase in the number of vehicles in China may also
628 have led to an increase in NMVOC emissions from transportation. ~~Thus, Therefore, the~~ **increases of NMVOC emission**
629 **during 2015–2017 estimated by our inversion inventory may be related to the increases in anthropogenic NMVOC emissions**
630 **from the chemical industry, solvent use, and vehicles, together with the increase in biogenic NMVOC emissions, may be the**
631 **main reasons for the increased NMVOC emissions during the 2013–2017 action plan. For the trends of biogenic NMVOC**
632 **emissions, the CAMS global emission inventory shows that there were only little changes in the biogenic NMVOC emissions**
633 **in China from 2013 to 2018 (Sect. 4.3.3), suggesting little contributions of the biogenic sources to the increased NMVOC**
634 **emission in China.** ~~According to the estimations of Li et al. (2020a), there was also an upward trend in China's biogenic~~
635 ~~NMVOC emissions from 2008 to 2018 because of the increased vegetation cover and air temperature. Compared to the~~
636 ~~emissions in 2008, China's biogenic NMVOC emissions increased by 20.18% in 2017, with an average annual rate of increase~~
637 ~~of 2.03%. Therefore, the increases in NMVOC emissions from the chemical industry, solvent use, and vehicles, together with~~
638 ~~the increase in biogenic NMVOC emissions, may be the main reasons for the increased NMVOC emissions during the 2013–~~
639 ~~2017 action plan.~~ Figure S86 further shows the changes in NMVOC emissions over different regions of China, which suggests
640 consistent increases in NMVOC emissions from 2015 to 2017 over different regions. According to the top-down estimations,
641 NMVOC emissions increased by 30.5%, 25.2%, 18.5%, 10.9%, 50.5% and 63.1% over the NCP, SE, NE, SW, NW and Central
642 regions, respectively. Again, the NW and Central regions exhibited the largest emission increases among the six regions, which
643 is consistent with their elevated levels of human activity and weak emission controls.

644 The decrease in NO_x and NMVOC emissions after 2018 suggests that the emission control strategy of the Chinese
645 government had reached a point of optimization. The 2018–2020 action plan not only strengthened the controls over the
646 industrial and power sectors, but also the transportation sector, especially for diesel vehicles with high NO_x emissions. For
647 example, the Chinese government released the “Action Plan for the Control of Diesel Trucks”, and vigorously promoted an
648 adjustment of the transportation structure of China by gradually improving the availability of rail transport. As a result, there
649 was a downward trend in NO_x emissions in China. The top-down estimated reductions of NO_x emissions were approximately
650 0.81 Tg (17.2%) over NCP, 0.98 Tg (14.0%) over SE, 0.37 Tg (9.4%) over NE, 0.51 Tg (12.2%) over SW, 0.13 Tg (11.0%)
651 over NW, and 0.32 Tg (9.2%) over Central (Fig. S75). The decrease in NMVOC emissions after 2018 may on the one hand
652 have been related to the strengthening of vehicle controls during the 2018–2020 action plan, whilst on the other hand it may
653 have been related to the promotion of clean heating plans in the northern region, which reduced the emissions of NMVOCs
654 from residential sources. However, the decreases in NMVOC emissions were smaller than those in NO_x, which were estimated
655 to be 0.84 Tg (6.9%) over NCP, 0.47 Tg (2.8%) over SE, 0.98 Tg (10.1%) over NE, and 0.53 Tg (14.1%) over NW (Fig. S6).
656 Different from other regions, the NMVOC emissions over the SW and Central regions remained almost unchanged during the
657 2018–2020 action plan (Fig. S86).

658 4.2.3 Changes in the distribution pattern of emissions in China

659 Due to the different emission control intensities over the different regions of China, the emission distribution patterns of
660 the different species may also have been altered, which could have influenced the distributions of air pollution in China. Based
661 on CAQIEI, we further investigated the emission distribution patterns, as well as their changes, during the two action plans.
662 Maps of the emission changes of different species during ~~2015–2017~~ **the 2013–2017 action plan** and ~~the~~ **2018–2020 action plan**
663 are presented in Fig. 8. The shares of emissions in 2015, 2017 and 2020 by each subregion of China are also presented (Fig.

664 9). It can be seen that the emission changes during the 2015–2017 ~~2013–2017~~ ~~action plan~~ were more heterogenous than those
665 during ~~the~~ 2018–2020 ~~action plan~~. The air pollutant emissions after the 2018–2020 action plan showed consistent reductions
666 over most regions of China, while there were obvious emission increases detected ~~from 2015 to 2017~~ ~~over the 2013–2017~~
667 ~~action plan~~. This is consistent with the different emission control ~~eff~~~~ct~~~~s~~~~i~~~~e~~~~n~~~~c~~~~i~~~~e~~~~s~~~~i~~~~e~~~~n~~~~c~~~~i~~~~e~~~~s~~ during the two clean air action plans as
668 mentioned in previous sections. Due to its strictest emission control policies, the NCP region showed consistent emission
669 reductions of SO₂, NO_x, CO, PM_{2.5} and PM₁₀ during the two clean air action plans. Accordingly, the shares of emissions in the
670 NCP region continued to decrease during the two action plan periods (Fig. 9). For example, the share of SO₂ emissions in the
671 NCP region decreased from 19.4% to 15.4% ~~after the~~ ~~during the period of~~ 2015–2017 ~~action plan~~, and from 15.4% to 12.7%
672 ~~during~~ ~~after~~ the 2018–2020 action plan. In contrast, NMVOC emissions increased obviously over the NCP region ~~from~~ ~~during~~
673 ~~the~~ 2015–2017 ~~action plan~~, and decreased during ~~the~~ 2018–2020 ~~action plan~~. However, its share did not change
674 significantly ~~during the two action plans~~, being roughly 20% throughout both periods. As for other regions, increases of SO₂,
675 NO_x, PM_{2.5}, PM₁₀ and NMVOC emissions during ~~2015–2017~~ ~~the 2013–2017~~ ~~action plan~~ could be found over the Central
676 region. More specifically, the emission increases were mainly located in the Fenwei Plain area of the Central region, which
677 was due to the fact that this area was not included as a key region of emission controls during the 2013–2017 action plan.
678 However, the Fenwei Plain area was added as a key emission control region during the 2018–2020 action plan, which is
679 consistent with the emission reductions for these species over the Central region (Fig. 8). As a result, the shares of SO₂ and
680 PM_{2.5} emissions in the Central region increased ~~during 2015–2017~~ ~~in the 2013–2017~~ ~~action plan~~ but decreased ~~in the~~ ~~during~~
681 ~~2018–2020~~ ~~action plan~~ (Fig. 9). However, the shares of NO_x, PM₁₀ and NMVOC emissions continued to increase over the
682 Central region during the two clean air action plans, which suggests larger roles of air pollutant emissions in that region. In
683 contrast, the share of CO emissions in the Central region continued to decrease in the two action plans, from 17.7% in 2015 to
684 13.4% in 2020.

685 In terms of the shares of emissions in eastern and western China, the top-down estimation suggests an increased share of
686 NO_x, PM_{2.5}, PM₁₀ and NMVOC emissions in western China after the two clean air action plans (Fig. 9), which indicates slower
687 emission reductions for these species in western China. However, the share of CO emissions in western China was reduced
688 after the two clean air action plans. Although the share of SO₂ emissions in western China increased during ~~the~~ 2015–2017
689 ~~action plan~~, it turned to a decrease ~~during~~ ~~in the~~ 2018–2020 ~~action plan~~.

690 4.3 Comparisons with different ~~bottom-up~~ emission inventories

691 In this section, the CAQIEI is compared with the previous long-term bottom-up and top-down emission inventories in
692 China to validate our inversion results and provide the clues for the potential uncertainty in the current air pollutant emission
693 inventories. The bottom-up emission inventories used in the comparison include MEIC (Zheng et al., 2018), ABaCAS (Li et
694 al., 2023), HTAPv3 (Crippa et al., 2023), EDGARv6 (Jalkanen et al., 2012) and CEDS (McDuffie et al., 2020), while the top-
695 down emission inventory is obtained from the updated Tropospheric Chemistry Reanalysis (TCR-2) (Miyazaki et al., 2020b).
696 However, it is difficult to directly compare our inversion results with these emission inventories considering that the inversion
697 emission includes both anthropogenic and natural emissions. To better compare our inversion results with previous inventories,
698 the natural emission sources, including soil NO_x emissions and biogenic emissions obtained from the CAMS global emission
699 inventory (<https://ads.atmosphere.copernicus.eu/cdsapp#!/dataset/cams-global-emission-inventories?tab=overview>; last
700 accessed 26 July 2023) and the biomass burning emissions obtained from the Global Fire Assimilation System (GFAS) (Kaiser
701 et al., 2012) are taken as a reference to account for the influences of natural sources. The CAMS and GFAS emission inventory
702 are used because they are state-of-art natural emission inventories and can provide us with long-term estimations of natural
703 emissions. Since the latest year of most emission inventories is 2018, the comparisons were conducted between 2015 and 2018.
704 Note that due to the complexity in the estimations of natural sources, significant uncertainty exists in the estimated natural

705 emissions. As a result, the comparison results would be sensitive to the used natural emission inventories, especially for the
706 species with large amount of natural emission, such as the NMVOC and particulate matter. Therefore, it should be aware of
707 that the comparison conducted here and the derived implications are on the basis of the natural emissions estimated by CAMS
708 and GFAS. In addition, the natural dust emissions are not considered in the comparisons, which would influence the
709 comparisons of the PM emissions.

710 4.3.1 Magnitude

711 ~~In this subsection, we compare CAQIEI with previous long term bottom-up and top-down emission inventories in~~
712 ~~China to validate our inversion results and identify the potential uncertainty in the current understanding of China's~~
713 ~~air pollutant emissions. The emission inventories adopted were MEIC (Zheng et al., 2018), ABaCAS (Li et al., 2023),~~
714 ~~HTAPv3 (Crippa et al., 2023), EDGARv6 (Jalkanen et al., 2012), CEDS (Meduffie et al., 2020), and the top-down~~
715 ~~emission estimates from the updated Tropospheric Chemistry Reanalysis (TCR-2) (Miyazaki et al., 2020b).~~
716 ~~(<https://ads.atmosphere.copernicus.eu/edsapp#!/dataset/cams-global-emission-inventories?tab=overview>; last~~
717 ~~accessed 26 July 2023) Since the latest year of most emission inventories is 2018, the comparisons were conducted~~
718 ~~between 2015 and 2018. In particular, the comparison with MEIC is highlighted considering its wide application in~~
719 ~~Chinese air pollution studies. Considering that the top-down estimation includes both anthropogenic and natural~~
720 ~~sources, the natural emission sources, including soil NO_x emissions and biogenic emissions obtained from the CAMS~~
721 ~~global emission inventory ([https://ads.atmosphere.copernicus.eu/edsapp#!/dataset/cams-global-emission-](https://ads.atmosphere.copernicus.eu/edsapp#!/dataset/cams-global-emission-inventories?tab=overview)~~
722 ~~[inventories?tab=overview](https://ads.atmosphere.copernicus.eu/edsapp#!/dataset/cams-global-emission-inventories?tab=overview); last accessed 26 July 2023) and the biomass burning emissions obtained from the Global~~
723 ~~Fire Assimilation System (GFAS) (Kaiser et al., 2012), were also analyzed to help explain the discrepancies between~~
724 ~~our inversion results and previous inventories.~~

725 4.3.1.1 NO_x

726 Figure 10 shows the average emissions of different air pollutants in China during 2015–2018 obtained from CAQIEI and
727 the previous emission inventories plus the natural sources we considered. Comparisons of the emission estimations on the
728 regional scale and gridded scale are also presented (Fig. 11 and Fig. S9). The results show that the CAQIEI has slightly higher
729 NO_x emissions in China than the other inventories. Considering that CAQIEI includes both anthropogenic and natural sources,
730 this discrepancy could be explained by the natural NO_x sources. According to the estimations of CAMS and GFAS, the soil
731 and biomass-burning NO_x emissions are approximately 1.9 and 0.08 Tg/yr, which explains well the higher NO_x emissions
732 given by CAQIEI. After consideration of the natural sources, MEIC, HTAPv3 and EDGARv6 agree well with our inversion
733 results on the national scale, with their differences within 1.0–7.4%. ~~This confirms well our inversion results and suggests that~~
734 ~~there is no significant bias in the estimations of total NO_x emissions in China for these inventories. The NO_x emission estimated~~
735 ~~by ABaCAS, CEDS and TCR-2 may have low bias in their estimated NO_x emissions considering their are slightly lower smaller~~
736 ~~values than CAQIEI and other emission inventories. However, the differences between CAQIEI and these inventories were~~
737 ~~found to range from 15.9% to 21.3%, which is consistent with within the previous estimated uncertainties of NO_x emissions in~~
738 ~~China (Kurokawa and Ohara, 2020; Li et al., 2017b; Li et al., 2023). These results suggest that the total NO_x emissions in~~
739 ~~CAQIEI are generally consistent with the current estimations of the anthropogenic and natural NO_x emissions in China. On~~
740 ~~the regional scale, the top-down estimated NO_x emissions show good agreement with the previous emission inventories over~~
741 ~~the NCP and SE regions, with their differences ranging from 1.0%–26.8%, suggesting good consistency lower uncertainties in~~
742 ~~the estimations of NO_x emissions over these two regions. This makes sense because NCP and SE are the two most developed~~
743 ~~regions in China, and where surveys and research on emissions are most sufficient. The differences uncertainties are larger~~
744 ~~over the other regions. In the NE region, CAQIEI has higher NO_x emissions than the other inventories, by 5–70%,~~
745 ~~suggesting higher anthropogenic or biomass-burning emissions over there. The estimations made by MEIC, CEDS and TRC-~~
746 ~~2 are closer to our estimates, with their differences being approximately 5.4–23.3%, while the differences are larger for~~
747 ~~ABaCAS, HTAPv3 and EDGARv6 (36.7–70.0%). This suggests that anthropogenic or biomass-burning emissions may be~~
748 ~~underestimated over the NE region. Over the SW and Central regions, there are large diversity in the previous emission~~
749 ~~inventories with estimations by HTAPv3 and EDGARv6 almost double those of MEIC, ABaCAS, CEDS and TCR-2. The~~
750 ~~CAQIEI suggests a midst estimation which is within the range of previous emission inventories higher than MEIC, ABaCAS,~~

751 ~~CEDS and TCR-2 by 29.4–40.8% and 22.4–47.4%, respectively, but is lower than HTAPv3 and EDGARv6 by about 30%,~~
752 ~~suggesting higher uncertainties of estimated NO_x emissions over these two regions.~~ In the NW region, CAQIEI is consistently
753 higher than ~~otherthe previous~~ inventories, by 22.7–64.2%, ~~which which~~ suggests a potential missing source of the NO_x
754 emissions significant low bias may exist in current estimations of NO_x emissions over this region.

755 4.3.1.2 SO₂

756 For SO₂ emissions, since natural sources contribute little (only about 0.02 Tg/yr) to them in China, the discrepancies
757 between CAQIEI and previous emission inventories are mainly attributable to the differences in anthropogenic emissions. As
758 shown in Fig. 10, CAQIEI agrees well with HTAPv3 and CEDS on the national scale, with their differences being
759 approximately ±2%, but is higher than MEIC, ABaCAS and TCR-2 by 17.4–32.9%, ~~suggesting a negative bias in their~~
760 ~~estimated SO₂ emissions in China.~~ In contrast, EDGARv6 may have a positive bias in its estimated SO₂ emissions, which are
761 roughly double those of CAQIEI and other inventories. On the regional scale, our results agree well with MEIC, ABaCAS,
762 HTAPv3, CEDS and TCR-2 over the NCP region, with their differences ranging from 1.0 to 18.1%, ~~suggesting lower~~
763 ~~uncertainties in SO₂ emissions over this region.~~ In the SE region, CAQIEI ~~suggests~~ lower SO₂ emissions than previous
764 emission inventories, except TCR-2. The differences are relatively smaller (~~by around –15%~~) for the MEIC and ABaCAS
765 inventories by around –15%, but larger for HTAPv3, EDGARv6 and CEDS (ranging from –47.3% to –113.2%). ~~This suggests~~
766 ~~that current global emission inventories may overestimate the SO₂ emissions in the SE region.~~ In contrast, CAQIEI ~~is suggests~~
767 higher SO₂ emissions than all previous emission inventories over the NE region by about 14.8–132.0%, ~~indicating which~~
768 ~~suggests a possible missing sources consistent negative bias may exist in current estimations of SO₂ emissions over this~~
769 ~~regionthere.~~ Similarly, ~~the~~ CAQIEI ~~and HTAPv3 suggests~~ higher SO₂ emissions than ~~the~~ MEIC, ABaCAS, CEDS and TCR-
770 2, by 27.0–75.6%, in the NW region, and by 44.3–77.7% in the Central region, ~~suggesting a negative bias in estimations of~~
771 ~~SO₂ emissions over these two regions. The SO₂ emissions estimated by HTAPv3 are closer to our inversion results, with their~~
772 ~~differences being about 6.9–12.6%.~~

773 4.3.1.3 CO

774 For CO emissions, CAQIEI is substantially higher than the previous emission inventories, with the estimated CO
775 emissions of CAQIEI being about three times higher than the bottom-up inventories and more than double those of the top-
776 down estimates made by TCR-2. According to GFAS, the average rate of CO biomass-burning emissions in China from 2015
777 to 2018 was about 3.4 Tg/yr. Yin et al. (2019), based on MODIS fire radiative energy data, also estimated China's CO biomass-
778 burning emissions to be about 5.0 (2.3–7.8) Tg/yr. The biogenic CO emissions obtained from the CAMS global emission
779 inventory were approximately 2.3 Tg/yr. According to these estimates, natural CO emissions in China have a magnitude of
780 about 10¹, which is rather small compared with anthropogenic sources, and cannot explain the large discrepancies between
781 CAQIEI and other inventories. Thus, ~~the CAQIEI suggest much higher anthropogenic CO emissions in China than the existing~~
782 ~~emission inventories there may be a large negative bias in current estimations of anthropogenic CO emissions in China.~~ In fact,
783 the potential underestimation of CO anthropogenic emissions has been ~~investigated~~ revealed in previous studies and is regarded
784 as the main reason for the negative bias in global or hemispheric CO simulations (Stein et al., 2014; Gaubert et al., 2020).
785 Regionally, Kong et al. (2020) compared a suite of 13 modeling results from six different CTMs—namely, NAQPMS, CMAQ,
786 WRF-Chem, NU-WRF, NHM-Chem and GEOS-Chem—with observations over the NCP and Pearl River Delta regions under
787 the framework of the Model Inter-Comparison Study for Asia III (MICS-Asia III), and found consistent negative biases in the
788 CO simulations of all models, pointing toward potential underestimations of CO emissions in China. Previous inversion studies
789 have also reported ~~a significant underestimation of higher a posteriori~~ CO emissions ~~than~~ their a priori emission inventories
790 (Bergamaschi et al., 2000; Miyazaki et al., 2012; Petron et al., 2002; Petron et al., 2004; Tang et al., 2013; Gaubert et al., 2020).
791 For example, the ~~constrained CO emissions inversion results~~ reported by Gaubert et al. (2020) are 80% higher than suggested

792 ~~that CEDS underestimates CO emissions by 80% over their~~ northern China. ~~Therefore, Our~~ inversion results are consistent
793 with ~~these previous inversion~~ studies, ~~suggesting higher which supports the point on the underestimation of~~ anthropogenic CO
794 emissions in China. However, direct evidence in support of such high CO emissions in China ~~reported by our study~~ is still
795 limited currently. Thus, we compiled more inversion results within the period of 2013–2020 from previous studies to further
796 validate our inversion results, which are summarized in Table 6. It can be clearly seen that there are large differences in the
797 estimated CO emissions between the inversion results based on surface observations and those based on satellite data. Our
798 inversion results are consistent with the results of Feng et al. (2020), with China's CO emissions in December 2017 estimated
799 at approximately 1500.0 kt/day and 1388.1 kt/day, respectively. In addition, Feng et al. (2020) used the CMAQ model to
800 constrain CO emissions, which is different from the model we used. This may indicate that the model uncertainty would not
801 significantly influence the inversion results of CO emissions. However, the top-down estimated CO emissions based on
802 satellite data (163.6–553.4 kt/day) are much lower than those based on surface observations, although they are all higher than
803 their *a priori* emissions. The lower CO emission estimations based on satellite data assimilation may be attributable to the
804 lower sensitivities of satellite data to surface concentrations, suggesting that the assimilation of satellite data alone may not be
805 adequate to correct the negative biases in the *a priori* emissions. This deficiency has also been revealed by Miyazaki et al.
806 (2020b), who found undercorrected surface CO emissions in the extratropics of the Northern Hemisphere in TCR-2. However,
807 the assimilation of surface observations can be influenced by the uncertainties in the modeled vertical mixing, which could
808 lead to the uncertainties in the inversed CO emissions based on surface observations. Therefore, the inversed CO emissions in
809 CAQIEI could be partly supported by previous inversion studies based on surface observations, but more evidence is still
810 needed to justify the magnitude of the inversed CO emissions. Besides anthropogenic sources, the chemical production of CO
811 via oxidation of methane (CH₄) and NMVOCs, as well as the CO sinks via the hydroxyl radical (OH) reaction, also influence
812 the simulation of CO (Stein et al., 2014; Gaubert et al., 2020; Müller et al., 2018). Due to the important role of OH in the
813 chemical production and sinks of CO, the inversion of CO emissions is sensitive to the modeled OH abundance and the
814 emissions of CH₄ and NMVOCs. According to the estimation of Müller et al. (2018), the magnitude of inversed CO emissions
815 in China could differ by more than 40% when different levels of OH concentrations are used in the model. Thus, the much
816 higher estimations of CO emissions in our inversion results may also be partly explained by the underestimation of CO
817 chemical production or the overestimation of the CO sink.

818 4.3.1.4 PM_{2.5}

819 In terms of PM_{2.5}, ~~the CAQIEI suggests about 20% higher emissions~~ than ABA-CAS, HTAPv3 and EDGARv6 ~~by about~~
820 ~~20%~~, and ~~by 47.7% higher~~ than MEIC on the national scale, ~~suggesting that anthropogenic, biomass-burning, and/or fine-dust~~
821 ~~emissions may be underestimated~~. Larger ~~discrepancies underestimations~~ mainly occur in the NE and NW regions, where
822 CAQIEI is about 27.2–114.9% and 83.2–143.2% higher than the previous inventories. The ~~differences in the~~
823 ~~estimated underestimated~~ PM_{2.5} emissions may be related to the ~~uncertainties underestimations in the of~~ biomass-burning or
824 anthropogenic sources in the NE region (Wu et al., 2020b), while in the NW region, ~~besides the possible underestimation of~~
825 ~~anthropogenic sources as seen from the other species,~~ the ~~errors in the underestimated~~ fine-dust emissions may also contribute
826 to the ~~differences underestimation in the estimated of~~ PM_{2.5} emissions there. The differences in the estimated PM_{2.5} emissions
827 are relatively smaller in the NCP and SE regions, ranging from –18.9% to 20.4%, ~~suggesting which shows~~ better agreement in
828 the estimated PM_{2.5} emissions over these two regions. ~~This confirms our inversion results and indicates lower uncertainty in~~
829 ~~the estimated PM_{2.5} emissions over the NCP and SE regions.~~ In the SW region, CAQIEI is closer to HTAPv3 and EDGARv6,
830 with their differences being about 6.3% and –9.5% respectively, and is higher than MEIC and ABA-CAS by 54.2% and 28.6%.
831 ~~suggesting higher uncertainty in the estimated PM_{2.5} emissions over there.~~

832 4.3.1.5 PM₁₀

833 For PM₁₀ emissions, it is difficult to directly compare CAQIEI with previous emission inventories since CAQIEI not only
834 contains anthropogenic and biomass-burning emissions, but also coarse-dust emissions. As a result, the estimated emissions
835 of PM₁₀ by CAQIEI are substantially higher than those by previous inventories, especially over the NW, Central and NE
836 regions (Fig. 11), which are the typical natural windblown dust-source regions in China (Zeng et al., 2020). Besides the
837 naturally windblown dust of arid desert regions (Prospero et al., 2002), large amounts of coarse-dust emissions also stem from
838 anthropogenic sources, including anthropogenic fugitive, combustion and industrial dust from urban sources (AFCID) (Philip
839 et al., 2017), and anthropogenic windblown dust from human-disturbed soils due to changes in land-use practices, deforestation
840 and agriculture (Tegen et al., 1996). Therefore, although the other regions are not typical natural windblown dust-source
841 regions in China, there are still high levels of coarse-dust emissions from anthropogenic sources there (also called “urban
842 dust”), ~~which may be the main reason for the large deviation in the estimated PM₁₀ emissions differences between CAQIEI~~
843 ~~and previous inventories over these regions may reflect the underestimated and/or the unconsidered urban dust in previous~~
844 ~~emission inventories. On the one hand, although AFCID is included in MEIC, ABaCAS, HTAPv3 and EDGARv6, it is~~
845 ~~difficult for current bottom-up emission inventories to completely represent fugitive sources (Philip et al., 2017). On the other~~
846 ~~hand, in addition, the anthropogenic windblown dust emissions has not been included in current bottom-up emission~~
847 ~~inventories, which is an important source of coarse dust in urban areas according to the estimations of Li et al. (2016) and~~
848 ~~another important contributor to, which is an important source of coarse dust in urban areas according to the estimations of Li~~
849 ~~et al. (2016) the differences between CAQIEI and previous emission inventories. Besides, similar to the situation with PM_{2.5}~~
850 ~~emissions, anthropogenic and biomass-burning emissions may also be underestimated for PM₁₀ emissions, which could partly~~
851 ~~explain the large differences between CAQIEI and previous inventories.~~

852 4.3.1.6 NMVOCs

853 For NMVOC emissions, since CAQIEI includes both anthropogenic and natural sources, its estimated NMVOC emissions
854 are much higher than those estimated by previous emission inventories. After consideration of natural sources, ~~the CAQIEI~~
855 ~~suggests close estimations of the NMVOC emissions agrees well with the MEIC, HTAPv3 and CEDS inventories on the~~
856 ~~national scale, with their differences being about 1.5–12.5%, which validates our inversion results and the estimated NMNOV~~
857 ~~emissions for these inventories. The estimated NMVOC emission by ABaCAS and EDGARv6 may have a negative bias in~~
858 ~~their estimated NMVOC emissions, which are slightly lower than CAQIEI by 17.8% and 24.6%, respectively. On the regional~~
859 ~~scale, the comparison of CAQIEI with previous inventories suggests that there may be higher NMVOC emissions over the~~
860 ~~northern China (NCP, NE and NW), with the top-down estimated NMVOC emissions are about 30.4–81.4%, 27.3–72.1%,~~
861 ~~79.3–116.8%, and 8.7–57.5% higher than those of the previous emission inventories over these regions. This suggests that~~
862 ~~NMVOC emissions may be underestimated in northern China, especially over the Central region. In contrast, the CAQIEI~~
863 ~~suggests lower NMVOC emissions over the SE region may be overestimated, with the estimated NMVOC emissions of~~
864 ~~CAQIEI being about 21.2–27.6% lower than those of MEIC, ABaCAS, HTAPv3 and CEDS. These results are consistent with~~
865 ~~the previous inversion results based on the satellite observations, which suggest higher NMVOC emissions over the NCP~~
866 ~~region and lower NMVOC emissions over the south China (Souri et al., 2020). Over the SW region, CAQIEI shows good~~
867 ~~agreement with MEIC, ABaCAS and CEDS, with CAQIEI being slightly lower than these inventories by 1.0–8.9%, but is~~
868 ~~lower than HTAPv3 and EDGARv6 by may overestimate the NMVOC emissions over the SW region, with their results being~~
869 ~~about 38.6% and 29.1%, respectively higher than those of CAQIEI. Again, it should be noted that the comparisons of NMVOC~~
870 ~~emission are conducted on the basis of natural emissions estimated by CAMS and GFAS, and could be more sensitive to the~~
871 ~~used natural sources than other species considering the larger contributions of the natural source to the NMVOC emissions.~~

872 4.3.2 Seasonality

873 Figure 12 presents the monthly profiles of different air pollutants obtained from different emission inventories. Note that
874 the natural sources have been added to the previous inventories to facilitate the comparisons. The results show that different
875 emission inventories give similar monthly profiles of NO_x and CO emissions, with higher emissions during wintertime and
876 lower emissions during summertime, which suggests relatively lower uncertainty in the estimated monthly profiles for these
877 two species. For SO₂ emissions, CAQIEI yields stronger monthly variation than the other inventories, with a higher proportion
878 from January to March and lower proportion during summertime. Due to the influences of dust emissions, the top-down
879 estimated PM_{2.5} and PM₁₀ emissions show higher proportions than the other emission inventories during the spring season,
880 especially for PM₁₀. However, the proportion of emissions during autumn and winter are lower than in the other inventories.
881 The monthly profiles of NMVOC emissions are generally consistent, with higher emissions during summer due to the enhanced
882 biogenic emissions. However, the profile of CAQIEI is flatter than the previous inventories, and suggests a higher proportion
883 during springtime. In addition, the timings of peak values of NMVOC emissions are also different between CAQIEI and the
884 previous inventories, with CAQIEI showing peak values during May–July but the other inventories suggesting peaks during
885 June–August.

886 4.3.3 Emission changes during 2015–2018

887 The top-down estimated emission changes of different air pollutants during 2015–2018 were also compared with previous
888 emission inventories, ~~the results of which are shown in Fig. 13.~~ Figure 13 shows the time series of the total emissions of
889 different species from 2013 to 2020 obtained from the CAQIEI and other emission inventories. Comparisons of the emission
890 changes over the regional scales are also presented in Fig. S10–S15. Before the comparison, we firstly analyze the trends of
891 natural sources in China to investigate their influences on the emission changes of different species based on the CAMS
892 emission inventory and GFAS. Note that we only consider the soil, biogenic and biomass-burning emissions for the natural
893 sources; the trends of dust emissions in China are not analyzed, which may lead to uncertainty when comparing the emission
894 changes of PM_{2.5} and PM₁₀. As shown in Fig. S167, the natural sources of NO_x and NMVOC emissions changed little during
895 2013–2018, ~~suggesting that the emission trends of these two species would be mainly driven by anthropogenic sources.~~ The
896 other species had small decreasing trends from 2013 to 2018. However, considering the small contributions of natural sources
897 to their emissions, these small trends would not significantly influence their emission trends. For the dust emissions, previous
898 studies have indicated a declining trend in dust activity in China from 2001 to 2020 (Wu et al., 2022; Wang et al., 2021), due
899 to weakened surface wind and increased vegetation cover and soil moisture. These results suggest that the emission trends in
900 the CAQIEI would be mainly driven by the anthropogenic sources for the gaseous air pollutants based on the estimations of
901 CAMS and GFAS, while Thus, its estimated emission trends of PM_{2.5} and PM₁₀ there would be influenced by the declining
902 trends in dust emissions in China, which should be noted when comparing the emission changes of PM_{2.5} and PM₁₀.

903 As shown in Fig. 143, all the emission inventories agree that the NO_x, SO₂, CO, PM_{2.5} and PM₁₀ emissions in China were
904 reduced from 2015 to 2018, except for the increases of CO emissions estimated by TCR-2, which confirms the effectiveness
905 of the emission control policies implemented during the clean air action plans. Meanwhile, most emission inventories agree
906 that SO₂ is the species with the largest emission reduction rates, followed by PM_{2.5}, indicating better emission mitigation
907 effects of these two species (Fig. 14). However, the CAQIEI suggested lower emission reduction rates than the other emission
908 inventories for most species emission reduction rates estimated by CAQIEI are generally lower than those estimated by
909 previous emission inventories, especially for NO_x, PM₁₀ and NMVOCs (Fig. 14), ~~which suggests that the mitigation effects of~~
910 ~~the air quality control during 2015–2018 may be overestimated by previous inventories.~~ The estimated emission reduction
911 rate of NO_x obtained from CAQIEI is about –2.7%, which is lower than the values of MEIC (–9.7%), ABaCAS (–23.0%),
912 HTAPv3 (–13.0%) and CEDS (–9.0%). ~~As we discussed in Sect. 4.2.2.2, the small reductions of NO_x emission in CAQIEI~~
913 ~~would be related to the increased vehicle emissions and the undesirable mitigation effects of the industry control. In fact, these~~

914 ~~factors have been considered in some bottom-up emission inventories, such as MEIC. The differences between our inversion~~
915 ~~results and previous inventories thus reflect uncertainty in the quantifications of the effects of these factors on the NO_x~~
916 ~~emissions due to the lack of sufficient statistics on mobile vehicle or other sectors. Our inversion results suggest larger adverse~~
917 ~~effects of these two factors on the reductions of NO_x emissions in China.~~ According to Fig. S178, the differences between
918 CAQIEI and these inventories mainly occur in the SE, SW, NW and Central regions, with the emission reduction rate estimated
919 by CAQIEI being substantially lower than those estimated by previous inventories. In particular, CAQIEI suggests increases
920 of NO_x emissions over the Central region, ~~which is opposite to the previous emission inventories which was not captured by~~
921 ~~previous inventories.~~ Better agreement is achieved over the NCP and NE regions, with the emission reduction rate estimated
922 by CAQIEI being closer to those of MEIC, HTAPv3 and CEDS, ~~suggesting lower uncertainty in the estimated NO_x emission~~
923 ~~reduction rate over these two regions.~~ The NO_x emission reduction rates estimated by EDGARv6 (-3.3%) and TCR-2 (-1.7%)
924 are closer to our results on the national scale, but they ~~underestimate the estimated lower~~ NO_x emission reduction rate ~~than our~~
925 ~~estimate~~ over the NCP and NE regions.

926 Similarly, the emission reduction rate of PM₁₀ obtained from CAQIEI (-10.8%) is ~~much~~ lower than those estimated by
927 MEIC (-27.9%), ABaCAS (-33.0%) and HTAPv3 (-27.8%) on the national scale (Fig. 143). A lower PM₁₀ emission reduction
928 rate of CAQIEI than these inventories also exists in the different regions of China, except SW (Fig. S178). In particular,
929 different from previous emission inventories, CAQIEI suggests that PM₁₀ emissions may have actually increased over the
930 Central region. Considering that dust emissions may have decreased from 2015 to 2018 owing to weakened dust events (Wang
931 et al., 2021), the increase in PM₁₀ emissions over the Central region may reflect the increases in anthropogenic sources.
932 Meanwhile, we also found that CAQIEI estimated the emission reduction rate of PM₁₀ to be smaller than that of PM_{2.5}. This is
933 different from previous emission inventories, which show similar emission reduction rates for PM_{2.5} and PM₁₀. Considering
934 that PM₁₀ emissions include PM_{2.5} and PM_{10-2.5} emissions, the lower emission reduction rate of PM₁₀ than PM_{2.5} in CAQIEI
935 suggests that PM_{10-2.5} emissions may have decreased slower than PM_{2.5} emissions from 2015 to 2018, ~~which was not captured by~~
936 ~~previous inventories.~~

937 In terms of NMVOCs, most previous inventories, including MEIC, EDGARv6 and CEDS, suggest a weak decrease in
938 China, with the estimated rates of change in emissions ranging from -0.8% to -4.6%. The emission reduction rate estimated
939 by ABaCAS is larger, reaching up to -14.2%. In contrast, ~~the~~ CAQIEI ~~suggests~~ ~~indicates~~ an opposite emission change to these
940 inventories, with estimated NMVOC emissions increasing by 26.6% from 2015 to 2018. HTAPv3 also suggests an increase in
941 NMVOC emissions, but with a much lower rate of increase (2.7%). Similar results could also be found on the regional scale
942 (Fig. S178), especially over the NCP, NE and Central regions, where NMVOC emissions could have increased by 38.0%,
943 38.3% and 60.0%, respectively, according to the estimates of CAQIEI. ~~As we discussed in Sect. 4.2.2.2, the increases of~~
944 ~~NMVOC emission estimated in CAQIEI may be related to the increased anthropogenic NMVOC emissions from the chemical~~
945 ~~industry, solvent use, and vehicles. Therefore, similar to the NO_x emissions, the differences between CAQIEI and previous~~
946 ~~inventories reflects the uncertainty in the quantifications of the impacts of these factors, and suggest larger adverse effects of~~
947 ~~these factors on the emission reductions of NMVOC emission than the previous inventories. However, none of the previous~~
948 ~~emission inventories captured this increasing trend over these regions. Considering that biogenic NMVOC emissions changed~~
949 ~~little from 2015 to 2018 according to the estimates of the CAMS inventory, the increases of NMVOC emissions possibly arise~~
950 ~~from the increased anthropogenic sources. This is consistent with the estimate of Li et al. (2019c), who found persistent growth~~
951 ~~of anthropogenic NMVOC emissions in China from 1900 to 2017. However, the drivers of the increased NMVOC emissions~~
952 ~~still need to be investigated, considering the uncertainty in the estimated trends of biogenic NMVOC emissions. Different from~~
953 ~~the CAMS inventory, Li et al. (2020a) found an increasing trend in biogenic emissions in China from 2008 to 2018, especially~~
954 ~~over northern China, which can partly explain the increased NMVOC emissions in China. Therefore, more analysis is needed~~
955 ~~to better understand the potential drivers of the increased NMVOC emissions in China.~~

956 The differences in the estimated emission reduction rates between CAQIEI and previous inventories are relatively smaller
957 for SO₂ and PM_{2.5} emissions, ~~suggesting lower uncertainty in the estimated emission reduction rates for these two species~~. The
958 emission reduction rate of SO₂ estimated by CAQIEI is close to that estimated by MEIC and CEDS, ranging from -34.7% to
959 -44.3%. ABA-CAS and HTAPv3 estimate a larger emission reduction rate of about -58.5% and -53.7%, respectively.
960 EDGARv6 and TCR-2 may ~~greatly~~ underestimate the reduction rate of SO₂, with estimates of only about -7.0% and -9.1%,
961 respectively. This may be because EDGARv6 underestimates the FGD (flue-gas desulfurization devices) penetration or SO₂
962 removal efficiencies of FGD in China. On the regional scale (Fig. S178), the top-down estimated SO₂ emission reduction rate
963 agrees reasonably with that of MEIC over the NCP, NE and SE regions, but these inventories estimate different SO₂ emission
964 reduction rates over the SW, NW, and Central regions. The reduction rates estimated by MEIC over the SW and Central
965 regions is higher than those given by CAQIEI, but lower over the NW region. The other emission inventories also give different
966 emission reduction rates. ~~This suggests there are large high levels of uncertainty in the estimated SO₂ emission reduction
967 rates over these three regions. For example, CEDS shows similar results to our estimate over the SW and Central regions,
968 while the rate given by HTAPv3 is closer to MEIC. This suggests there are high levels of uncertainty in the estimated SO₂
969 emission reduction rates over these three regions.~~ In terms of PM_{2.5}, CAQIEI's estimated emission reduction rate agrees well
970 with those of MEIC and HTAPv3 on the national scale, ~~which is suggesting that the emission reduction rate of PM_{2.5} in China
971 was~~ about 24–27% from 2015 to 2018. ~~The emission reduction rate of PM_{2.5} estimated by EDGARv6 are lower than our
972 estimates and other inventories, which were may underestimate the reduction rate of PM_{2.5}, at~~ about 9%. On the regional scale,
973 our results show good ~~consistency with consistency with~~ MEIC and HTAPv3 over the NCP, NE, SE and SW regions, but they
974 have large differences over the NW and SW regions, ~~indicating higher uncertainty in the estimated reduction rate over western
975 China.~~

976 Different from the other species, the CO emission reduction rate estimated by CAQIEI (-21.3%) is higher than in most
977 of the previous inventories, including MEIC (-13.0%), ABA-CAS (-11.6%), EDGARv6 (-4.7%), and CEDS (-11.7%),
978 suggesting ~~that the large~~ mitigation effects on CO emissions ~~may be underestimated by these than other~~ inventories. HTAPv3
979 agrees with our results, with an estimated emission reduction rate of about -22.0%. On the regional scale (Fig. S178), our
980 result is consistent with MEIC over the NCP and SE regions, with estimated emission reduction rates for CO of around 24%
981 and 15%, respectively, while in other regions the emission reduction rate estimated by CAQIEI is higher than that estimated
982 by MEIC. ~~The The larger emission reduction rate for CO in our results is supported by HTAPv3 over the NE, SW, NW and
983 Central regions, as well as by CEDS over the SW, NW and Central regions. This suggests that the emission reduction rates for
984 CO may be underestimated by MEIC over these regions.~~ TCR-2 shows opposite changes in CO emissions compared with the
985 other inventories insofar as it suggests increases of CO emissions over different regions of China. Since the emissions in TCR-
986 2 are constrained by satellite observations, the differences between our results and those of TCR-2 highlight that the
987 observations used to constrain the emissions may have a large influence on the estimated emission changes. In this case, the
988 assimilation of surface observations (our study) is shown to be superior to the assimilation of satellite observations (TCR-2),
989 as our results are more consistent with other bottom-up inventories.

990 4.4 Uncertainty estimation of CAQIEI

991 ~~Finally, the uncertainty of the inversed emission inventory product is estimated in this section to facilitate users'
992 understanding of the data's accuracy. Within the framework of EnKF, the analysis perturbation X^a estimated by using Eq. (3)
993 could provide the information regarding the uncertainty of the inversed emission inventory. The Coefficient of variation
994 (hereinafter, CV), defined as the standard deviation divided by the average, with a larger value denoting higher uncertainty, is
995 calculated based on the analysis perturbation to measure the uncertainty of the inverse emission inventory. Based on this
996 method, the uncertainty (CV) of the a posteriori emission was estimated as follows: 92.3% (PM_{2.5}), 88.8% (PM₁₀), 26.7%~~

997 (SO₂), 46.8% (CO), 31.8% (NO_x) and 65.5% (NMVOC). However, it should be noted that such uncertainty was only calculated
998 under the framework of the EnKF constructed in this study, which is dependent on the assigned value of the a priori emission
999 uncertainty, observation errors and the number of assimilated observations. In addition, we only considered the a priori
1000 emission uncertainty and the observation errors during the inversion. The influences of the other error sources, such as
1001 uncertainty in the chemistry transport model, meteorology simulations and the inversion method were not considered.
1002 Therefore, the current estimated uncertainty should be considered as a lower bound for the real uncertainty. More systematic
1003 analysis that thoroughly consider the uncertainty sources regarding the emission inversion should be conducted in future to
1004 give a more accurate estimation of the uncertainty in our products.

1005 5 Discussion and conclusion

1006 A long-term, top-down emissions inventory of major air pollutants in China was developed and validated in this study by
1007 assimilating surface observations from CNEMC using the modified EnKF method and NAQPMS. It includes gridded emission
1008 maps of NO_x, SO₂, CO, primary PM_{2.5}, primary PM₁₀, and NMVOCs in China from 2013 to 2020, on a monthly basis, with a
1009 horizontal resolution of 15 km × 15 km. This new top-down emissions inventory, named CAQIEI, provides new insights into
1010 the air pollutant emissions and their changes in China during the country's two clean air action periods, ~~which has not been~~
1011 ~~reported by previous inventories~~. The estimated total emissions for the year 2015 in China are 25.2 Tg of NO_x, 17.8 Tg of SO₂,
1012 465.4 Tg of CO, 15.0 Tg of PM_{2.5}, 40.1 Tg of PM₁₀ and 46.0 Tg of NMVOCs. ~~Comparisons of~~ Comparisons of CAQIEI with
1013 previous inventories, including MEIC, ABaCAS, HTAPv3, EDGARv6, CEDS and TCR-2, on the basis of the natural
1014 emissions obtained from CAMS and GFAS, ~~including MEIC, ABaCAS, HTAPv3, EDGARv6, CEDS and TCR-2~~, showed
1015 reasonable agreement for the estimation of NO_x, SO₂ and NMVOC emissions in China, ~~which confirms our inversion results~~
1016 ~~and suggests lower uncertainty in the estimated total emissions in China for these species.~~ The PM_{2.5} emissions obtained from
1017 CAQIEI (13.2 Tg) are slightly higher than in the previous emission inventories (8.3–11.1 Tg), ~~suggesting possible~~
1018 ~~underestimations of the anthropogenic, biomass-burning or fine dust emissions in current estimations, while~~. The CO
1019 emissions estimated by CAQIEI (426.8 Tg) are substantially higher than in previous inventories (120.7–237.7 Tg). ~~However,~~
1020 ~~the reasons for such a large gap are still not clear indicating that CO emissions may be greatly underestimated currently.~~
1021 ~~Although previous model simulation and inversion studies generally support the underestimation of CO emissions in China,~~
1022 ~~the reasons for such a large underestimation are still not clear~~, but might be attributable to both the underestimation of CO
1023 sources (e.g., anthropogenic, biomass-burning and chemical-production sources) according to previous model simulation and
1024 inversion studies (Bergamaschi et al., 2000; Miyazaki et al., 2012; Petron et al., 2002; Petron et al., 2004; Tang et al., 2013;
1025 Gaubert et al., 2020), e.g., anthropogenic, biomass-burning and chemical-production sources, and/or the overestimation of CO
1026 sinks in the model (Müller et al., 2018). In addition, comparisons with previous inversion studies suggest there are larger
1027 differences in the top-down estimated CO emissions based on surface and satellite observations. Our inversion results are
1028 consistent with previous inversions based on surface observations, but are much higher than those based on satellite
1029 observations, suggesting large uncertainty in inversion-estimated CO emissions in China. Therefore, more research is needed
1030 to better understand the reasons behind the negative biases in CO simulation, and to explain the differences between our results
1031 and those of previous inventories. Similar to situation with CO emissions, the PM₁₀ emissions estimated by CAQIEI (37.7 Tg)
1032 are also substantially higher than in previous inventories (11.1–15.9 Tg). However, this will be mainly associated with the
1033 emissions of coarse dust, which were not included in previous inventories. The estimation of dust emissions in China is subject
1034 to high levels of uncertainty, with the estimated dust fluxes based on different dust emission schemes differing by several
1035 orders of magnitude (Zeng et al., 2020). Therefore, our inversion results could provide a reference for the magnitude of coarse-
1036 dust emissions in China, which could then help to reduce the large uncertainty in estimations of dust emissions in China.

1037 Several potential important deficiencies in current emission estimations were also ~~revealed~~ ~~indicated~~ by CAQIEI on the
1038 regional scale. For example, ~~the CAQIEI suggests substantially higher there are significant negative biases in the estimated~~ ~~air~~
1039 ~~pollutant emissions than the previous emission inventories~~ over the NW and Central regions, ~~suggesting that the air pollutant~~
1040 ~~emissions in western China may be greatly underestimated by current emission inventories. As a result~~ ~~Thus, the significant~~ air
1041 pollutant issues may be ~~more severe than we expected~~ ~~neglected~~ over these two regions, ~~which may have led to serious adverse~~
1042 ~~impacts in terms of human health and ecosystems~~. Meanwhile, ~~our inversion results suggest higher~~ NMVOC emissions ~~are~~
1043 ~~shown to be substantially underestimated~~ over ~~the~~ northern China but ~~suggest lower NMVOC emissions overestimated~~ in
1044 southern China, ~~which is consistent with the previous inversion studies based on the satellite~~. China is now facing increasingly
1045 severe O₃ pollution and has an urgent need for a coordinated control of O₃ and PM_{2.5}. Our results ~~shed new light on the nature~~
1046 ~~of~~ ~~may provide valuable information on the~~ NMVOC emissions in China, which is important for a proper understanding of O₃
1047 pollution and the development of effective control strategies nationally. ~~Higher emissions~~ ~~Consistent negative biases~~ were also
1048 ~~found~~ ~~identified~~ in the NE region ~~for the emissions of all species based on our inversion results~~. The NE region is a typical area
1049 for open-area biomass burning, with significant emissions from straw combustion (Wu et al., 2020b). The ~~higher emissions~~
1050 ~~estimated by our inversion result may indicate higher underestimation of emissions there may reflect the underestimation of~~
1051 biomass-burning emissions ~~over there~~. This is consistent with recent estimations of biomass-burning emissions by Xu et al.
1052 (2023) and Wu et al. (2020b), who showed higher biomass-burning emissions in China than previous estimations, including
1053 those of GFEDv4.1s (<https://www.globalfiredata.org/data.html>), FINNv1.5 (<https://www.acom.ucar.edu/Data/fire/>), and
1054 GFASv1.2 (<https://www.ecmwf.int/en/forecasts/dataset/global-fire-assimilation-system>).

1055 Based on CAQIEI, we further quantified the emission changes of different air pollutants in China during the two clean
1056 air action plans. The results confirmed the effectiveness of these campaigns on the mitigation of air pollutant emissions in
1057 China, with estimated emission reductions of 15.1% for NO_x, 54.5% for SO₂, 35.7% for CO, 44.4% for PM_{2.5}, and 33.6% for
1058 PM₁₀ from 2015 to 2020. In contrast, NMVOC emissions increased by 21.0% from 2015 to 2020. Comparisons of the estimated
1059 emission reduction rates during the two clean air action plans suggested that emission reductions were larger during the 2018–
1060 2020 ~~action plan~~ than during ~~the 2015–2017~~ ~~action plan~~. The estimated rates of change in emissions were 5.9% for NO_x,
1061 –23.8% for SO₂, –9.8% for CO, –14.5% for PM_{2.5}, –7.2% for PM₁₀, and 27.6% for NMVOCs during ~~the 2015–2017~~ ~~action~~
1062 ~~plan~~, which were smaller than the –12.1% for NO_x, –23.5% for SO₂, –18.3% for CO, –26.6% for PM_{2.5}, –25.5% for PM₁₀,
1063 and –4.5% for NMVOCs during ~~the 2018–2020~~ ~~action plan~~. On the one hand, this is due to the fact that more sectors were
1064 controlled during the 2018–2020 action plan. Besides the industrial and power sectors, which were the main points of control
1065 in the 2013–2017 action plan, the residential sector, transportation sector, and non-point sources like blowing-dust emissions,
1066 were also strengthened in the 2018–2020 action plan. Consequently, the emission reduction rates of CO, PM_{2.5} and PM₁₀ during
1067 ~~the 2018–2020~~ ~~action plan~~ were higher than those during the 2015–2017 ~~when the 2013–2017~~ ~~20~~ action plan ~~was implemented~~.
1068 However, the reduction of SO₂ emissions was similar during the two action plan periods. This is because most SO₂ emissions
1069 stem from the industrial sector and power plants, which together contribute about 77% of all emissions (Zheng et al., 2018).
1070 Thus, the additional control of other sectors in the 2018–2020 action plan may not have ~~significant~~ ~~significantly~~ impacted the
1071 mitigation of SO₂ emissions. On the other hand, strict emission controls were implemented or strengthened in more areas of
1072 China during the 2018–2020 action plans. For example, the inversion results indicated that there were obvious increases of
1073 SO₂, NO_x, PM_{2.5}, PM₁₀ and NMVOC emissions during ~~the 2015–2017~~ ~~action plan~~ over the Central region, especially in the
1074 Fengwei Plain area, where the emission controls were relatively weak during the 2013–2017 action plan. However, all species
1075 showed obvious emission reductions ~~almost the whole China over the Fengwei Plain area, and almost the whole of China,~~
1076 during the 2018–2020 action plan.

1077 The estimated rates of change in emissions during 2015–2018 were also compared with those estimated by previous
1078 emission inventories. Although both CAQIEI and previous inventories showed declines of air pollutant emissions in China,
1079 the emission reduction rates estimated by CAQIEI were generally smaller than those estimated by previous inventories,

1080 especially for NO_x, PM₁₀ and NMVOCs, suggesting ~~a smaller~~ mitigation effects of the air pollution control measures
1081 ~~than the previous emission inventories suggested~~ may be overestimated currently. In particular, China's NMVOC emissions
1082 were shown to have increased by 26.6% from 2015 to 2018, especially over NCP (38.0%), NE (38.3%) and Central (60.0%),
1083 ~~which was not captured by all previous inventories. The potential overestimation of the NO_x emission reduction rate was~~
1084 ~~mainly a feature of the SE, SW, NW and Central regions; however, over the NCP and NE regions, our results agreed well with~~
1085 ~~those of MEIC, HTAPv3 and CEDS, suggesting smaller uncertainty in the estimated reduction of NO_x emissions over these~~
1086 ~~two regions. The potential overestimation of the PM₁₀ emission reduction rate was a feature in most regions of China, possibly~~
1087 ~~related to the smaller reduction rate of the country's PM emissions.~~ CO was found to be an exception insofar as the emission
1088 reduction rate estimated by CAQIEI was larger than that of most previous emission inventories, ~~suggesting that the mitigation~~
1089 ~~effects of CO emission control measures may be underestimated~~, except in the NCP region. The estimated emission reduction
1090 rates of SO₂ and PM_{2.5} were relatively closer to those of previous inventories, suggesting better consistency ~~relatively lower~~
1091 ~~uncertainty~~ in the estimated ~~pace of~~ emission reduction for these two species.

1092 Overall, the inversion inventory developed in this study ~~sheds new light~~ could provide us with value information on the
1093 complex variations of air pollutant emissions in China during its two recent clean air action periods, which could
1094 significantly help improve our understanding of air pollutant emissions and related changes in air quality in China. For example,
1095 the increases of O₃ and nitrate concentrations may be associated with the undesirable emission reduction effects of the 2013–
1096 2017 action plans. The ~~estimated lower possible overestimation of the~~ NO_x emission reduction rate by ~~previous~~
1097 ~~inventories~~ CAQIEI may also help explain the weak responses of nitrogen deposition fluxes to the clean air action plans.
1098 Meanwhile, this top-down emissions inventory can be used to supply the input data for CTMs or serve as a comparable
1099 reference for future inversion studies based on other methods or observation data, which is expected to improve the
1100 performance of model simulations and air quality forecasts, and facilitate the development of inversion method.

1101 6 Limitations

1102 ~~However, due to the complexity of the emission estimation, it is inevitable that there are some limitations in our inversion~~
1103 ~~results. Here We summarise some issues that might affect the quality of the CAQIEI which were known at the time of~~
1104 ~~publication to assist the potential users in properly using this data products. However, there are some limitations to our~~
1105 ~~inventory that potential users should be aware of.~~

1106 ~~(1) Firstly, T~~ the changes in the number of observation sites ~~may have would~~ induced spurious emission trends during
1107 2013–2014, especially over western China, although the influence of the number of observation sites is smaller over the NCP
1108 and SE regions because of their higher density of observation sites. ~~Therefore, it is recommended that not to use the emissions~~
1109 ~~in 2013 and 2014 when analyzing the emission trends in China. This limitation makes it difficult to estimate the overall~~
1110 ~~emission control effects of 2013 – 2017 action plan. Consequently, the emission change rate during the 2015–2017 were~~
1111 ~~sampled in this study to represent the emission control effects of the 2013–2017 action plan, but it may not necessarily reflect~~
1112 ~~the overall reduction rate of the action plan for the entire period.~~ In addition, although the number of observation sites has
1113 become stable since 2015, the limited number of observation sites makes it difficult to fully constrain China's air pollutant
1114 emissions, especially for the natural sources considering that the majority of the observation sites are located in the urban
1115 areas with respect to natural sources in remote areas ~~Therefore, the uncertainty in the estimated emissions over the remote~~
1116 ~~areas are expected to be higher than those over the urban areas, especially for the species with large amount of natural emission,~~
1117 ~~such as PM and NMVOC.~~ For example, the coarse-dust emissions over western China are expected to be underestimated by
1118 CAQIEI because of the limited availability of observation sites. ~~Therefore, adding observations there will help improve the~~
1119 accuracy of the inversion estimates.

1120 (2) Secondly, The natural and anthropogenic emissions are not differentiated in our inversion method, leading to higher
1121 emissions of PM₁₀ and NMVOCs than in other emission inventories. This also hinders the comparisons of our inversion results
1122 with the previous inventories. Therefore, potential readers should be aware of that the current comparisons of our inversion
1123 results and previous inventories are on the basis of the natural emissions estimated by CAMS and GFAS, which does not
1124 necessarily indicate large uncertainties in anthropogenic sources within the bottom-up inventories. The impacts are expected
1125 to be smaller for the NO_x, SO₂ and CO due to the small contributions of natural sources to their emission, but would be larger
1126 for NMVOC and PM which has large amount of natural emission. Consequently, the estimated changes in emissions of
1127 different air pollutants are also influenced by natural emissions, which should be considered in the comparisons of our inversion
1128 results with those of previous emission inventories. Assimilation of isotope data, speciated PM_{2.5} and NMVOC observations
1129 may help differentiate the natural and anthropogenic emissions, and address this problem in future.

1130 (3) The NMVOC emissions may have larger uncertainty than the other species. On the one hand, a significant amount of
1131 NMVOC emission would originate from suburban or rural regions. Therefore, although the O₃ observations at the urban sites
1132 could provide information on the NMVOC emissions over the suburban or rural areas according to covariance estimated by
1133 the ensemble simulation, the NMVOC emissions may not be fully constrained due to the lack of observation sites over the
1134 suburban or rural areas. On the other hand, due to the lack of long-term NMVOC observations, the NMVOC emissions were
1135 constrained by the O₃ concentrations in this study. Although the feasibility of this approach has been demonstrated by previous
1136 inversion studies, the nonlinear NO_x-VOC-O₃ interactions could inevitably introduces greater uncertainty into the inversion of
1137 NMVOC than other species. Therefore, more attention should be paid while using the inversion results of NMVOC, and more
1138 robust analysis of the effects of nonlinear NO_x-VOC-O₃ interactions and the number of observation sites should be performed
1139 in future to better illustrate the feasibility of assimilating O₃ to constrain the NMVOC emissions.

1140 (4) Thirdly, The errors in the meteorological simulation and the CTMs were not considered in the emission inversions,
1141 which would leading to uncertainty in our estimated emissions. However, it is difficult to consider the meteorological and
1142 model errors in the assimilation process. A multi-model inversion framework, for example that of Miyazaki et al. (2020a),
1143 may help alleviate the influences of model errors on emission inversions in future. Meanwhile, Using other models (e.g., WRF-
1144 Chem, CMAQ) to validate our inversion inventory could also help us assess the impacts of model uncertainty on the emission
1145 inversions. Meanwhile, because of the many uses that require a rapid update of emissions, it may be time to organize an
1146 intercomparison study focused on the emission inversions.

1148 **76 data availability**

1149 The CAQIEI inventory can be freely download at <https://doi.org/10.57760/sciencedb.13151> (Kong et al., 2023), which
1150 includes monthly grid maps of the air pollutant emissions from 2013 to 2020. The contained species include NO_x, SO₂, CO,
1151 primary PM_{2.5}, primary PM₁₀ and NMVOC. The horizontal resolution is 15km. There are totally 8 Network Common Data
1152 Form files (NetCDF), which were named by the date and contains the monthly emissions of different air pollutants in China
1153 in each year. The description of the content of each NetCDF file and some important notes when using this dataset are also
1154 available in README.txt on the website.

1161
1162
1163
1164
1165
1166
1167
1168
1169
1170

1171 **Tables**

1172 **Table 1. Corresponding relationships between the chemical observations and adjusted emissions**

Species	Description	Observations used for inversions of this species
BC	Black carbon	PM _{2.5}
OC	Organic carbon	PM _{2.5}
PMF	Fine-mode unspciated aerosol	PM _{2.5}
PMC	Coarse-mode unspciated aerosol	PM ₁₀ – PM _{2.5}
NO _x	Nitrogen oxide	NO ₂
SO ₂	Sulfur dioxide	SO ₂
CO	Carbon monoxide	CO
NMVOCs	Non-methane volatile organic compounds	MDA8h O ₃

1173
1174
1175
1176
1177
1178
1179
1180
1181
1182
1183
1184
1185
1186
1187
1188
1189
1190

1191
 1192
 1193
 1194
 1195
 1196
 1197
 1198
 1199
 1200
 1201
 1202

Table 2. Evaluation statistics of the *a posteriori* (*a priori*) model simulation for different species

	PM _{2.5} (µg/m ³)				PM ₁₀ (µg/m ³)			
	R	MBE	NMB (%)	RMSE	R	MBE	NMB (%)	RMSE
Hourly	0.77 (0.53)	2.1 (13.3)	4.5 (28.6)	32.4 (55.6)	0.72 (0.44)	-3.7 (-11.5)	-4.6 (-14.3)	53.1 (74.4)
Daily	0.89 (0.61)	2.1 (13.3)	4.4 (28.4)	20.0 (46.3)	0.88 (0.51)	-3.7 (-11.2)	-4.6 (-14.1)	31.6 (62.2)
Monthly	0.94 (0.68)	2.1 (13.3)	4.5 (28.3)	11.7 (32.5)	0.90 (0.56)	-3.6 (-11.3)	-4.5 (-14.1)	21.2 (44.1)
Yearly	0.94 (0.62)	2.2 (11.9)	4.4 (24.3)	9.1 (27.7)	0.89 (0.52)	-3.8 (-13.4)	-4.6 (-16.1)	18.5 (38.7)
	SO ₂ (µg/m ³)				NO ₂ (µg/m ³)			
	R	MBE	NMB (%)	RMSE	R	MBE	NMB (%)	RMSE
Hourly	0.64 (0.16)	-1.8 (19.0)	-9.1 (93.8)	24.9 (58.7)	0.67 (0.45)	-1.2 (-0.9)	-3.9 (-2.7)	19.9 (25.5)
Daily	0.80 (0.20)	-1.8 (19.0)	-9.2 (94.5)	16.0 (51.4)	0.80 (0.51)	-1.2 (-0.8)	-3.7 (-2.6)	12.8 (20.1)
Monthly	0.85 (0.20)	-1.9 (18.9)	-9.3 (93.1)	12.4 (45.8)	0.84 (0.57)	-1.2 (-0.8)	-3.8 (-2.6)	9.4 (15.6)
Yearly	0.83 (0.18)	-2.4 (17.0)	-10.8 (75.9)	11.6 (42.4)	0.82 (0.63)	-1.3 (-1.6)	-3.9 (-5.0)	8.1 (13.0)
	CO (mg/m ³)				O ₃ (µg/m ³)			
	R	MBE	NMB (%)	RMSE	R	MBE	NMB (%)	RMSE
Hourly	0.69 (0.38)	-0.1 (-0.4)	-8.8 (-45.6)	0.6 (0.8)	0.71 (0.51)	5.6 (-8.4)	9.5 (-14.0)	34.9 (41.6)
Daily	0.81 (0.42)	-0.1 (-0.4)	-8.6 (-45.5)	0.4 (0.7)	0.71 (0.40)	5.7 (-8.4)	9.5 (-14.1)	26.1 (33.8)
Monthly	0.83 (0.42)	-0.1 (-0.4)	-8.7 (-45.7)	0.3 (0.7)	0.76 (0.47)	5.6 (-8.4)	9.4 (-14.1)	19.6 (26.0)
Yearly	0.82 (0.27)	-0.1 (-0.5)	-9.0 (-47.6)	0.3 (0.7)	0.53 (0.11)	5.1 (-7.8)	8.7 (-13.4)	14.2 (20.5)

1203
 1204
 1205
 1206
 1207
 1208
 1209
 1210

1211
1212
1213
1214
1215
1216
1217
1218
1219
1220
1221

1222 **Table 3. Inversion-estimated emissions (Tg/yr) of different species in China as well as the six regions for year 2015**

	China	NCP	SE	NE	SW	NW	Central
NO _x	25.2	5.1	7.1	4.5	4.2	1.2	3.2
SO ₂	17.8	3.5	3.3	4.0	2.6	0.8	3.6
CO	465.4	82.2	106.7	78.7	82.8	32.6	82.3
PM _{2.5}	14.9	2.7	3.3	3.1	2.9	1.2	1.9
PM ₁₀	40.1	8.7	7.5	8.2	5.5	4.1	6.2
NM VOC	46.0	9.0	13.7	8.5	7.8	2.7	4.2

1223
1224
1225
1226
1227
1228
1229

Table 4. The calculated annual trends of PM_{2.5} and PM₁₀ emissions in China based on CAQIEI

	PM _{2.5} (Tg/year)			PM ₁₀ (Tg/year)		
	2015–2020	2015–2017	2018–2020	2015–2020	2015–2017	2018–2020
China	-1.4*	-1.1	-1.5	-2.6*	-1.4	-4.6
NCP	-0.32*	-0.30	-0.32	-0.64*	-0.88	-0.99
SE	-0.32*	-0.21	-0.44	-0.52*	-0.48	-0.84
NE	-0.24*	-0.25	-0.11	-0.52*	-0.22	-0.73
SW	-0.21*	-0.26	-0.20	-0.40*	-0.26	-0.56
NW	-0.09	-0.08	-0.12	-0.20*	-0.32	-0.32
Central	-0.15	0.01	-0.32	-0.27	-0.32	-1.14

* Trend is significant at the 0.05 significance level

1230
1231
1232
1233
1234
1235
1236
1237

1238
1239
1240
1241
1242
1243
1244
1245
1246
1247
1248
1249

Table 5. The calculated annual trends of the four gaseous emissions in China based on CAQIEI

	SO ₂ (Tg/year)			CO (Tg/year)		
	2015–2020	2015–2017	2018–2020	2015–2020	2015–2017	2018–2020
China	-2.1*	-2.1	-1.3	-36.0*	-22.8	-33.5
NCP	-0.57*	-0.69	-0.21	-8.4*	-4.30	-7.23
SE	-0.34*	-0.39	-0.20	-6.1*	-3.54	-8.37
NE	-0.44*	-0.44	-0.21	-6.2*	-1.74	-3.91
SW	-0.22*	-0.27	-0.17	-3.8*	-2.36	-4.54
NW	-0.08*	-0.08	-0.08	-3.0*	-0.73	-2.95
Central	-0.46*	-0.25	-0.40	-8.7*	-10.14	-6.55
	NO _x (Tg/year)			NMVOC (Tg/year)		
	2015–2020	2015–2017	2018–2020	2015–2020	2015–2017	2018–2020
China	-0.67	0.74	-1.6	1.9	6.3	-1.3
NCP	-0.32	0.05	-0.40	0.66	1.37	-0.42
SE	-0.22	0.18	-0.49	0.50	1.73	-0.24
NE	-0.17	0.03	-0.19	0.03	0.79	-0.49
SW	-0.06	0.10	-0.26	0.23*	0.43	0.03
NW	-0.03	0.11	-0.06	0.10	0.69	-0.27
Central	0.04	0.28	-0.16	0.55*	1.33	0.09

* Trend is significant at the 0.05 significance level

1250
1251
1252
1253
1254
1255
1256
1257
1258
1259
1260
1261
1262

1263
1264
1265
1266
1267
1268
1269
1270
1271
1272
1273
1274

Table 6 The top-down estimated CO emissions in China from previous inventories

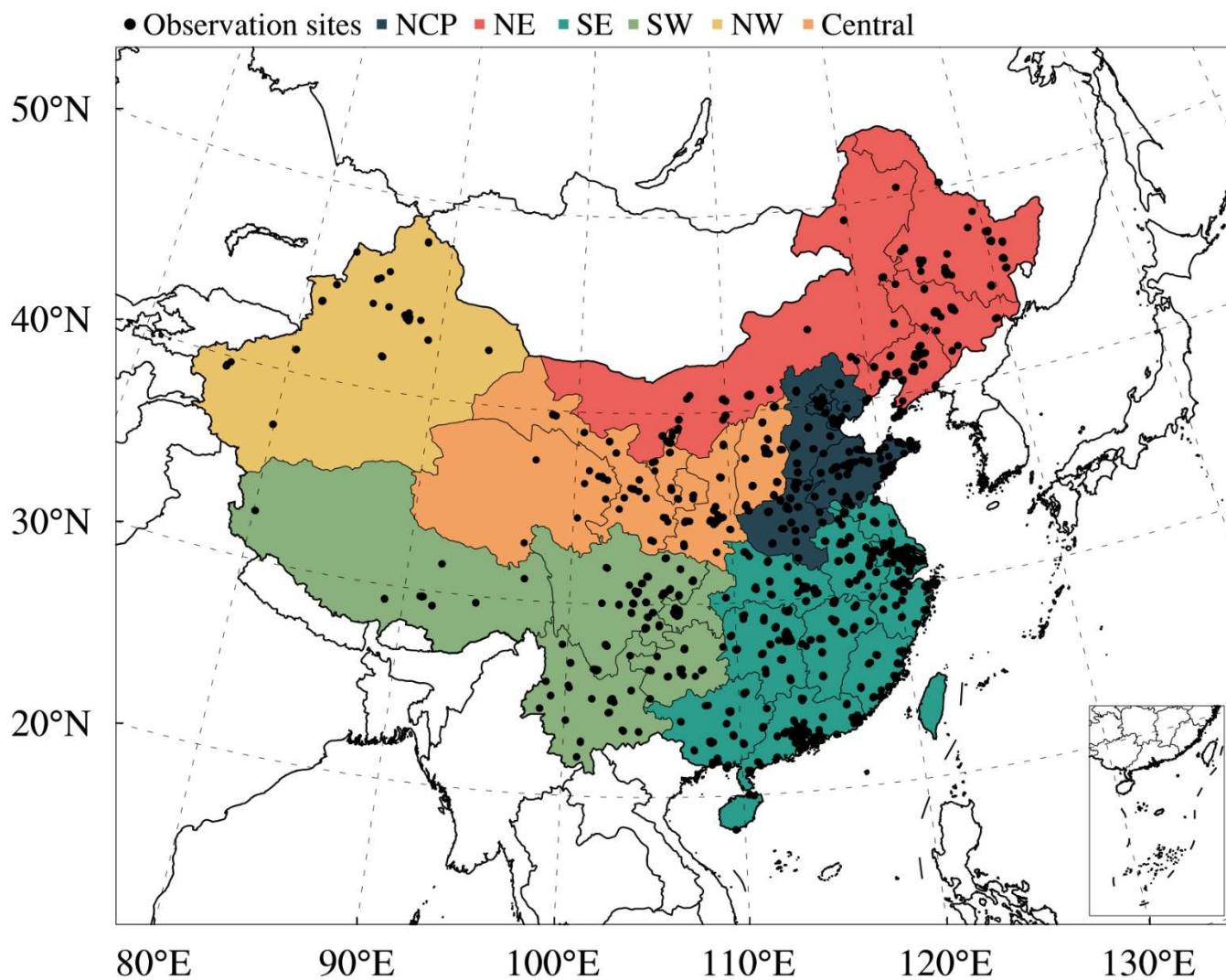
Reference	Region	Period	Method	Assimilated observation	<i>A priori</i> CO emission (kt/day)	<i>A posteriori</i> CO emission (kt/day)
Feng et al. (2020)	China	December 2013			586.4	1678.0
	Mainland	December 2017	EnKF with	Surface	499.3	1388.1
	NCP	December 2013	CMAQ model	observation	143.9	394.3
		December 2017			120.5	340.7
Muller et al. (2018)	China	2013	4DVar with IMAGES model	IASI CO observation with different constraints on OH levels	454.8	367.1–553.4
Gaubert et al. (2020)	Central China	May 2016	DART/CAM-CHEM	MOPITT CO observation	193.6	220.3
	North China				93.5	163.6
Jiang et al. (2017)	East China	2013	4DVar with GEOS-Chem	MOPITT CO observation	564.5	439.5–484.4
		2014				430.4–481.1
		2015				397.5–439.7
Zheng et al. (2019)	China	2010–2017 average	Bayesian inversion	MOPITT CO, OMI HCHO, and GOSAT CH ₄ observation	-	444.4

1275
1276
1277
1278
1279
1280
1281

1282
1283
1284
1285
1286
1287
1288
1289
1290

1291 **Figures**

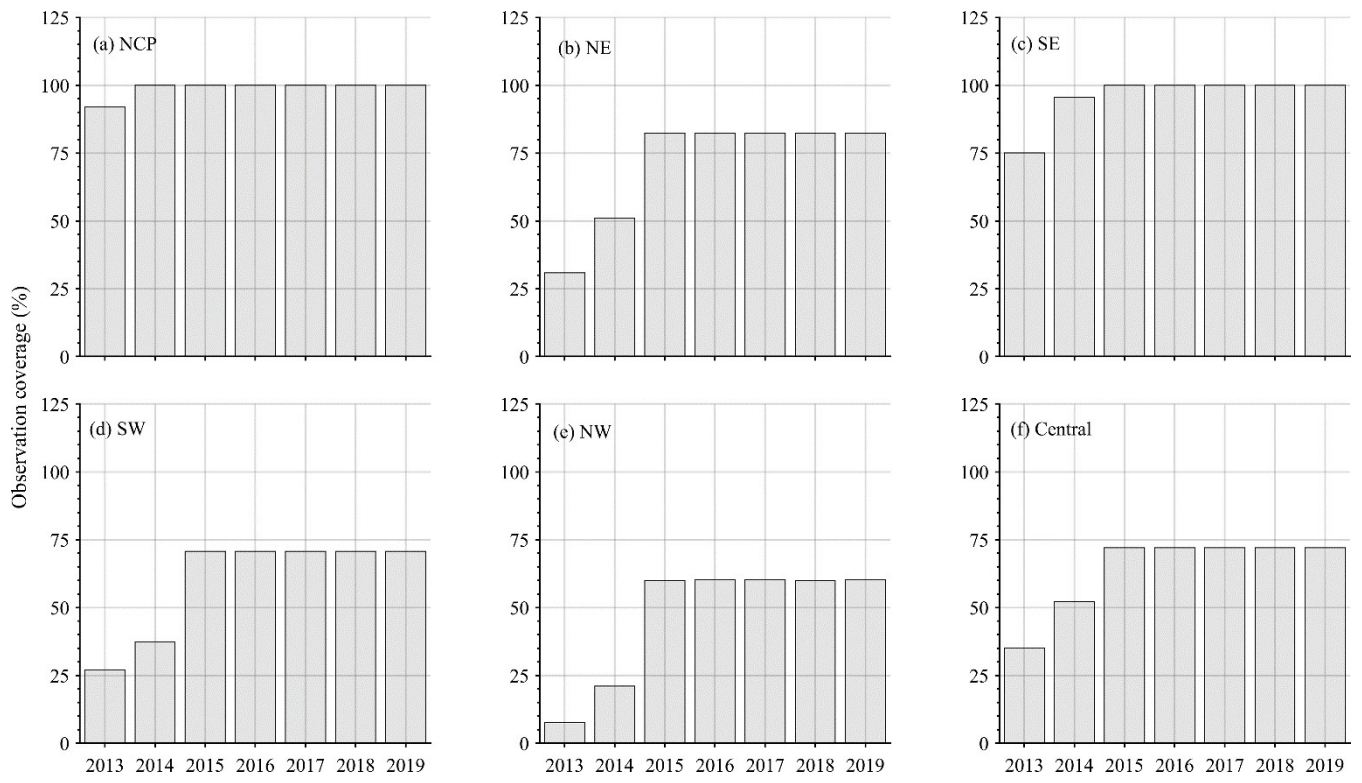
1292



1293

1294 **Figure 1: Modeling domain of the ensemble simulation overlaid with the distributions of observation sites from CNEMC. Different**
1295 **colors denote the different regions in mainland China—namely, the North China Plain (NCP), Northeast China (NE), Southwest**
1296 **China (SW), Southeast China (SE), Northwest China (NW) and Central China (Central).**

1297



1298

1299 **Figure 2: Time series of the observational coverage from 2013 to 2020 over different regions of China.**

1300

1301

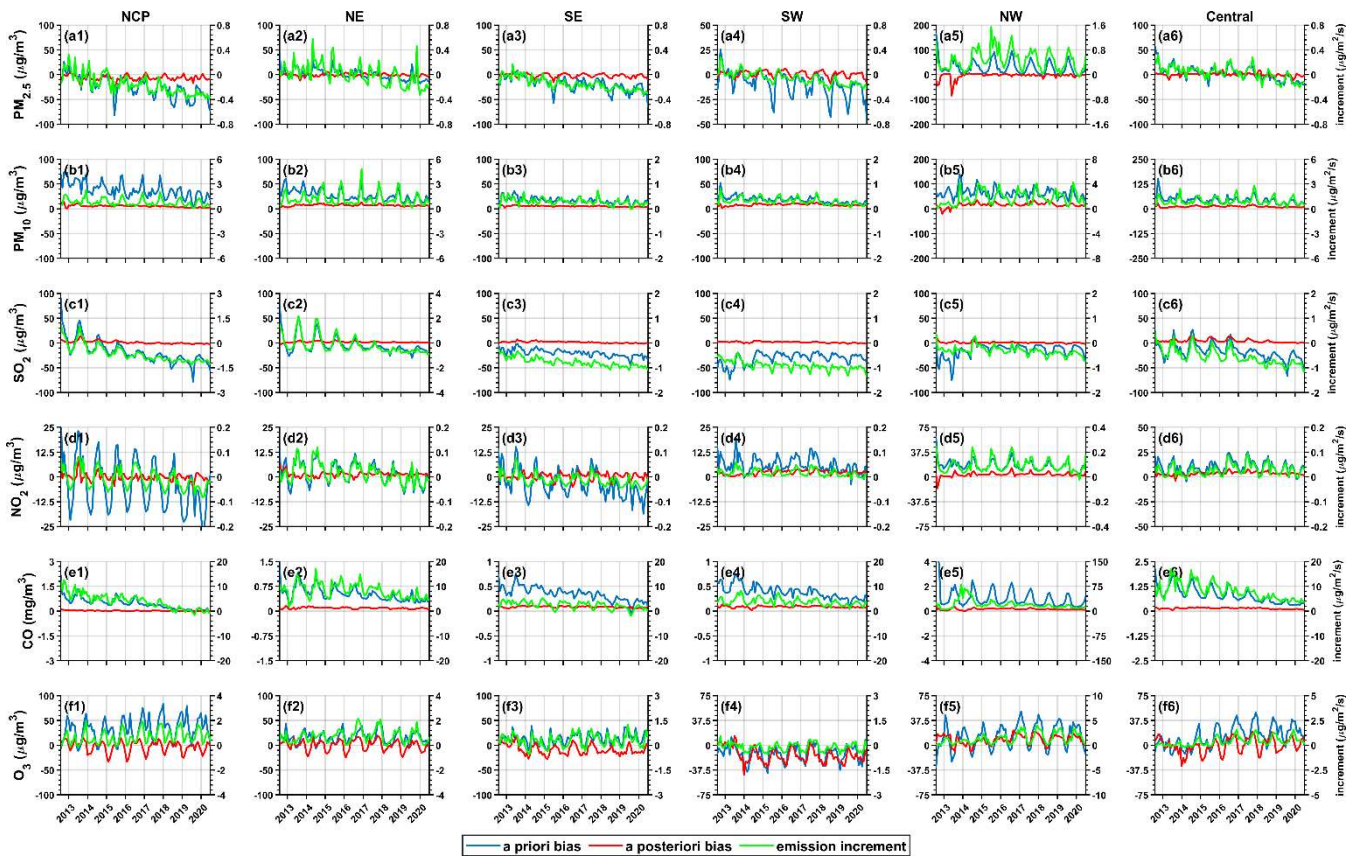
1302

1303

1304

1305

1306



1307

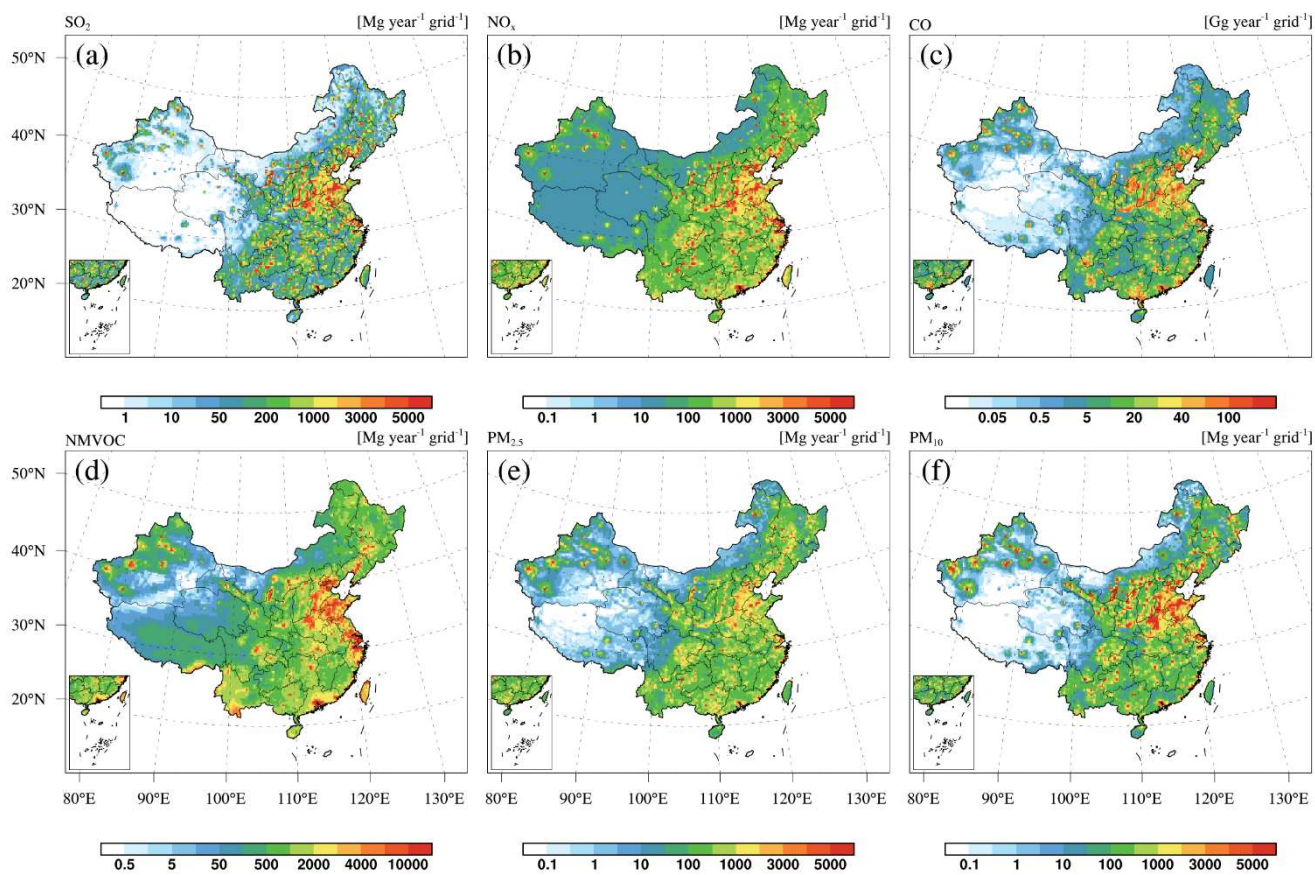
1308

1309

Figure 3: Time series of the *a priori* bias (blue lines), the *a posteriori* bias (red lines), and the emission increment (green lines) from 2013 to 2020 for different species over the six regions of China.

1310

1311



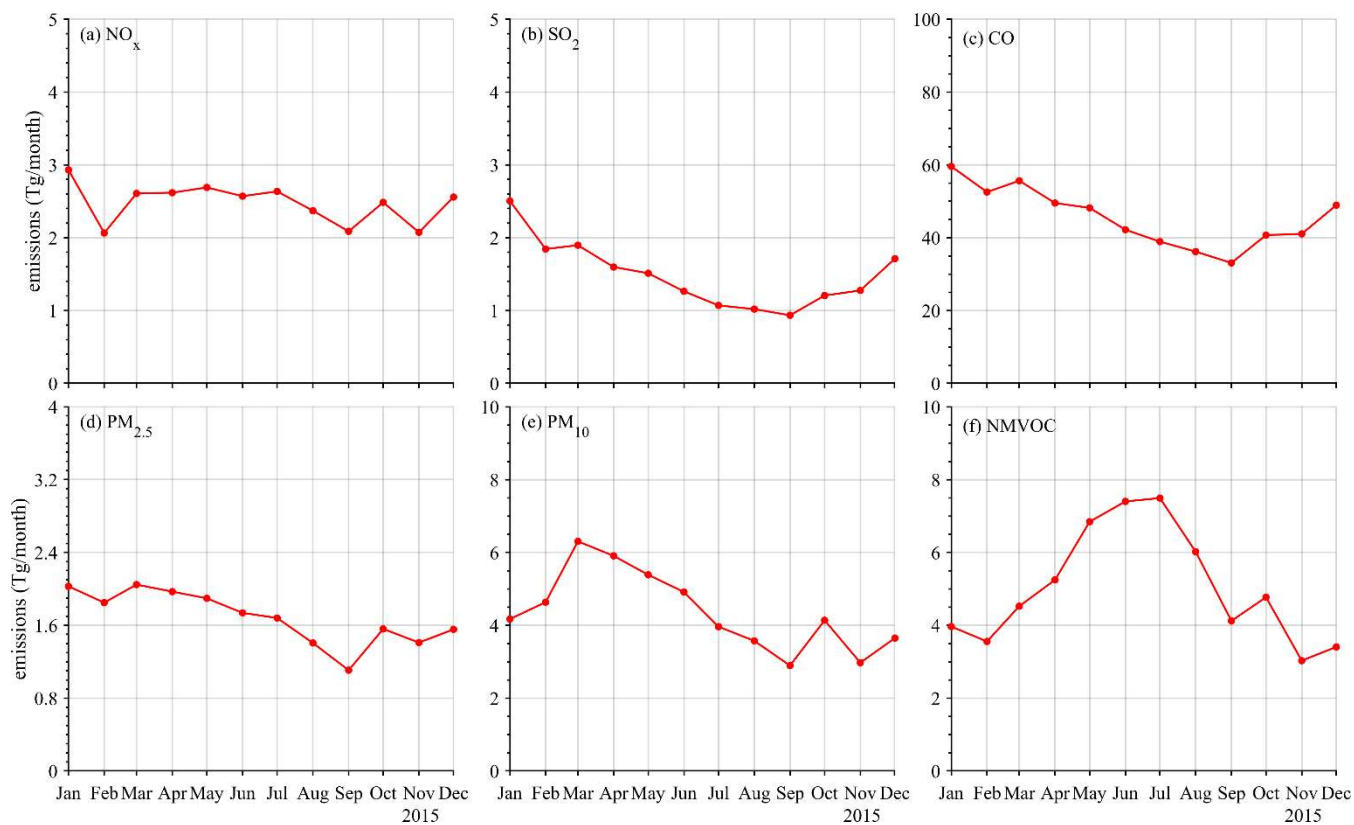
1312

1313 **Figure 4: Spatial distributions of the emissions of (a) SO_2 , (b) NO_x , (c) CO, (d) NMVOCs, (e) $\text{PM}_{2.5}$, and (f) PM_{10} in 2015 obtained**
 1314 **from CAQIEI.**

1315

1316

1317



1318

1319 **Figure 5: Monthly series of emissions of (a) NO_x, (b) SO₂, (c) CO, (d) PM_{2.5}, (e) PM₁₀, and (f) NMVOCs in 2015 obtained from**
 1320 **CAQIEL.**

1321

1322

1323

1324

1325

1326

1327

1328

1329

1330

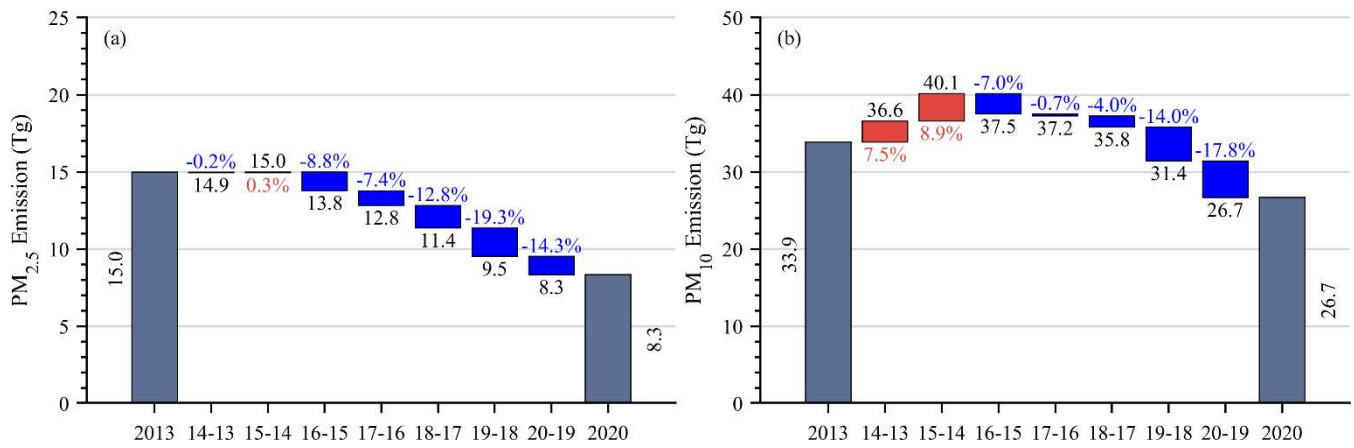
1331

1332

1333

1334

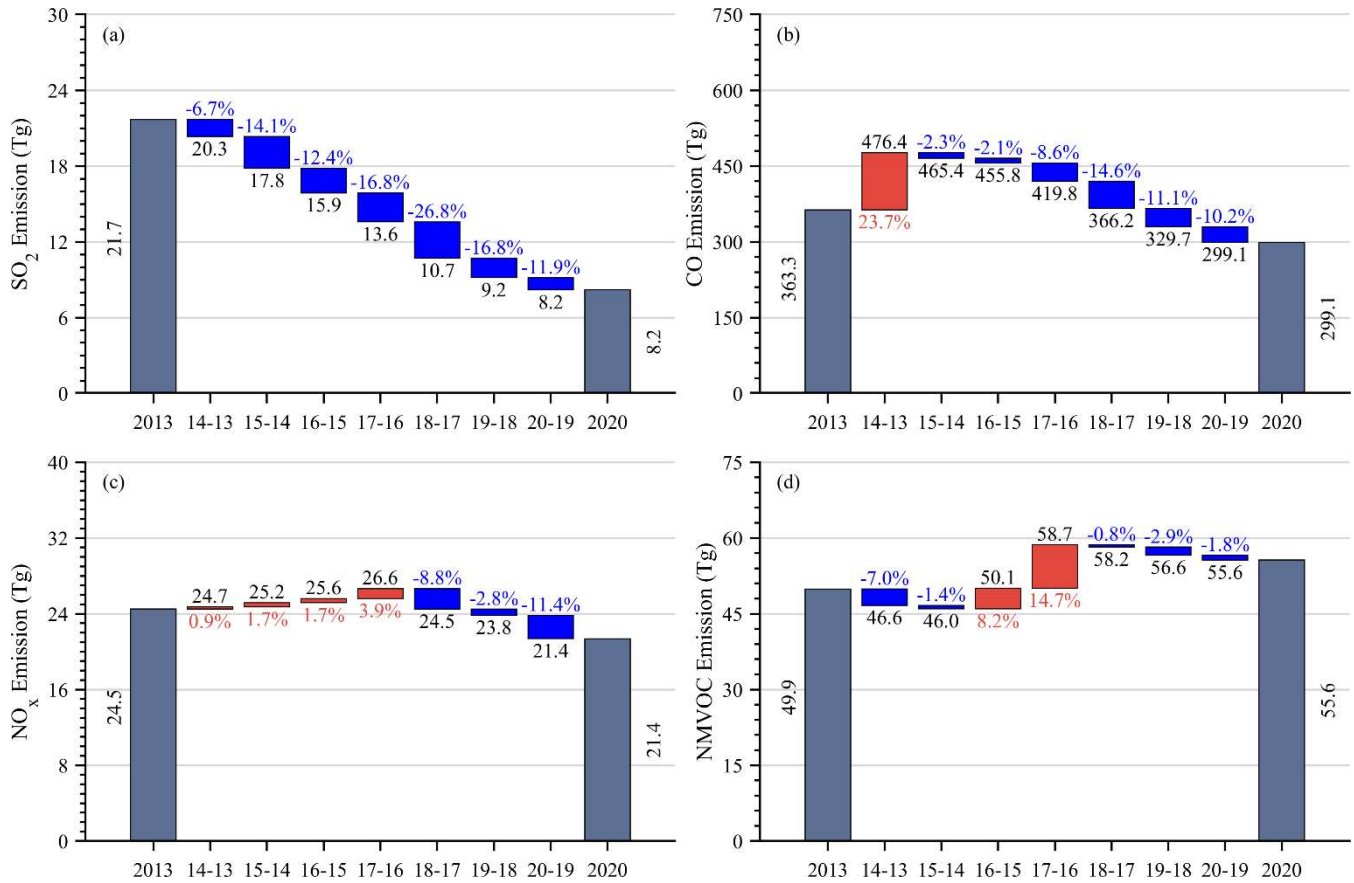
1335



1336

1337

Figure 6: Emission changes in (a) PM_{2.5} and (b) PM₁₀ obtained from CAQIEI from 2013 to 2020.

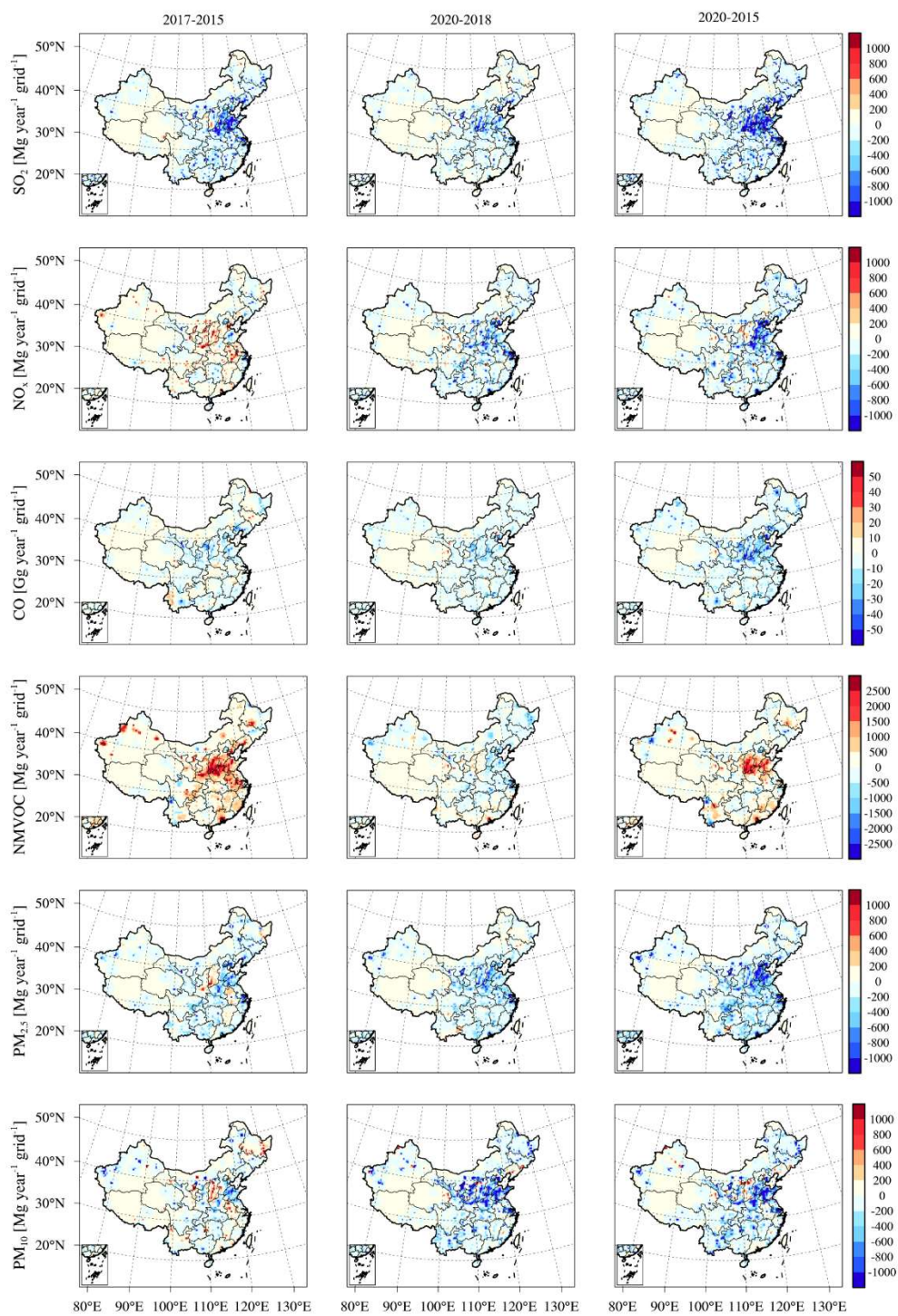


1338

1339

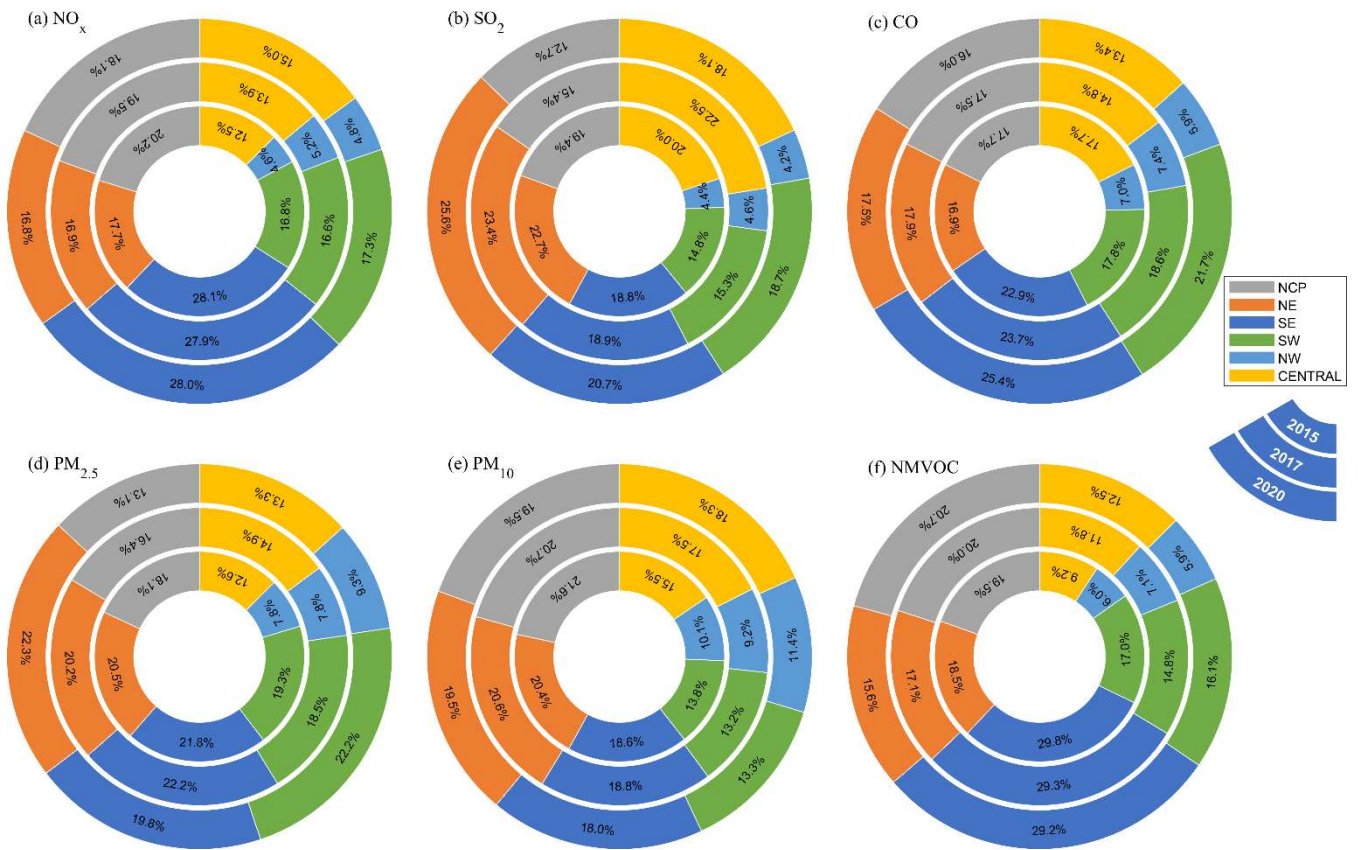
Figure 7: Emission changes in (a) SO₂, (b) CO, (c) NO_x, and (d) NMVOCs obtained from CAQIEI from 2013 to 2020.

1340



1341

1342 **Figure 8: Spatial distributions of the emission changes of different species during 2015–2017 (left panels), 2018–2020 (middle panels),**
 1343 **and 2015–2020 (right panels) obtained from CAQIEI from 2013 to 2020.**

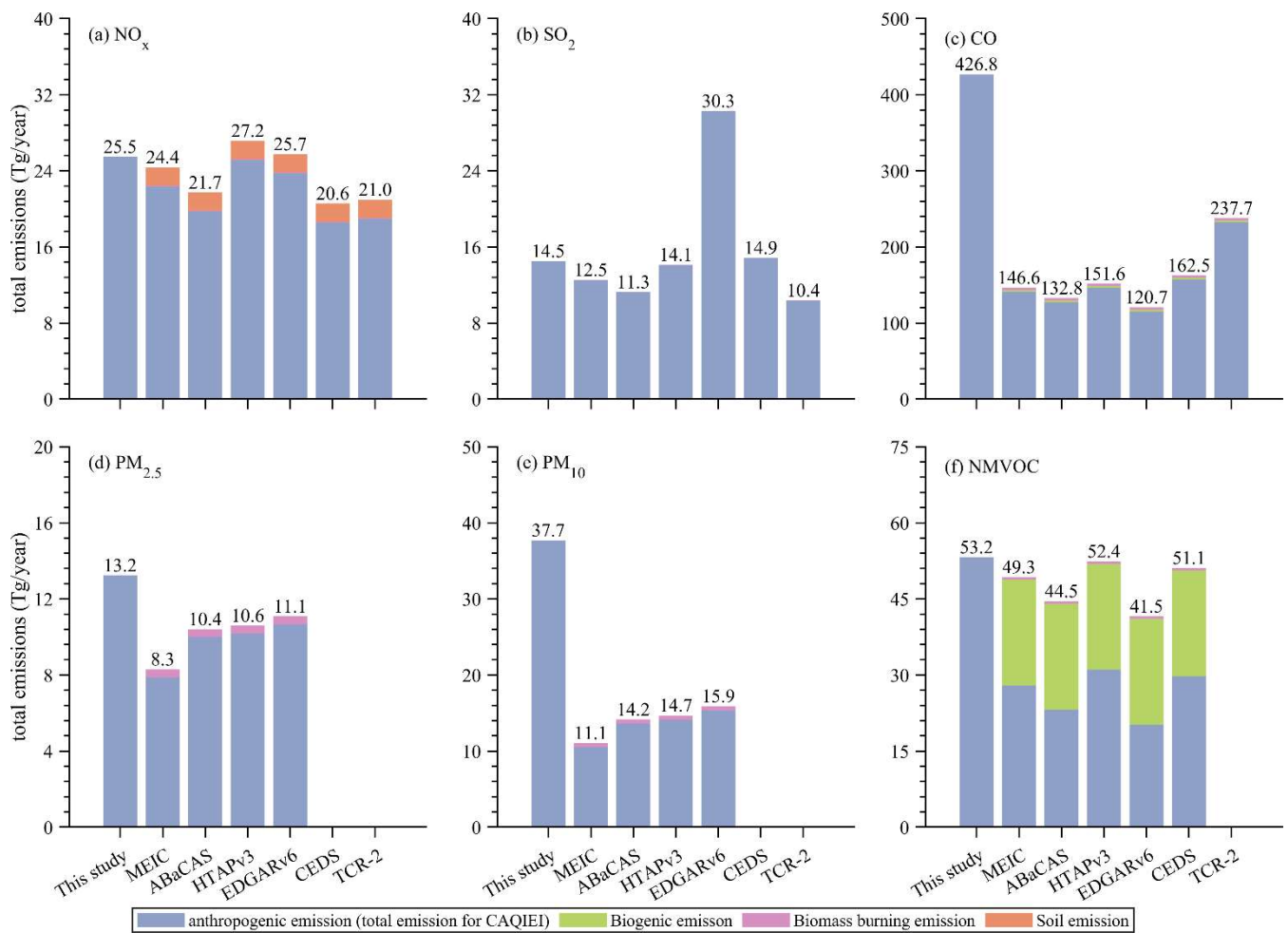


1344

1345 **Figure 9: Emission distributions of (a) NO_x, (b) SO₂, (c) CO, (d) PM_{2.5}, (e) PM₁₀, and (f) NMVOCs among different regions in China**
 1346 **obtained from CAQIEI in 2015, 2017 and 2020.**

1347

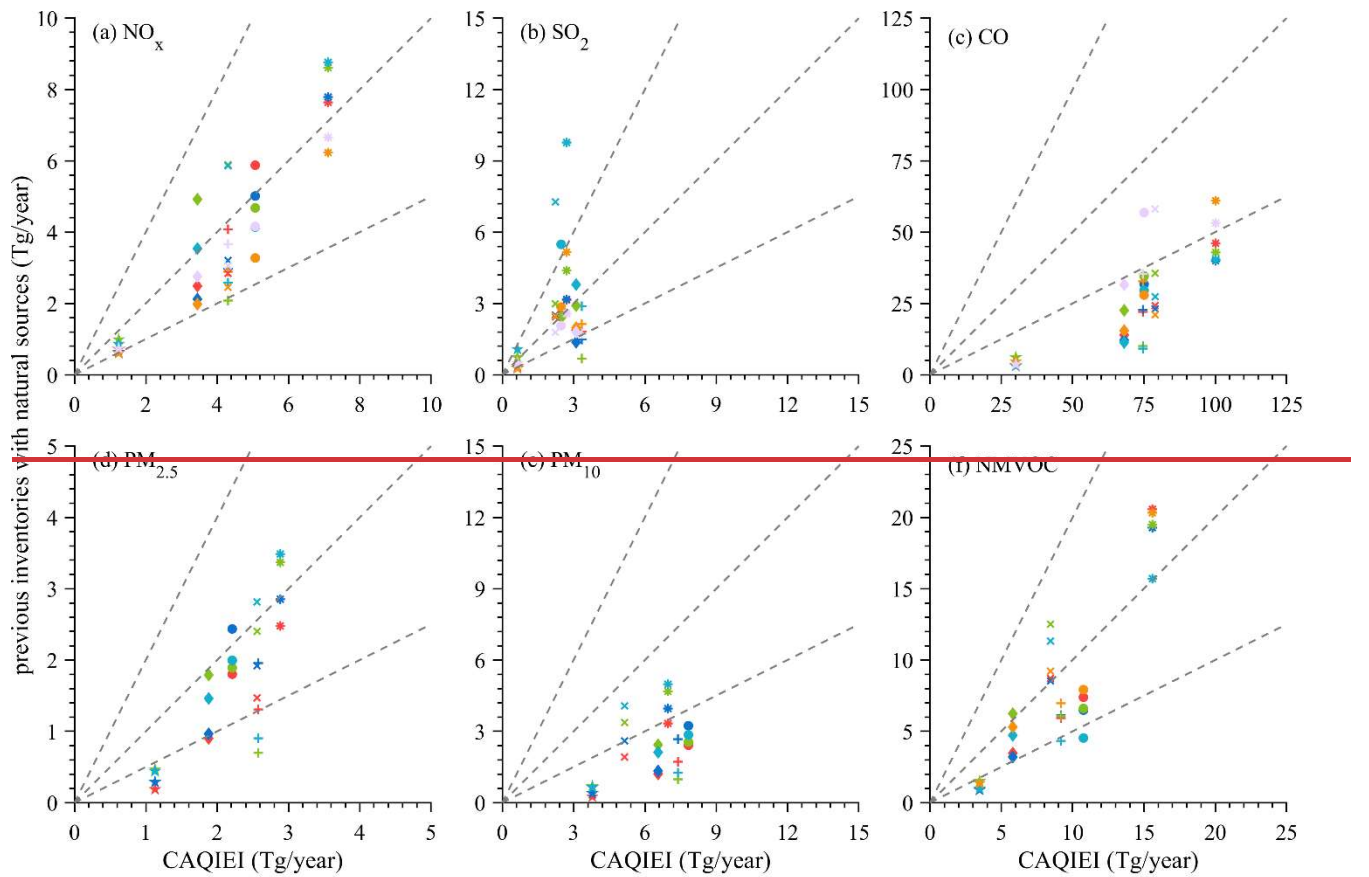
1348



1349

1350 **Figure 10: Comparisons of the averaged emissions of (a) NO_x, (b) SO₂, (c) CO, (d) PM_{2.5}, (e) PM₁₀, and (f) NMVOCs over China**
 1351 **from 2015 to 2018 between CAQIEI and previous inventories added with natural sources.**

1352



● MEIC ● ABaCAS ● HTAPv3 ● EDGARv6 ● CEDS ● TCR ● NCP + NE * SE * SW * NW ◆ Central

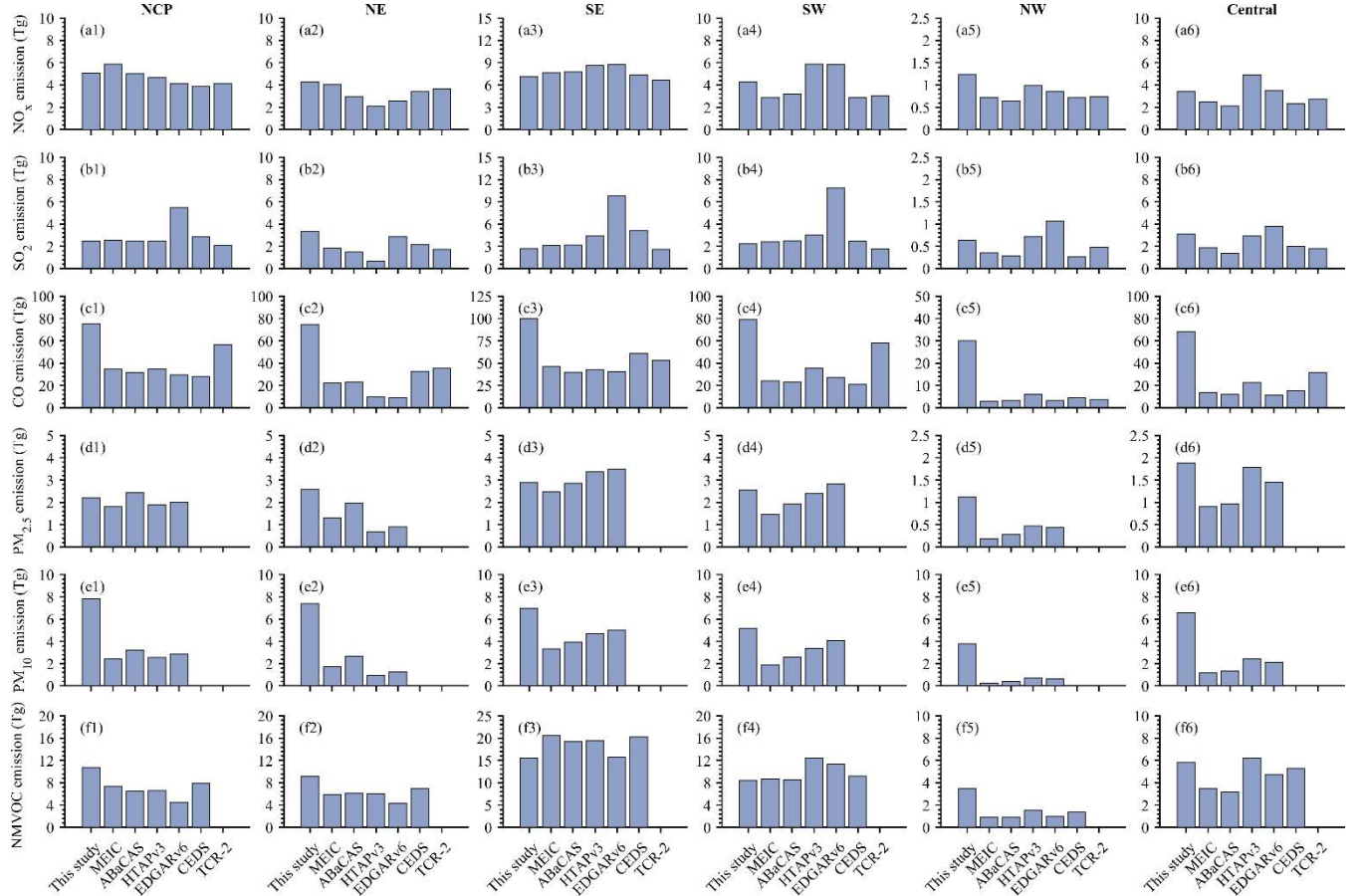
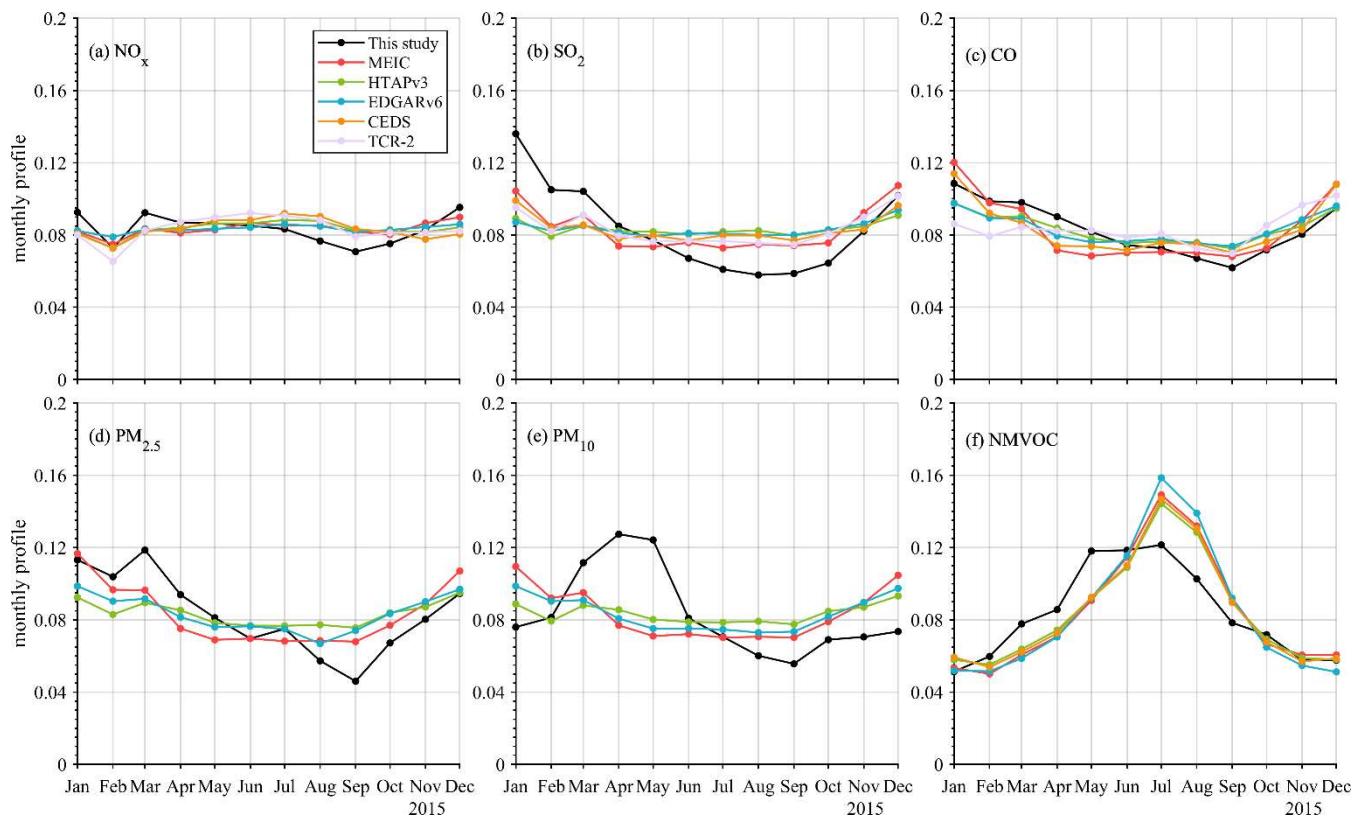


Figure 11: Comparisons of the averaged emissions of (a) NO_x , (b) SO_2 , (c) CO, (d) $\text{PM}_{2.5}$, (e) PM_{10} , and (f) NMVOCs over different regions in China from 2015 to 2018 between CAQIEI and previous inventories added with natural sources.

1359

1360

1361



1362

1363

1364

1365

1366

1367

1368

1369

1370

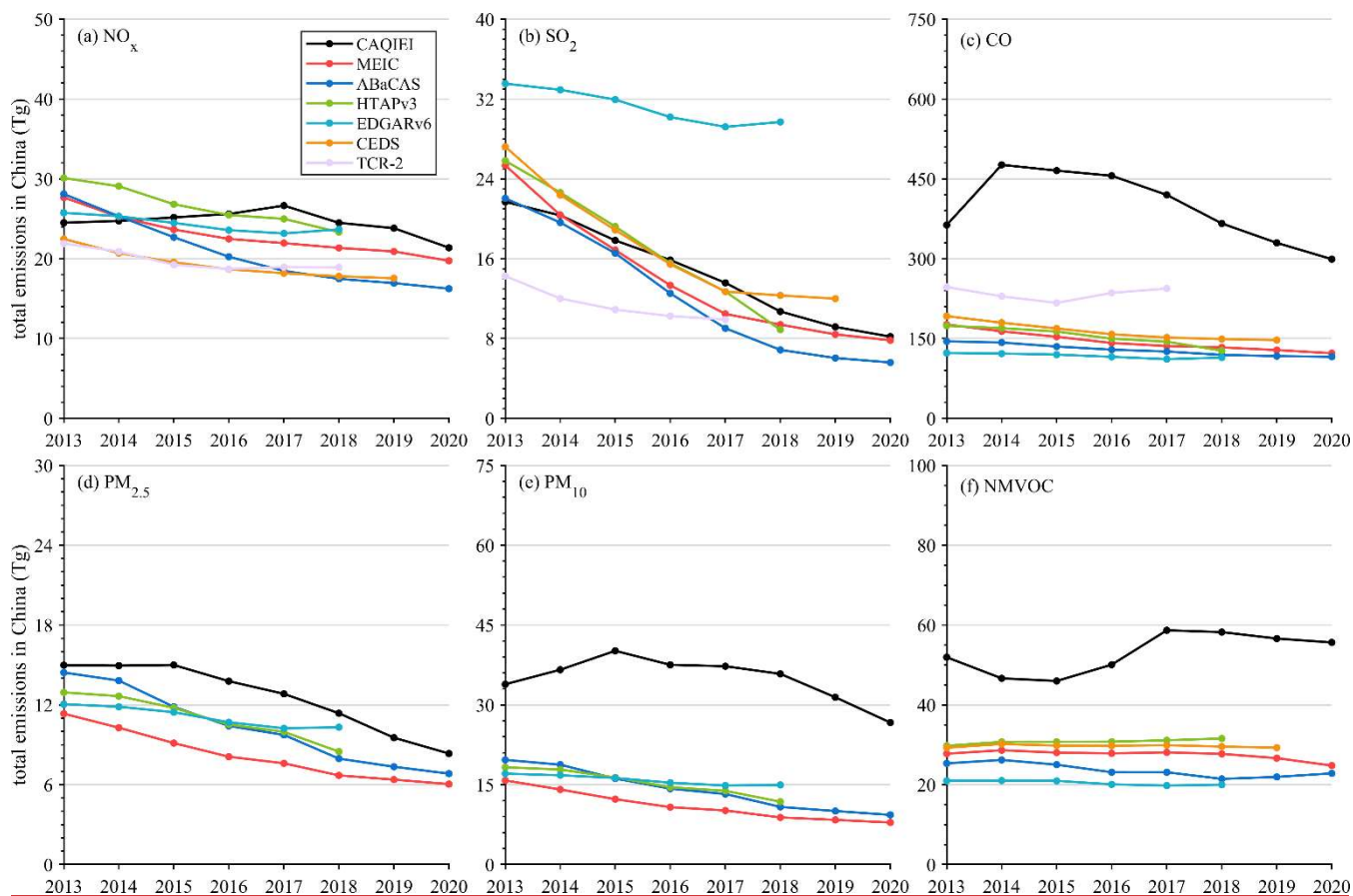
1371

1372

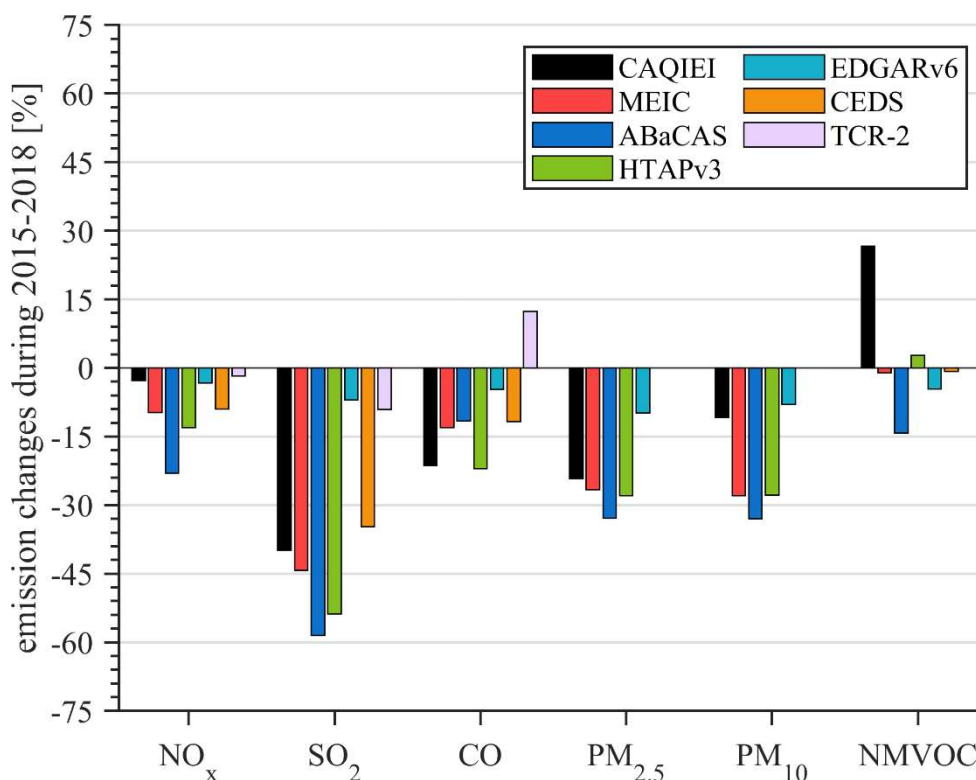
1373

1374

Figure 12: Comparisons of the monthly profiles of (a) NO_x, (b) SO₂, (c) CO, (d) PM_{2.5}, (e) PM₁₀, and (f) NMVOCs over China averaged from 2015 to 2018 between CAQIEI and previous inventories added with natural sources.



1375
 1376 **Figure 13: Time series of annual emissions of (a) NO_x , (b) SO_2 , (c) CO, (d) $\text{PM}_{2.5}$, (e) PM_{10} and (f) NMVOC over China from 2013 to**
 1377 **2020 obtained from CAQIEI and previous inventories. Note that the natural sources were not included in the previous inventories**
 1378 **in this figure.**



1385

1386 **Figure 143:** Comparisons of the calculated emission changes of (a) NO_x, (b) SO₂, (c) CO, (d) PM_{2.5}, (e) PM₁₀, and (f) NMVOCs over
 1387 China from 2015 to 2018 between CAQIEI and previous inventories.

1388 **Author contributions**

1389 X.T., Z.W., and J.Z. conceived and designed the project; L.K., H.W., X.T., and L.W. established the data assimilation system;
 1390 Q.W. and L.K. performed the meteorology simulations; L.K., H.C., and J.L. conducted the ensemble simulation with the
 1391 NAQPMS model; J.L., L.Z., W.W., B.L., Q.W., D.C. and Y.P. provided the air quality monitoring data; H.W. performed the
 1392 quality control of the observation data; and L.K. performed the inversion estimation, generated the figures, and wrote the paper,
 1393 with comments provided by G.R.C.

1394 **Competing interests**

1395 The authors declare no competing financial interest.

1396 **Acknowledgements**

1397 We acknowledge the use of surface air quality observation data from CNEMC and the strong support from the National Key
 1398 Scientific and Technological Infrastructure project “Earth System Science Numerical Simulator Facility” (EarthLab), which
 1399 provide us with ample computational resources to fill the requirement of the inversion of multiple years using the ensemble
 1400 method at a high grid resolution of 15km.

1401 **Financial support**

1402 This research has been sponsored by the National Natural Science Foundation of China (Grant Nos. 42175132, 92044303,
 1403 42205119), the National Key R&D Program (Grant No. 2020YFA0607802), the CAS Information Technology Program (Grant
 1404 No. CAS-WX2021SF-0107-02).

1405 **References**

- 1406 Athanasopoulou, E., Tombrou, M., Pandis, S. N., and Russell, A. G.: The role of sea-salt emissions and heterogeneous chemistry in the air
1407 quality of polluted coastal areas, *Atmos. Chem. Phys.*, 8, 5755-5769, <https://doi.org/10.5194/acp-8-5755-2008>, 2008.
- 1408 Bergamaschi, P., Hein, R., Heimann, M., and Crutzen, P. J.: Inverse modeling of the global CO cycle 1. Inversion of CO mixing ratios, *J.*
1409 *Geophys. Res.-Atmos.*, 105, 1909-1927, <https://doi.org/10.1029/1999jd900818>, 2000.
- 1410 Bobbink, R., Hornung, M., and Roelofs, J. G. M.: The effects of air-borne nitrogen pollutants on species diversity in natural and semi-natural
1411 European vegetation, *J. Ecol.*, 86, 717-738, <https://doi.org/10.1046/j.1365-2745.1998.8650717.x>, 1998.
- 1412 Brasseur, G. P., Hauglustaine, D. A., Walters, S., Rasch, P. J., Müller, J.-F., Granier, C., and Tie, X. X.: MOZART, a global chemical
1413 transport model for ozone and related chemical tracers: 1. Model description, *J. Geophys. Res.-Atmos.*, 103, 28265-28289,
1414 <https://doi.org/10.1029/98JD02397>, 1998.
- 1415 [Cao, H. S., Fu, T. M., Zhang, L., Henze, D. K., Miller, C. C., Lerot, C., Abad, G. G., De Smedt, I., Zhang, Q., van Roozendaal, M., Hendrick,
1416 F., Chance, K., Li, J., Zheng, J. Y., and Zhao, Y. H.: Adjoint inversion of Chinese non-methane volatile organic compound emissions
1417 using space-based observations of formaldehyde and glyoxal, *Atmos. Chem. Phys.*, 18, 15017-15046, \[https://10.5194/acp-18-15017-
1418 2018\]\(https://doi.org/10.5194/acp-18-15017-2018\), 2018.](https://doi.org/10.5194/acp-18-15017-2018)
- 1419
- 1420 Cohen, A. J., Brauer, M., Burnett, R., Anderson, H. R., Frostad, J., Estep, K., Balakrishnan, K., Brunekreef, B., Dandona, L., Dandona, R.,
1421 Feigin, V., Freedman, G., Hubbell, B., Jobling, A., Kan, H., Knibbs, L., Liu, Y., Martin, R., Morawska, L., Pope, C. A., Shin, H., Straif,
1422 K., Shaddick, G., Thomas, M., van Dingenen, R., van Donkelaar, A., Vos, T., Murray, C. J. L., and Forouzanfar, M. H.: Estimates and
1423 25-year trends of the global burden of disease attributable to ambient air pollution: an analysis of data from the Global Burden of
1424 Diseases Study 2015, *Lancet*, 389, 1907-1918, [https://doi.org/10.1016/s0140-6736\(17\)30505-6](https://doi.org/10.1016/s0140-6736(17)30505-6), 2017.
- 1425 Crippa, M., Guizzardi, D., Butler, T., Keating, T., Wu, R., Kaminski, J., Kuenen, J., Kurokawa, J., Chatani, S., Morikawa, T., Pouliot, G.,
1426 Racine, J., Moran, M. D., Klimont, Z., Manseau, P. M., Mashayekhi, R., Henderson, B. H., Smith, S. J., Suchyta, H., Muntean, M.,
1427 Solazzo, E., Banja, M., Schaaf, E., Pagani, F., Woo, J. H., Kim, J., Monforti-Ferrario, F., Pisoni, E., Zhang, J., Niemi, D., Sassi, M.,
1428 Ansari, T., and Foley, K.: The HTAP_v3 emission mosaic: merging regional and global monthly emissions (2000–2018) to support
1429 air quality modelling and policies, *Earth Syst. Sci. Data*, 15, 2667-2694, <https://doi.org/10.5194/essd-15-2667-2023>, 2023.
- 1430 Dee, D. P. and Da Silva, A. M.: Data assimilation in the presence of forecast bias, *Q. J. R. Meteorol. Soc.*, 124, 269-295,
1431 <https://doi.org/10.1002/qj.49712454512>, 1998.
- 1432 Elbern, H., Strunk, A., Schmidt, H., and Talagrand, O.: Emission rate and chemical state estimation by 4-dimensional variational inversion,
1433 *Atmos. Chem. Phys.*, 7, 3749-3769, <https://doi.org/10.5194/acp-7-3749-2007>, 2007.
- 1434 Elguindi, N., Granier, C., Stavrakou, T., Darras, S., Bauwens, M., Cao, H., Chen, C., van der Gon, H., Dubovik, O., Fu, T. M., Henze, D.
1435 K., Jiang, Z., Keita, S., Kuenen, J. J. P., Kurokawa, J., Liousse, C., Miyazaki, K., Muller, J. F., Qu, Z., Solmon, F., and Zheng, B.:
1436 Intercomparison of Magnitudes and Trends in Anthropogenic Surface Emissions From Bottom-Up Inventories, Top-Down Estimates,
1437 and Emission Scenarios, *Earth Future*, 8, 20, <https://doi.org/10.1029/2020ef001520>, 2020.
- 1438 Evensen, G.: Sequential data assimilation with a nonlinear quasi-geostrophic model using Monte Carlo methods to forecast error statistics,
1439 *J. Geophys. Res.-Oceans*, 99, 10143-10162, <https://doi.org/10.1029/94JC00572>, 1994.
- 1440 Fan, H., Zhao, C., Yang, Y., and Yang, X.: Spatio-Temporal Variations of the PM_{2.5}/PM₁₀ Ratios and Its Application to Air Pollution Type
1441 Classification in China, *Front. Environ. Sci.*, 9, <https://doi.org/10.3389/fenvs.2021.692440>, 2021.
- 1442 [Feng, S., Jiang, F., Qian, T., Wang, N., Jia, M., Zheng, S., Chen, J., Ying, F., and Ju, W.: Constraint of non-methane volatile organic
1443 compound emissions with TROPOMI HCHO observations and its impact on summertime surface ozone simulation over China,
1444 *EGUsphere*, 2024, 1-34, \[https://10.5194/egusphere-2023-2654\]\(https://doi.org/10.5194/egusphere-2023-2654\), 2024.](https://doi.org/10.5194/egusphere-2023-2654)
- 1445 Feng, S., Jiang, F., Wu, Z., Wang, H., Ju, W., and Wang, H.: CO Emissions Inferred From Surface CO Observations Over China in December
1446 2013 and 2017, *J. Geophys. Res.-Atmos.*, 125, e2019JD031808, <https://doi.org/10.1029/2019JD031808>, 2020.
- 1447 Fu, X., Wang, T., Gao, J., Wang, P., Liu, Y. M., Wang, S. X., Zhao, B., and Xue, L. K.: Persistent Heavy Winter Nitrate Pollution Driven
1448 by Increased Photochemical Oxidants in Northern China, *Environ. Sci. Technol.*, 54, 3881-3889,
1449 <https://doi.org/10.1021/acs.est.9b07248>, 2020.
- 1450 Gaubert, B., Emmons, L. K., Raeder, K., Tilmes, S., Miyazaki, K., Arellano Jr, A. F., Elguindi, N., Granier, C., Tang, W., Barré, J., Worden,
1451 H. M., Buchholz, R. R., Edwards, D. P., Franke, P., Anderson, J. L., Saunio, M., Schroeder, J., Woo, J. H., Simpson, I. J., Blake, D.

1452 R., Meinardi, S., Wennberg, P. O., Crounse, J., Teng, A., Kim, M., Dickerson, R. R., He, H., Ren, X., Pusede, S. E., and Diskin, G. S.:
1453 Correcting model biases of CO in East Asia: impact on oxidant distributions during KORUS-AQ, *Atmos. Chem. Phys.*, 20, 14617-
1454 14647, <https://doi.org/10.5194/acp-20-14617-2020>, 2020.

1455 [Goldberg, D. L., Saide, P. E., Lamsal, L. N., de Foy, B., Lu, Z. F., Woo, J. H., Kim, Y., Kim, J., Gao, M., Carmichael, G., and Streets, D. G.:](#)
1456 [A top-down assessment using OMI NO₂ suggests an underestimate in the NO_x emissions inventory in Seoul, South Korea, during](#)
1457 [KORUS-AQ, *Atmos. Chem. Phys.*, 19, 1801-1818, <https://doi.org/10.5194/acp-19-1801-2019>, 2019.](#)

1458 Granier, C., Lamarque, J., Mieville, A., Muller, J., Olivier, J., Orlando, J., Peters, J., Petron, G., Tyndall, G., and Wallens, S.: POET, a
1459 database of surface emissions of ozone precursors, available at: <http://www.aero.jussieu.fr/projet/ACCENT/POET.php> (last access: 09
1460 October 2023), 2005.

1461 Hauglustaine, D. A., Brasseur, G. P., Walters, S., Rasch, P. J., Muller, J. F., Emmons, L. K., and Carroll, C. A.: MOZART, a global chemical
1462 transport model for ozone and related chemical tracers 2. Model results and evaluation, *J. Geophys. Res.-Atmos.*, 103, 28291-28335,
1463 <https://doi.org/10.1029/98jd02398>, 1998.

1464 Henze, D. K., Seinfeld, J. H., and Shindell, D. T.: Inverse modeling and mapping US air quality influences of inorganic PM_{2.5} precursor
1465 emissions using the adjoint of GEOS-Chem, *Atmos. Chem. Phys.*, 9, 5877-5903, <https://doi.org/10.5194/acp-9-5877-2009>, 2009.

1466 Hernández, D. L., Vallano, D. M., Zavaleta, E. S., Tzankova, Z., Pasari, J. R., Weiss, S., Selmants, P. C., and Morozumi, C.: Nitrogen
1467 Pollution Is Linked to US Listed Species Declines, *BioScience*, 66, 213-222, <https://doi.org/10.1093/biosci/biw003>, 2016.

1468 Jalkanen, J. P., Johansson, L., Kukkonen, J., Brink, A., Kalli, J., and Stipa, T.: Extension of an assessment model of ship traffic exhaust
1469 emissions for particulate matter and carbon monoxide, *Atmos. Chem. Phys.*, 12, 2641-2659, <https://doi.org/10.5194/acp-12-2641-2012>,
1470 2012.

1471 Janssens-Maenhout, G., Crippa, M., Guizzardi, D., Dentener, F., Muntean, M., Pouliot, G., Keating, T., Zhang, Q., Kurokawa, J.,
1472 Wankmuller, R., van der Gon, H. D., Kuenen, J. J. P., Klimont, Z., Frost, G., Darras, S., Koffi, B., and Li, M.: HTAP_v2.2: a mosaic
1473 of regional and global emission grid maps for 2008 and 2010 to study hemispheric transport of air pollution, *Atmos. Chem. Phys.*, 15,
1474 11411-11432, <https://doi.org/10.5194/acp-15-11411-2015>, 2015.

1475 Jiang, Z., Worden, J. R., Worden, H., Deeter, M., Jones, D. B. A., Arellano, A. F., and Henze, D. K.: A 15-year record of CO emissions
1476 constrained by MOPITT CO observations, *Atmos. Chem. Phys.*, 17, 4565-4583, <https://doi.org/10.5194/acp-17-4565-2017>, 2017.

1477 Kaiser, J. W., Heil, A., Andreae, M. O., Benedetti, A., Chubarova, N., Jones, L., Morcrette, J. J., Razinger, M., Schultz, M. G., Suttie, M.,
1478 and van der Werf, G. R.: Biomass burning emissions estimated with a global fire assimilation system based on observed fire radiative
1479 power, *Biogeosciences*, 9, 527-554, <https://doi.org/10.5194/bg-9-527-2012>, 2012.

1480 Kan, H., Chen, R., and Tong, S.: Ambient air pollution, climate change, and population health in China, *Environ. Int.*, 42, 10-19,
1481 <https://doi.org/10.1016/j.envint.2011.03.003>, 2012.

1482 Kong, L., Tang, X., Wang, Z. F., Zhu, J., Li, J. J., Wu, H. J., Wu, Q. Z., Chen, H. S., Zhu, L. L., Wang, W., Liu, B., Wang, Q., Chen D. H.,
1483 Pan Y. P., Li, J., Wu, L., and Carmichael, G. R.: Inversed Emission Inventory for Chinese Air Quality (CAQIEI) version 1.0, *Science*
1484 *Data Bank [dataset]*, <https://doi.org/10.57760/sciencedb.13151>, 2023.

1485 Kong, L., Tang, X., Zhu, J., Wang, Z., Pan, Y., Wu, H., Wu, L., Wu, Q., He, Y., Tian, S., Xie, Y., Liu, Z., Sui, W., Han, L., and Carmichael,
1486 G.: Improved Inversion of Monthly Ammonia Emissions in China Based on the Chinese Ammonia Monitoring Network and Ensemble
1487 Kalman Filter, *Environ. Sci. Technol.*, 53, 12529-12538, <https://doi.org/10.1021/acs.est.9b02701>, 2019.

1488 Kong, L., Tang, X., Zhu, J., Wang, Z., Sun, Y., Fu, P., Gao, M., Wu, H., Lu, M., Wu, Q., Huang, S., Sui, W., Li, J., Pan, X., Wu, L., Akimoto,
1489 H., and Carmichael, G. R.: Unbalanced emission reductions of different species and sectors in China during COVID-19 lockdown
1490 derived by multi-species surface observation assimilation, *Atmos. Chem. Phys.*, 23, 6217-6240, [https://doi.org/10.5194/acp-23-6217-](https://doi.org/10.5194/acp-23-6217-2023)
1491 2023, 2023.

1492 Kong, L., Tang, X., Zhu, J., Wang, Z., Li, J., Wu, H., Wu, Q., Chen, H., Zhu, L., Wang, W., Liu, B., Wang, Q., Chen, D., Pan, Y., Song, T.,
1493 Li, F., Zheng, H., Jia, G., Lu, M., Wu, L., and Carmichael, G. R.: A 6-year-long (2013–2018) high-resolution air quality reanalysis
1494 dataset in China based on the assimilation of surface observations from CNEMC, *Earth Syst. Sci. Data*, 13, 529-570,
1495 <https://doi.org/10.5194/essd-13-529-2021>, 2021.

1496 Kong, L., Tang, X., Zhu, J., Wang, Z., Fu, J. S., Wang, X., Itahashi, S., Yamaji, K., Nagashima, T., Lee, H. J., Kim, C. H., Lin, C. Y., Chen,
1497 L., Zhang, M., Tao, Z., Li, J., Kajino, M., Liao, H., Wang, Z., Sudo, K., Wang, Y., Pan, Y., Tang, G., Li, M., Wu, Q., Ge, B., and
1498 Carmichael, G. R.: Evaluation and uncertainty investigation of the NO₂, CO and NH₃ modeling over China under the framework of
1499 MICS-Asia III, *Atmos. Chem. Phys.*, 20, 181-202, <https://doi.org/10.5194/acp-20-181-2020>, 2020.

1500 Koohkan, M. R., Bocquet, M., Roustan, Y., Kim, Y., and Seigneur, C.: Estimation of volatile organic compound emissions for Europe using
1501 data assimilation, *Atmos. Chem. Phys.*, 13, 5887-5905, <https://doi.org/10.5194/acp-13-5887-2013>, 2013.

1502 Koukouli, M. E., Theys, N., Ding, J. Y., Zyrichidou, I., Mijling, B., Balis, D., and Johannes, V. R.: Updated SO₂ emission estimates over
1503 China using OMI/Aura observations, *Atmos. Meas. Tech.*, 11, 1817-1832, [10.5194/amt-11-1817-2018](https://doi.org/10.5194/amt-11-1817-2018), 2018.

1504 Krotkov, N. A., McLinden, C. A., Li, C., Lamsal, L. N., Celarier, E. A., Marchenko, S. V., Swartz, W. H., Bucsela, E. J., Joiner, J., Duncan,
1505 B. N., Boersma, K. F., Veefkind, J. P., Levelt, P. F., Fioletov, V. E., Dickerson, R. R., He, H., Lu, Z. F., and Streets, D. G.: Aura OMI
1506 observations of regional SO₂ and NO₂ pollution changes from 2005 to 2015, *Atmos. Chem. Phys.*, 16, 4605-4629,
1507 <https://doi.org/10.5194/acp-16-4605-2016>, 2016.

1508 Krupa, S. V.: Effects of atmospheric ammonia (NH₃) on terrestrial vegetation: a review, *Environ. Pollut.*, 124, 179-221,
1509 [https://doi.org/10.1016/s0269-7491\(02\)00434-7](https://doi.org/10.1016/s0269-7491(02)00434-7), 2003.

1510 Kurokawa, J. and Ohara, T.: Long-term historical trends in air pollutant emissions in Asia: Regional Emission inventory in ASia (REAS)
1511 version 3, *Atmos. Chem. Phys.*, 20, 12761-12793, <https://doi.org/10.5194/acp-20-12761-2020>, 2020.

1512 Kurokawa, J., Ohara, T., Morikawa, T., Hanayama, S., Janssens-Maenhout, G., Fukui, T., Kawashima, K., and Akimoto, H.: Emissions of
1513 air pollutants and greenhouse gases over Asian regions during 2000-2008: Regional Emission inventory in ASia (REAS) version 2,
1514 *Atmos. Chem. Phys.*, 13, 11019-11058, <https://doi.org/10.5194/acp-13-11019-2013>, 2013.

1515 Lei, L., Zhou, W., Chen, C., He, Y., Li, Z. J., Sun, J. X., Tang, X., Fu, P. Q., Wang, Z. F., and Sun, Y. L.: Long-term characterization of
1516 aerosol chemistry in cold season from 2013 to 2020 in Beijing, China, *Environ. Pollut.*, 268, 9, [10.1016/j.envpol.2020.115952](https://doi.org/10.1016/j.envpol.2020.115952), 2021.

1517 Li, C., McLinden, C., Fioletov, V., Krotkov, N., Carn, S., Joiner, J., Streets, D., He, H., Ren, X., Li, Z., and Dickerson, R. R.: India Is
1518 Overtaking China as the World's Largest Emitter of Anthropogenic Sulfur Dioxide, *Sci Rep*, 7, 14304, [https://doi.org/10.1038/s41598-](https://doi.org/10.1038/s41598-017-14639-8)
1519 [017-14639-8](https://doi.org/10.1038/s41598-017-14639-8), 2017a.

1520 Li, H., Cheng, J., Zhang, Q., Zheng, B., Zhang, Y., Zheng, G., and He, K.: Rapid transition in winter aerosol composition in Beijing from
1521 2014 to 2017: response to clean air actions, *Atmos. Chem. Phys.*, 19, 11485-11499, <https://doi.org/10.5194/acp-19-11485-2019>, 2019a.

1522 Li, J., Wang, Z., Zhuang, G., Luo, G., Sun, Y., and Wang, Q.: Mixing of Asian mineral dust with anthropogenic pollutants over East Asia:
1523 a model case study of a super-duststorm in March 2010, *Atmos. Chem. Phys.*, 12, 7591-7607, 2012.

1524 Li, K., Jacob, D. J., Liao, H., Shen, L., Zhang, Q., and Bates, K. H.: Anthropogenic drivers of 2013-2017 trends in summer surface ozone in
1525 China, *Proc. Natl. Acad. Sci. U.S.A.*, 116, 422-427, <https://doi.org/10.1073/pnas.1812168116>, 2019b.

1526 Li, L. Y., Yang, W. Z., Xie, S. D., and Wu, Y.: Estimations and uncertainty of biogenic volatile organic compound emission inventory in
1527 China for 2008-2018, *Sci. Total Environ.*, 733, 10, <https://doi.org/10.1016/j.scitotenv.2020.139301>, 2020a.

1528 Li, M., Zhang, Q., Zheng, B., Tong, D., Lei, Y., Liu, F., Hong, C. P., Kang, S. C., Yan, L., Zhang, Y. X., Bo, Y., Su, H., Cheng, Y. F., and
1529 He, K. B.: Persistent growth of anthropogenic non-methane volatile organic compound (NMVOC) emissions in China during 1990-
1530 2017: drivers, speciation and ozone formation potential, *Atmos. Chem. Phys.*, 19, 8897-8913, [https://doi.org/10.5194/acp-19-8897-](https://doi.org/10.5194/acp-19-8897-2019)
1531 [2019](https://doi.org/10.5194/acp-19-8897-2019), 2019c.

1532 Li, M., Zhang, Q., Kurokawa, J. I., Woo, J. H., He, K., Lu, Z., Ohara, T., Song, Y., Streets, D. G., Carmichael, G. R., Cheng, Y., Hong, C.,
1533 Huo, H., Jiang, X., Kang, S., Liu, F., Su, H., and Zheng, B.: MIX: a mosaic Asian anthropogenic emission inventory under the
1534 international collaboration framework of the MICS-Asia and HTAP, *Atmos. Chem. Phys.*, 17, 935-963, [https://doi.org/10.5194/acp-](https://doi.org/10.5194/acp-17-935-2017)
1535 [17-935-2017](https://doi.org/10.5194/acp-17-935-2017), 2017b.

1536 Li, N., Long, X., Tie, X. X., Cao, J. J., Huang, R. J., Zhang, R., Feng, T., Liu, S. X., and Li, G. H.: Urban dust in the Guanzhong basin of
1537 China, part II: A case study of urban dust pollution using the WRF-Dust model, *Sci. Total Environ.*, 541, 1614-1624,
1538 <https://doi.org/10.1016/j.scitotenv.2015.10.028>, 2016.

1539 Li, R., Cui, L. L., Li, J. L., Zhao, A., Fu, H. B., Wu, Y., Zhang, L. W., Kong, L. D., and Chen, J. M.: Spatial and temporal variation of
1540 particulate matter and gaseous pollutants in China during 2014-2016, *Atmos. Environ.*, 161, 235-246,
1541 <https://doi.org/10.1016/j.atmosenv.2017.05.008>, 2017c.

1542 Li, S., Wang, S., Wu, Q., Zhang, Y., Ouyang, D., Zheng, H., Han, L., Qiu, X., Wen, Y., Liu, M., Jiang, Y., Yin, D., Liu, K., Zhao, B., Zhang,
1543 S., Wu, Y., and Hao, J.: Emission trends of air pollutants and CO₂ in China from 2005 to 2021, *Earth Syst. Sci. Data*, 15, 2279-2294,
1544 <https://doi.org/10.5194/essd-15-2279-2023>, 2023.

1545 Li, W., Shao, L., Wang, W., Li, H., Wang, X., Li, Y., Li, W., Jones, T., and Zhang, D.: Air quality improvement in response to intensified
1546 control strategies in Beijing during 2013-2019, *Sci. Total Environ.*, 744, <https://doi.org/10.1016/j.scitotenv.2020.140776>, 2020b.

1547 Liu, J., Tong, D., Zheng, Y. X., Cheng, J., Qin, X. Y., Shi, Q. R., Yan, L., Lei, Y., and Zhang, Q.: Carbon and air pollutant emissions from
1548 China's cement industry 1990-2015: trends, evolution of technologies, and drivers, *Atmos. Chem. Phys.*, 21, 1627-1647,
1549 <https://doi.org/10.5194/acp-21-1627-2021>, 2021.

1550 Liu, J., Mauzerall, D. L., Chen, Q., Zhang, Q., Song, Y., Peng, W., Klimont, Z., Qiu, X. H., Zhang, S. Q., Hu, M., Lin, W. L., Smith, K. R.,
1551 and Zhu, T.: Air pollutant emissions from Chinese households: A major and underappreciated ambient pollution source, *Proc. Natl.*
1552 *Acad. Sci. U.S.A.*, 113, 7756-7761, <https://doi.org/10.1073/pnas.1604537113>, 2016.

1553 Lu, X., Zhang, L., Wang, X. L., Gao, M., Li, K., Zhang, Y. Z., Yue, X., and Zhang, Y. H.: Rapid Increases in Warm-Season Surface Ozone
1554 and Resulting Health Impact in China Since 2013, *Environ. Sci. Technol. Lett.*, 7, 240-247, <https://doi.org/10.1021/acs.estlett.0c00171>,
1555 2020.

1556 Lu, X., Hong, J. Y., Zhang, L., Cooper, O. R., Schultz, M. G., Xu, X. B., Wang, T., Gao, M., Zhao, Y. H., and Zhang, Y. H.: Severe Surface
1557 Ozone Pollution in China: A Global Perspective, *Environ. Sci. Technol. Lett.*, 5, 487-494, <https://doi.org/10.1021/acs.estlett.8b00366>,
1558 2018.

1559 Ma, C. Q., Wang, T. J., Mizzi, A. P., Anderson, J. L., Zhuang, B. L., Xie, M., and Wu, R. S.: Multiconstituent Data Assimilation With WRF-
1560 Chem/DART: Potential for Adjusting Anthropogenic Emissions and Improving Air Quality Forecasts Over Eastern China, *J. Geophys.*
1561 *Res.-Atmos.*, 124, 7393-7412, <https://doi.org/10.1029/2019jd030421>, 2019.

1562 Martin, S. T., Hung, H. M., Park, R. J., Jacob, D. J., Spurr, R. J. D., Chance, K. V., and Chin, M.: Effects of the physical state of tropospheric
1563 ammonium-sulfate-nitrate particles on global aerosol direct radiative forcing, *Atmos. Chem. Phys.*, 4, 183-214,
1564 <https://doi.org/10.5194/acp-4-183-2004>, 2004.

1565 McDuffie, E. E., Smith, S. J., O'Rourke, P., Tibrewal, K., Venkataraman, C., Marais, E. A., Zheng, B., Crippa, M., Brauer, M., and Martin,
1566 R. V.: A global anthropogenic emission inventory of atmospheric pollutants from sector- and fuel-specific sources (1970-2017): an
1567 application of the Community Emissions Data System (CEDS), *Earth Syst. Sci. Data*, 12, 3413-3442, <https://doi.org/10.5194/essd-12-3413-2020>, 2020.

1569 Miyazaki, K. and Eskes, H.: Constraints on surface NO_x emissions by assimilating satellite observations of multiple species, *Geophys. Res.*
1570 *Lett.*, 40, 4745-4750, <https://doi.org/10.1002/grl.50894>, 2013.

1571 Miyazaki, K., Bowman, K. W., Yumimoto, K., Walker, T., and Sudo, K.: Evaluation of a multi-model, multi-constituent assimilation
1572 framework for tropospheric chemical reanalysis, *Atmos. Chem. Phys.*, 20, 931-967, <https://doi.org/10.5194/acp-20-931-2020>, 2020a.

1573 Miyazaki, K., Eskes, H. J., Sudo, K., Takigawa, M., van Weele, M., and Boersma, K. F.: Simultaneous assimilation of satellite NO₂, O₃,
1574 CO, and HNO₃ data for the analysis of tropospheric chemical composition and emissions, *Atmos. Chem. Phys.*, 12, 9545-9579,
1575 <https://doi.org/10.5194/acp-12-9545-2012>, 2012.

1576 Miyazaki, K., Bowman, K., Sekiya, T., Eskes, H., Boersma, F., Worden, H., Livesey, N., Payne, V. H., Sudo, K., Kanaya, Y., Takigawa,
1577 M., and Ogochi, K.: Updated tropospheric chemistry reanalysis and emission estimates, TCR-2, for 2005–2018, *Earth Syst. Sci. Data*,
1578 12, 2223-2259, <https://doi.org/10.5194/essd-12-2223-2020>, 2020b.

1579 Müller, J.-F., Stavrou, T., Bauwens, M., George, M., Hurtmans, D., Coheur, P.-F., Clerbaux, C., and Sweeney, C.: Top-Down CO
1580 Emissions Based On IASI Observations and Hemispheric Constraints on OH Levels, *Geophys. Res. Lett.*, 45, 1621-1629,
1581 <https://doi.org/10.1002/2017GL076697>, 2018.

1582 Muller, J. F., Stavrou, T., Bauwens, M., George, M., Hurtmans, D., Coheur, P. F., Clerbaux, C., and Sweeney, C.: Top-Down CO
1583 Emissions Based On IASI Observations and Hemispheric Constraints on OH Levels, *Geophys. Res. Lett.*, 45, 1621-1629,
1584 <https://doi.org/10.1002/2017gl076697>, 2018.

1585 Paulot, F., Jacob, D. J., Pinder, R. W., Bash, J. O., Travis, K., and Henze, D. K.: Ammonia emissions in the United States, European Union,
1586 and China derived by high-resolution inversion of ammonium wet deposition data: Interpretation with a new agricultural emissions
1587 inventory (MASAGE_NH₃), *J. Geophys. Res.-Atmos.*, 119, 4343-4364, <https://doi.org/10.1002/2013jd021130>, 2014.

1588 Peng, Z., Lei, L., Tan, Z. M., Zhang, M., Ding, A., and Kou, X.: Dynamics-based estimates of decline trend with fine temporal variations in
1589 China's PM_{2.5} emissions, *EGUsphere*, 2023, 1-34, <https://doi.org/10.5194/egusphere-2023-755>, 2023.

1590 Peng, Z., Lei, L. L., Liu, Z. Q., Su, J. N., Ding, A. J., Ban, J. M., Chen, D., Kou, X. X., and Chu, K. K.: The impact of multi-species surface
1591 chemical observation assimilation on air quality forecasts in China, *Atmos. Chem. Phys.*, 18, 18, [https://doi.org/10.5194/acp-18-17387-](https://doi.org/10.5194/acp-18-17387-2018)
1592 2018, 2018.

1593 Petron, G., Granier, C., Khattatov, B., Lamarque, J. F., Yudin, V., Muller, J. F., and Gille, J.: Inverse modeling of carbon monoxide surface
1594 emissions using Climate Monitoring and Diagnostics Laboratory network observations, *J. Geophys. Res.-Atmos.*, 107, 23,
1595 <https://doi.org/10.1029/2001jd001305>, 2002.

1596 Petron, G., Granier, C., Khattatov, B., Yudin, V., Lamarque, J. F., Emmons, L., Gille, J., and Edwards, D. P.: Monthly CO surface sources
1597 inventory based on the 2000-2001 MOPITT satellite data, *Geophys. Res. Lett.*, 31, 5, <https://doi.org/10.1029/2004gl020560>, 2004.

1598 Philip, S., Martin, R. V., Snider, G., Weagle, C. L., van Donkelaar, A., Brauer, M., Henze, D. K., Klimont, Z., Venkataraman, C., Guttikunda,
1599 S. K., and Zhang, Q.: Anthropogenic fugitive, combustion and industrial dust is a significant, underrepresented fine particulate matter
1600 source in global atmospheric models, *Environ. Res. Lett.*, 12, 7, <https://doi.org/10.1088/1748-9326/aa65a4>, 2017.

1601 Price, C., Penner, J., and Prather, M.: NO_x from lightning .1. Global distribution based on lightning physics, *J. Geophys. Res.-Atmos.*, 102,
1602 5929-5941, <https://doi.org/10.1029/96jd03504>, 1997.

1603 Prospero, J. M., Ginoux, P., Torres, O., Nicholson, S. E., and Gill, T. E.: Environmental characterization of global sources of atmospheric
1604 soil dust identified with the Nimbus 7 Total Ozone Mapping Spectrometer (TOMS) absorbing aerosol product, *Rev. Geophys.*, 40, 31,
1605 <https://doi.org/10.1029/2000rg000095>, 2002.

1606 Qu, Z., Henze, D. K., Capps, S. L., Wang, Y., Xu, X. G., Wang, J., and Keller, M.: Monthly top-down NO_x emissions for China (2005-2012):
1607 A hybrid inversion method and trend analysis, *J. Geophys. Res.-Atmos.*, 122, 4600-4625, <https://doi.org/10.1002/2016jd025852>, 2017.

1608 Qu, Z., Henze, D. K., Li, C., Theys, N., Wang, Y., Wang, J., Wang, W., Han, J., Shim, C., Dickerson, R. R., and Ren, X. R.: SO₂ Emission
1609 Estimates Using OMI SO₂ Retrievals for 2005-2017, *J. Geophys. Res.-Atmos.*, 124, 8336-8359, <https://doi.org/10.1029/2019jd030243>,
1610 2019.

1611 Randerson, J. T., Van Der Werf, G. R., Giglio, L., Collatz, G. J., and Kasibhatla, P. S.: Global Fire Emissions Database, Version 4.1
1612 (GFEDv4), ORNL DAAC, Oak Ridge, Tennessee, USA, <https://doi.org/10.3334/ORNLDAAC/1293>, 2017.

1613 [Ren, J., Guo, F., and Xie, S.: Diagnosing ozone-NO_x-VOC sensitivity and revealing causes of ozone increases in China based on 2013-
1614 2021 satellite retrievals. *Atmos. Chem. Phys.*, 22, 15035-15047, <https://10.5194/acp-22-15035-2022>, 2022.](#)

1615 Sakov, P. and Oke, P. R.: A deterministic formulation of the ensemble Kalman filter: an alternative to ensemble square root filters, *Tellus*
1616 *Ser. A-Dyn. Meteorol. Oceanol.*, 60, 361-371, <https://doi.org/10.1111/j.1600-0870.2007.00299.x>, 2008.

1617 Sindelarova, K., Granier, C., Bouarar, I., Guenther, A., Tilmes, S., Stavrou, T., Muller, J. F., Kuhn, U., Stefani, P., and Knorr, W.: Global
1618 data set of biogenic VOC emissions calculated by the MEGAN model over the last 30 years, *Atmos. Chem. Phys.*, 14, 9317-9341,
1619 <https://doi.org/10.5194/acp-14-9317-2014>, 2014.

1620 Song, C., Wu, L., Xie, Y., He, J., Chen, X., Wang, T., Lin, Y., Jin, T., Wang, A., Liu, Y., Dai, Q., Liu, B., Wang, Y.-n., and Mao, H.: Air
1621 pollution in China: Status and spatiotemporal variations, *Environ. Pollut.*, 227, 334-347, <https://doi.org/10.1016/j.envpol.2017.04.075>,
1622 2017.

1623 [Souri, A. H., Nowlan, C. R., Abad, G. G., Zhu, L., Blake, D. R., Fried, A., Weinheimer, A. J., Wisthaler, A., Woo, J. H., Zhang, Q., Miller,
1624 C. E. C., Liu, X., and Chance, K.: An inversion of NO_x and non-methane volatile organic compound \(NMVOC\) emissions using
1625 satellite observations during the KORUS-AQ campaign and implications for surface ozone over East Asia. *Atmos. Chem. Phys.*, 20,
1626 9837-9854, <https://10.5194/acp-20-9837-2020>, 2020.](#)

1627 [Stavrou, T., Muller, J. F., Bauwens, M., De Smedt, I., Van Roozendaal, M., De Maziere, M., Vigouroux, C., Hendrick, F., George, M.,
1628 Clerbaux, C., Coheur, P. F., and Guenther, A.: How consistent are top-down hydrocarbon emissions based on formaldehyde
1629 observations from GOME-2 and OMI?, *Atmos. Chem. Phys.*, 15, 11861-11884, <https://10.5194/acp-15-11861-2015>, 2015.](#)

1630 Stein, O., Schultz, M. G., Bouarar, I., Clark, H., Huijnen, V., Gaudel, A., George, M., and Clerbaux, C.: On the wintertime low bias of
1631 Northern Hemisphere carbon monoxide found in global model simulations, *Atmos. Chem. Phys.*, 14, 9295-9316,
1632 <https://doi.org/10.5194/acp-14-9295-2014>, 2014.

1633 Streets, D. G., Bond, T. C., Carmichael, G. R., Fernandes, S. D., Fu, Q., He, D., Klimont, Z., Nelson, S. M., Tsai, N. Y., Wang, M. Q., Woo,
1634 J. H., and Yarber, K. F.: An inventory of gaseous and primary aerosol emissions in Asia in the year 2000, *J. Geophys. Res.-Atmos.*,
1635 108, n/a-n/a, <https://doi.org/10.1029/2002JD003093>, 2003.

1636 Tandeo, P., Ailliot, P., Bocquet, M., Carrasi, A., Miyoshi, T., Pulido, M., and Zhen, Y. C.: A Review of Innovation-Based Methods to
1637 Jointly Estimate Model and Observation Error Covariance Matrices in Ensemble Data Assimilation, *Mon. Weather Rev.*, 148, 3973-
1638 3994, <https://doi.org/10.1175/mwr-d-19-0240.1>, 2020.

1639 Tang, M., Liu, Y., He, J., Wang, Z., Wu, Z., and Ji, D.: In situ continuous hourly observations of wintertime nitrate, sulfate and ammonium
1640 in a megacity in the North China plain from 2014 to 2019: Temporal variation, chemical formation and regional transport,
1641 *Chemosphere*, 262, <https://doi.org/10.1016/j.chemosphere.2020.127745>, 2021.

1642 Tang, X., Zhu, J., Wang, Z., Gbaguidi, A., Lin, C., Xin, J., Song, T., and Hu, B.: Limitations of ozone data assimilation with adjustment of
1643 NO_x emissions: mixed effects on NO₂ forecasts over Beijing and surrounding areas, *Atmos. Chem. Phys.*, 16, 6395-6405,
1644 <https://doi.org/10.5194/acp-16-6395-2016>, 2016.

1645 Tang, X., Zhu, J., Wang, Z., Wang, M., Gbaguidi, A., Li, J., Shao, M., Tang, G. Q., and Ji, D. S.: Inversion of CO emissions over Beijing
1646 and its surrounding areas with ensemble Kalman filter, *Atmos. Environ.*, 81, 676-686, <https://doi.org/10.1016/j.atmosenv.2013.08.051>,
1647 2013.

1648 Tegen, I., Lacis, A. A., and Fung, I.: The influence on climate forcing of mineral aerosols from disturbed soils, *Nature*, 380, 419-422,
1649 <https://doi.org/10.1038/380419a0>, 1996.

1650 van der Werf, G. R., Randerson, J. T., Giglio, L., Collatz, G. J., Mu, M., Kasibhatla, P. S., Morton, D. C., DeFries, R. S., Jin, Y., and van
1651 Leeuwen, T. T.: Global fire emissions and the contribution of deforestation, savanna, forest, agricultural, and peat fires (1997–2009),
1652 *Atmos. Chem. Phys.*, 10, 11707-11735, <https://doi.org/10.5194/acp-10-11707-2010>, 2010.

1653 von Schneidmesser, E., Monks, P. S., Allan, J. D., Bruhwiler, L., Forster, P., Fowler, D., Lauer, A., Morgan, W. T., Paasonen, P., Righi,
1654 M., Sindelarova, K., and Sutton, M. A.: Chemistry and the Linkages between Air Quality and Climate Change, *Chem. Rev.*, 115, 3856-
1655 3897, <https://doi.org/10.1021/acs.chemrev.5b00089>, 2015.

1656 Wang, S., Su, H., Chen, C., Tao, W., Streets, D. G., Lu, Z., Zheng, B., Carmichael, G. R., Lelieveld, J., Poeschl, U., and Cheng, Y.: Natural
1657 gas shortages during the "coal-to-gas" transition in China have caused a large redistribution of air pollution in winter 2017, *Proc. Natl.*
1658 *Acad. Sci. U.S.A.*, 117, 31018-31025, <https://doi.org/10.1073/pnas.2007513117>, 2020a.

1659 Wang, S. S., Yu, Y., Zhang, X. X., Lu, H. Y., Zhang, X. Y., and Xu, Z. W.: Weakened dust activity over China and Mongolia from 2001 to
1660 2020 associated with climate change and land-use management, *Environ. Res. Lett.*, 16, 12, <https://doi.org/10.1088/1748-9326/ac3b79>,
1661 2021.

1662 [Wang, X., Liang, X.-Z., Jiang, W., Tao, Z., Wang, J. X. L., Liu, H., Han, Z., Liu, S., Zhang, Y., Grell, G. A., and Peckham, S. E.: WRF-
1663 Chem simulation of East Asian air quality: Sensitivity to temporal and vertical emissions distributions, *Atmos. Environ.*, 44, 660-669,
1664 <https://doi.org/10.1016/j.atmosenv.2009.11.011>, 2010.](https://doi.org/10.1016/j.atmosenv.2009.11.011)

1665

1666 Wang, X. G. and Bishop, C. H.: A comparison of breeding and ensemble transform Kalman filter ensemble forecast schemes, *J. Atmos. Sci.*,
1667 60, 1140-1158, [https://doi.org/10.1175/1520-0469\(2003\)060<1140:Acobae>2.0.Co;2](https://doi.org/10.1175/1520-0469(2003)060<1140:Acobae>2.0.Co;2), 2003.

1668 Wang, X. Y., Lei, Y., Yan, L., Liu, T., Zhang, Q., and He, K. B.: A unit-based emission inventory of SO₂, NO_x and PM for the Chinese
1669 iron and steel industry from 2010 to 2015, *Sci. Total Environ.*, 676, 18-30, <https://doi.org/10.1016/j.scitotenv.2019.04.241>, 2019a.

1670 Wang, Y. C., Li, X., Wang, Q. Y., Zhou, B. H., Liu, S. X., Tian, J., Hao, Q., Li, G. H., Han, Y. M., Ho, S. S. H., and Cao, J. J.: Response of
1671 aerosol composition to the clean air actions in Baoji city of Fen-Wei River Basin, *Environ. Res.*, 210, 10,
1672 <https://doi.org/10.1016/j.envres.2022.112936>, 2022.

1673 Wang, Y. H., Gao, W. K., Wang, S., Song, T., Gong, Z. Y., Ji, D. S., Wang, L. L., Liu, Z. R., Tang, G. Q., Huo, Y. F., Tian, S. L., Li, J. Y.,
1674 Li, M. G., Yang, Y., Chu, B. W., Petaja, T., Kerminen, V. M., He, H., Hao, J. M., Kulmala, M., Wang, Y. S., and Zhang, Y. H.:
1675 Contrasting trends of PM_{2.5} and surface-ozone concentrations in China from 2013 to 2017, *Natl. Sci. Rev.*, 7, 1331-1339,
1676 <https://doi.org/10.1093/nsr/nwaa032>, 2020b.

1677 Wang, Y. S., Li, W. J., Gao, W. K., Liu, Z. R., Tian, S. L., Shen, R. R., Ji, D. S., Wang, S., Wang, L. L., Tang, G. Q., Song, T., Cheng, M.
1678 T., Wang, G. H., Gong, Z. Y., Hao, J. M., and Zhang, Y. H.: Trends in particulate matter and its chemical compositions in China from
1679 2013-2017, *Sci. China-Earth Sci.*, 62, 1857-1871, <https://doi.org/10.1007/s11430-018-9373-1>, 2019b.

1680 Wu, C. L., Lin, Z. H., Shao, Y. P., Liu, X. H., and Li, Y.: Drivers of recent decline in dust activity over East Asia, *Nat. Commun.*, 13, 10,
1681 <https://doi.org/10.1038/s41467-022-34823-3>, 2022.

1682

1683 World Health Organization (WHO): Ambient air pollution: a global assessment of exposure and burden of disease,
1684 <https://www.who.int/publications/i/item/9789241511353>, last access: 16 November 2023.

1685 Wu, H., Tang, X., Wang, Z., Wu, L., Li, J., Wang, W., Yang, W., and Zhu, J.: High-spatiotemporal-resolution inverse estimation of CO and
1686 NO_x emission reductions during emission control periods with a modified ensemble Kalman filter, *Atmos. Environ.*, 236, 117631,
1687 <https://doi.org/10.1016/j.atmosenv.2020.117631>, 2020a.

1688 Wu, H. J., Tang, X., Wang, Z. F., Wu, L., Lu, M. M., Wei, L. F., and Zhu, J.: Probabilistic Automatic Outlier Detection for Surface Air
1689 Quality Measurements from the China National Environmental Monitoring Network, *Adv. Atmos. Sci.*, 35, 1522-1532,
1690 <https://doi.org/10.1007/s00376-018-8067-9>, 2018.

1691 Wu, J., Kong, S. F., Wu, F. Q., Cheng, Y., Zheng, S. R., Qin, S., Liu, X., Yan, Q., Zheng, H., Zheng, M. M., Yan, Y. Y., Liu, D. T., Ding,
1692 S., Zhao, D. L., Shen, G. F., Zhao, T. L., and Qi, S. H.: The moving of high emission for biomass burning in China: View from multi-
1693 year emission estimation and human-driven forces, *Environ. Int.*, 142, 17, <https://doi.org/10.1016/j.envint.2020.105812>, 2020b.

1694 [Xing, J., Li, S. W., Jiang, Y. Q., Wang, S. X., Ding, D., Dong, Z. X., Zhu, Y., and Hao, J. M.: Quantifying the emission changes and](https://doi.org/10.5194/acp-20-14347-2020)
1695 [associated air quality impacts during the COVID-19 pandemic on the North China Plain: a response modeling study, *Atmos. Chem.*](https://doi.org/10.5194/acp-20-14347-2020)
1696 [Phys., 20, 14347-14359, <https://doi.org/10.5194/acp-20-14347-2020>, 2020.](https://doi.org/10.5194/acp-20-14347-2020)

1697

1698 Xu, Q., Wang, S., Jiang, J., Bhattarai, N., Li, X., Chang, X., Qiu, X., Zheng, M., Hua, Y., and Hao, J.: Nitrate dominates the chemical
1699 composition of PM_{2.5} during haze event in Beijing, China, *Sci. Total Environ.*, 689, 1293-1303,
1700 <https://doi.org/10.1016/j.scitotenv.2019.06.294>, 2019a.

1701 Xu, W., Sun, Y., Wang, Q., Zhao, J., Wang, J., Ge, X., Xie, C., Zhou, W., Du, W., Li, J., Fu, P., Wang, Z., Worsnop, D. R., and Coe, H.:
1702 Changes in Aerosol Chemistry From 2014 to 2016 in Winter in Beijing: Insights From High-Resolution Aerosol Mass Spectrometry,
1703 *J. Geophys. Res.-Atmos.*, 124, 1132-1147, <https://doi.org/10.1029/2018JD029245>, 2019b.

1704 Xu, Y., Huang, Z., Ye, J., and Zheng, J.: Hourly emissions of air pollutants and greenhouse gases from open biomass burning in China
1705 during 2016–2020, *Sci. Data*, 10, 629, <https://doi.org/10.1038/s41597-023-02541-0>, 2023.

1706 Yan, X. Y., Akimoto, H., and Ohara, T.: Estimation of nitrous oxide, nitric oxide and ammonia emissions from croplands in East, Southeast
1707 and South Asia, *Glob. Change Biol.*, 9, 1080-1096, <https://doi.org/10.1046/j.1365-2486.2003.00649.x>, 2003.

1708 Yin, L., Du, P., Zhang, M., Liu, M., Xu, T., and Song, Y.: Estimation of emissions from biomass burning in China (2003–2017) based on
1709 MODIS fire radiative energy data, *Biogeosciences*, 16, 1629-1640, <https://doi.org/10.5194/bg-16-1629-2019>, 2019.

1710 Zeng, Y., Wang, M., Zhao, C., Chen, S., Liu, Z., Huang, X., and Gao, Y.: WRF-Chem v3.9 simulations of the East Asian dust storm in May
1711 2017: modeling sensitivities to dust emission and dry deposition schemes, *Geosci. Model Dev.*, 13, 2125-2147,
1712 <https://doi.org/10.5194/gmd-13-2125-2020>, 2020.

1713 Zhang, Z. Y., Guan, H., Luo, L., Zheng, N. J., and Xiao, H. Y.: Response of fine aerosol nitrate chemistry to Clean Air Action in winter
1714 Beijing: Insights from the oxygen isotope signatures, *Sci. Total Environ.*, 746, 8, <https://doi.org/10.1016/j.scitotenv.2020.141210>, 2020.

1715 Zheng, B., Chevallier, F., Yin, Y., Ciais, P., Fortems-Cheiney, A., Deeter, M. N., Parker, R. J., Wang, Y. L., Worden, H. M., and Zhao, Y.
1716 H.: Global atmospheric carbon monoxide budget 2000-2017 inferred from multi-species atmospheric inversions, *Earth Syst. Sci. Data*,
1717 11, 1411-1436, <https://doi.org/10.5194/essd-11-1411-2019>, 2019.

1718 Zheng, B., Tong, D., Li, M., Liu, F., Hong, C. P., Geng, G. N., Li, H. Y., Li, X., Peng, L. Q., Qi, J., Yan, L., Zhang, Y. X., Zhao, H. Y.,
1719 Zheng, Y. X., He, K. B., and Zhang, Q.: Trends in China's anthropogenic emissions since 2010 as the consequence of clean air actions,
1720 *Atmos. Chem. Phys.*, 18, 14095-14111, <https://doi.org/10.5194/acp-18-14095-2018>, 2018.

1721 Zheng, Y. X., Xue, T., Zhang, Q., Geng, G. N., Tong, D., Li, X., and He, K. B.: Air quality improvements and health benefits from China's
1722 clean air action since 2013, *Environ. Res. Lett.*, 12, 9, <https://doi.org/10.1088/1748-9326/aa8a32>, 2017.

1723 Zhong, Q., Tao, S., Ma, J., Liu, J., Shen, H., Shen, G., Guan, D., Yun, X., Meng, W., Yu, X., Cheng, H., Zhu, D., Wan, Y., and Hu, J.: PM_{2.5}
1724 reductions in Chinese cities from 2013 to 2019 remain significant despite the inflating effects of meteorological conditions, *One Earth*,
1725 4, 448-458, <https://doi.org/10.1016/j.oneear.2021.02.003>, 2021.

1726 Zhou, M., Nie, W., Qiao, L., Huang, D. D., Zhu, S., Lou, S., Wang, H., Wang, Q., Tao, S., Sun, P., Liu, Y., Xu, Z., An, J., Yan, R., Su, H.,
1727 Huang, C., Ding, A., and Chen, C.: Elevated Formation of Particulate Nitrate From N₂O₅ Hydrolysis in the Yangtze River Delta
1728 Region From 2011 to 2019, *Geophys. Res. Lett.*, 49, e2021GL097393, <https://doi.org/10.1029/2021GL097393>, 2022a.

1729 Zhou, W., Lei, L., Du, A. D., Zhang, Z. Q., Li, Y., Yang, Y., Tang, G. Q., Chen, C., Xu, W. Q., Sun, J. X., Li, Z. J., Fu, P. Q., Wang, Z. F.,
1730 and Sun, Y. L.: Unexpected Increases of Severe Haze Pollution During the Post COVID-19 Period: Effects of Emissions, Meteorology,
1731 and Secondary Production, *J. Geophys. Res.-Atmos.*, 127, 14, <https://doi.org/10.1029/2021jd035710>, 2022b.

1732 Zhou, W., Gao, M., He, Y., Wang, Q. Q., Xie, C. H., Xu, W. Q., Zhao, J., Du, W., Qiu, Y. M., Lei, L., Fu, P. Q., Wang, Z. F., Worsnop, D.
1733 R., Zhang, Q., and Sun, Y. L.: Response of aerosol chemistry to clean air action in Beijing, China: Insights from two-year ACSM
1734 measurements and model simulations, *Environ. Pollut.*, 255, 11, <https://doi.org/10.1016/j.envpol.2019.113345>, 2019.
1735

Supplementary Material

Text S1: Assessment of the influences of site differences on the emission inversions

The emission increments at the observation sites (a posteriori minus a priori) for different species in China from 2013 to 2015 under the scenarios of fixed observation sites (blue lines) and varying observation sites (orange) were calculated to assess the influences of the site differences on the emission inversions (Fig. S2). In the fixed-site scenario, it is assumed that the number of observation sites remains constant at the 2013 level while in the varying-site scenario, the number of observation sites increases over time. The differences in emission increments between these two scenarios are used to analyze the impact of changes in the observation coverage on the emission inversions. Please note that, to simplify calculations, we only computed the emission increments at the locations of observation sites. Therefore, they may not be equal to the emission increments calculated for the entire grid as reported in the paper. However, they are still useful indicators for the effects of emission inversion. In addition, since we did not consider the temporal variation in the a priori emissions, the changes of the emission increments can be used to approximate the temporal variations of the a posterior emissions. It can be clearly seen that there are obvious differences in the emission increments between the two scenarios. The emission increment is larger in the varying-site scenario than that in the fixed-site scenario for all species due to the increases of observation sites. Moreover, as indicated in Fig. S2, the changes of observation sites were shown to significantly affect the estimation of the emission trend in 2013 and 2014. Most of species showed decreasing trends in their inversed emission under the fixed-site scenario. However, under the varying-site scenario, the decreasing trends were smaller for PM_{2.5}, NO_x and NMVOC, and the emissions of PM₁₀ and CO even showed increasing trends. This is due to that the emission increments were positive over most of observation sites for these species as demonstrated in Fig.3. Thus, the increases of observation site would lead to increases of positive emission increments and higher a posteriori emissions, which may counteract the decreasing trends or even lead to an opposite trend. These results provide the evidences that the increasing trends in the total emissions of PM₁₀ and CO from 2013 to 2015 seen in Fig. 6 and Fig. 7 are highly likely to be a spurious trend caused by the changes of observation coverage. The weak emission changes in PM_{2.5} and NO_x (Fig. 6 and Fig. 7) may also be related to the changes in the number of observation sites. The SO₂ emission is an except that its calculated trend is larger under the varying-site scenario than that under the fixed-site scenario. This is because that the emission increment for the SO₂ is generally negative over the most sites, thus the increased observation sites would lead to larger decreasing trend in the inversed emissions of SO₂. To date, these results highlighted the significant influences of the site differences on the estimated emissions and their trends. Therefore, we recommend not to use the emission in 2013 and 2014 when analyze the trends of the emissions.

Table S1 The average mean (standard deviation) of the calculated factor for the inflation of the ensemble member over different regions of China for different species

	<u>NCP</u>	<u>NE</u>	<u>SE</u>	<u>SW</u>	<u>NW</u>	<u>Central</u>
<u>PM_{2.5}</u>	<u>1.0 (0.2)</u>	<u>1.7 (1.6)</u>	<u>1.0 (0.0)</u>	<u>6.8 (8.5)</u>	<u>3.1 (3.8)</u>	<u>3.9 (3.9)</u>
<u>PM₁₀</u>	<u>1.4 (0.7)</u>	<u>7.2 (8.0)</u>	<u>2.4 (0.8)</u>	<u>78.1 (108.2)</u>	<u>26.3 (36.5)</u>	<u>36.0 (49.0)</u>
<u>SO₂</u>	<u>1.4 (0.7)</u>	<u>4.1 (3.2)</u>	<u>2.3 (0.8)</u>	<u>176.1 (254.6)</u>	<u>7.8 (6.5)</u>	<u>58.6 (72.5)</u>
<u>NO_x</u>	<u>1.0 (0.1)</u>	<u>1.7 (0.7)</u>	<u>1.2 (0.3)</u>	<u>8.1 (5.3)</u>	<u>2.8 (1.3)</u>	<u>5.4 (4.1)</u>
<u>CO</u>	<u>1.0 (0.1)</u>	<u>2.8 (2.3)</u>	<u>1.4 (0.4)</u>	<u>18.8 (16.8)</u>	<u>6.8 (6.9)</u>	<u>8.6 (10.0)</u>
<u>NMVOC</u>	<u>1.4 (0.6)</u>	<u>4.5 (4.4)</u>	<u>1.6 (0.5)</u>	<u>8.1 (8.6)</u>	<u>6.5 (5.8)</u>	<u>8.1 (10.1)</u>

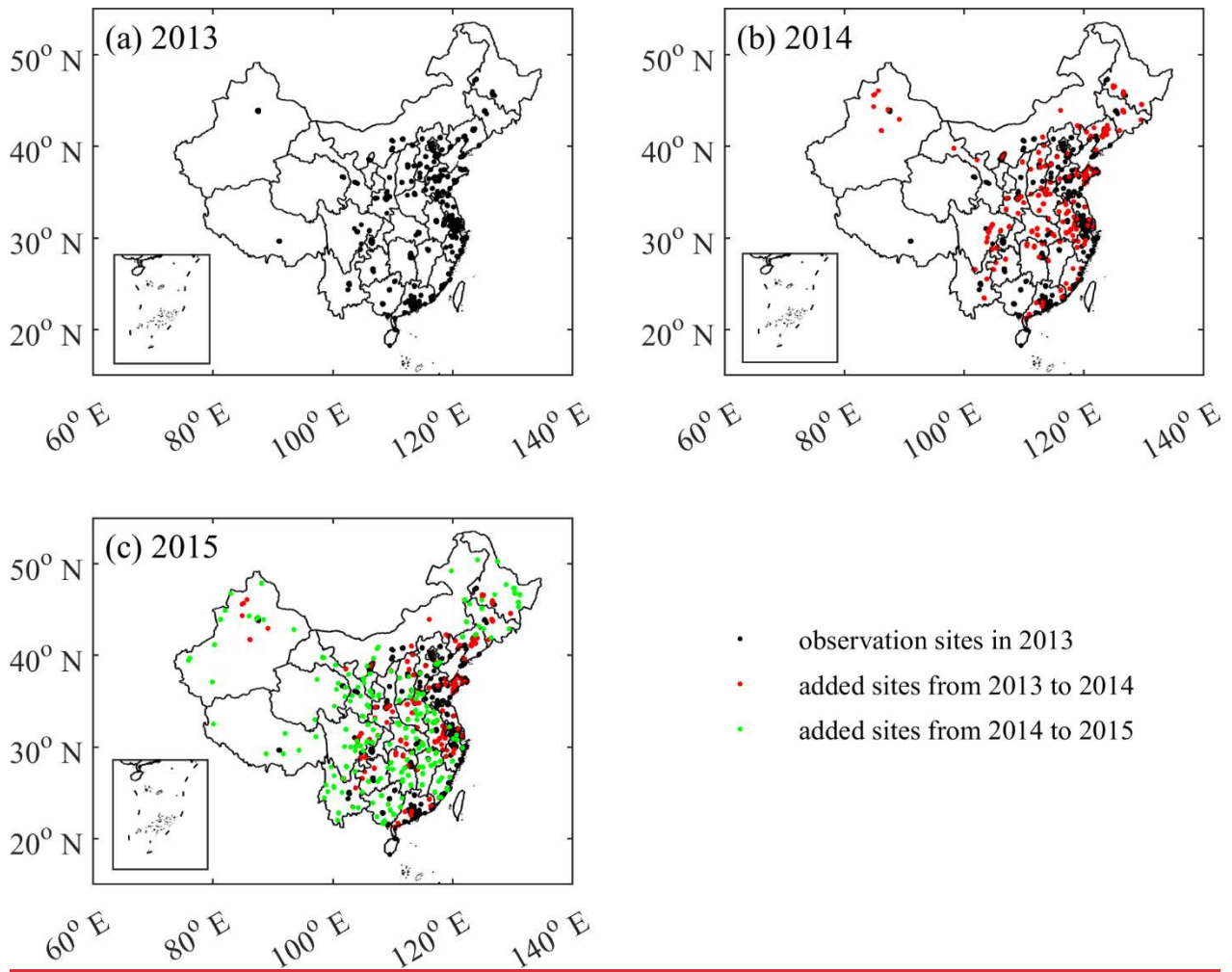


Figure S1: Spatial distributions of observation sites in (a) 2013, (b) 2014 and (c) 2015. The observation sites in 2013 were marked as black dots, while the added observation sites from 2013 to 2014 and those from 2014 to 2015 were marked as red and green dots, respectively.

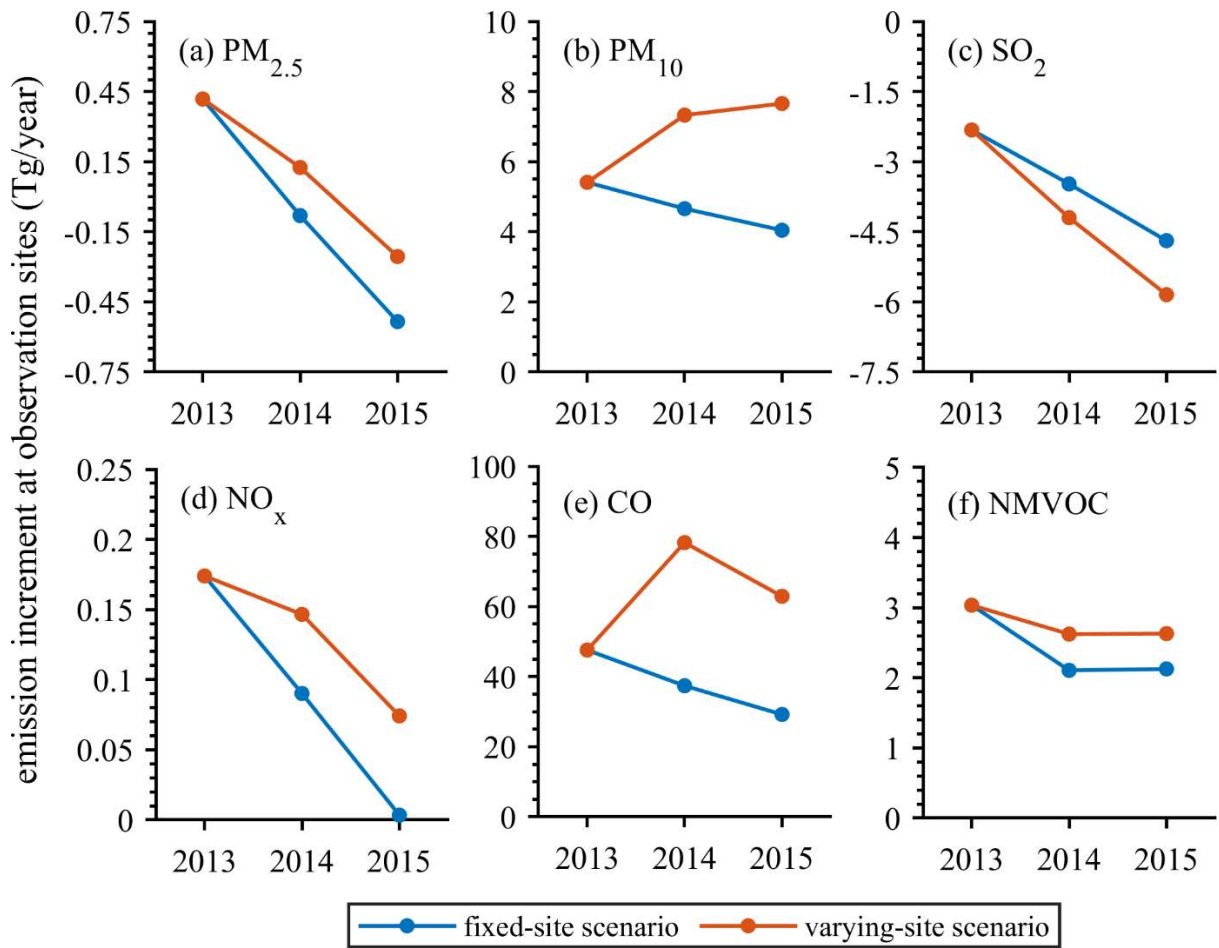


Figure S2: The calculated total emission increments at the observation sites for different species under the fixed-site scenario and varying-site scenario.

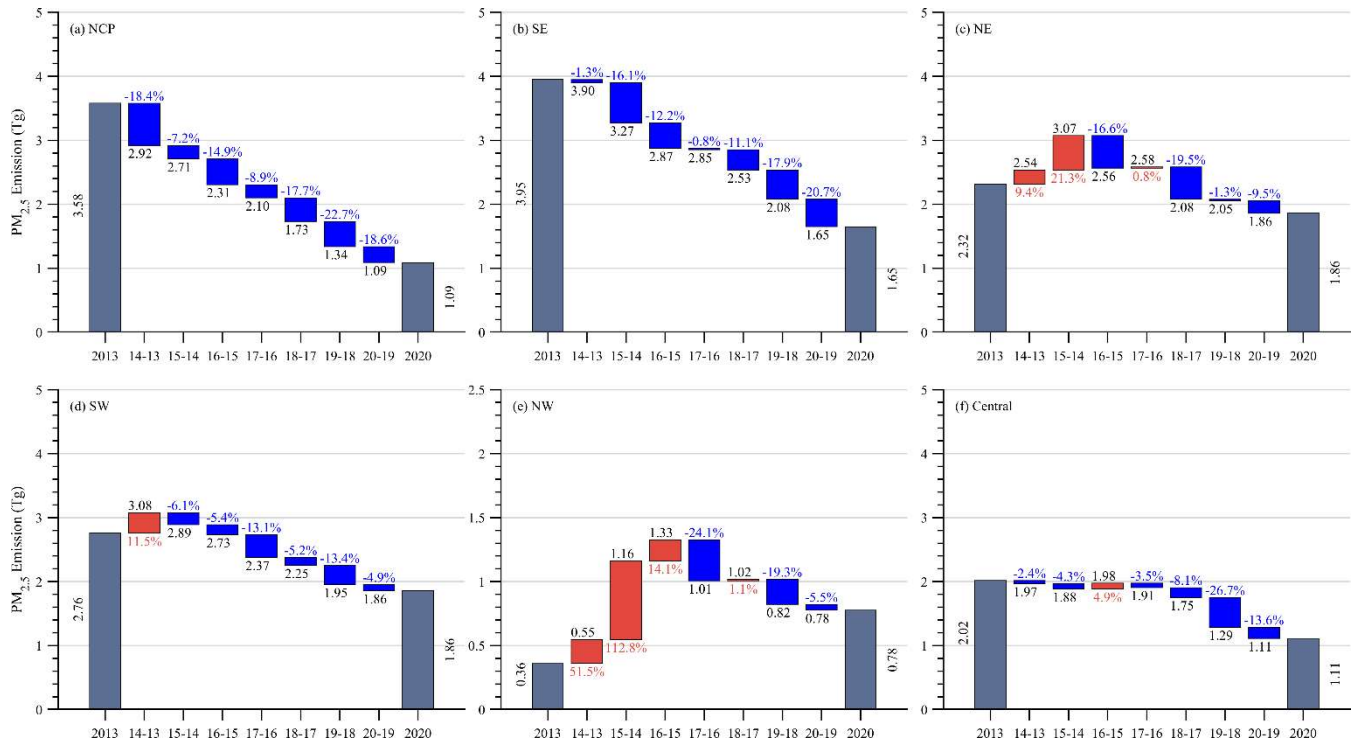


Figure S31: Emission changes of PM_{2.5} from 2013 to 2020 over different regions of China obtained from CAQIEL.

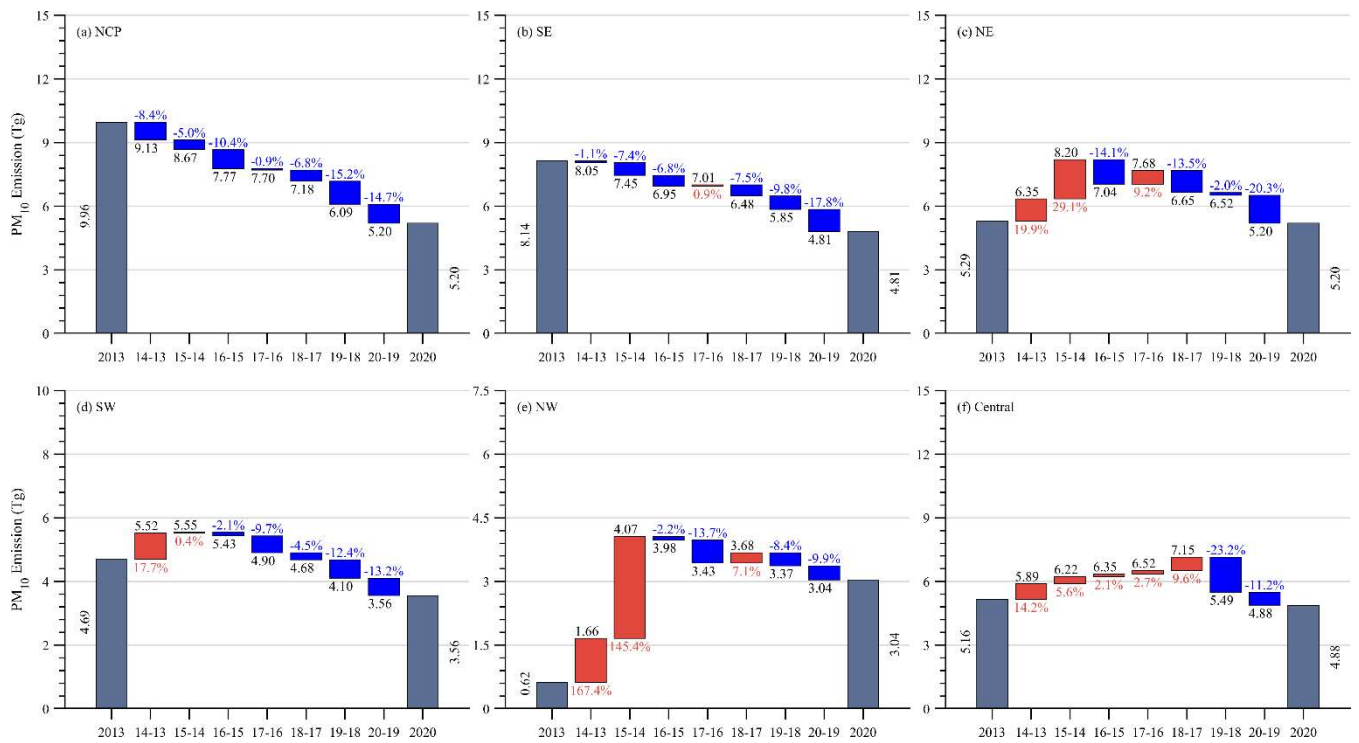


Figure S42: Same as Fig. S31 but for PM₁₀.

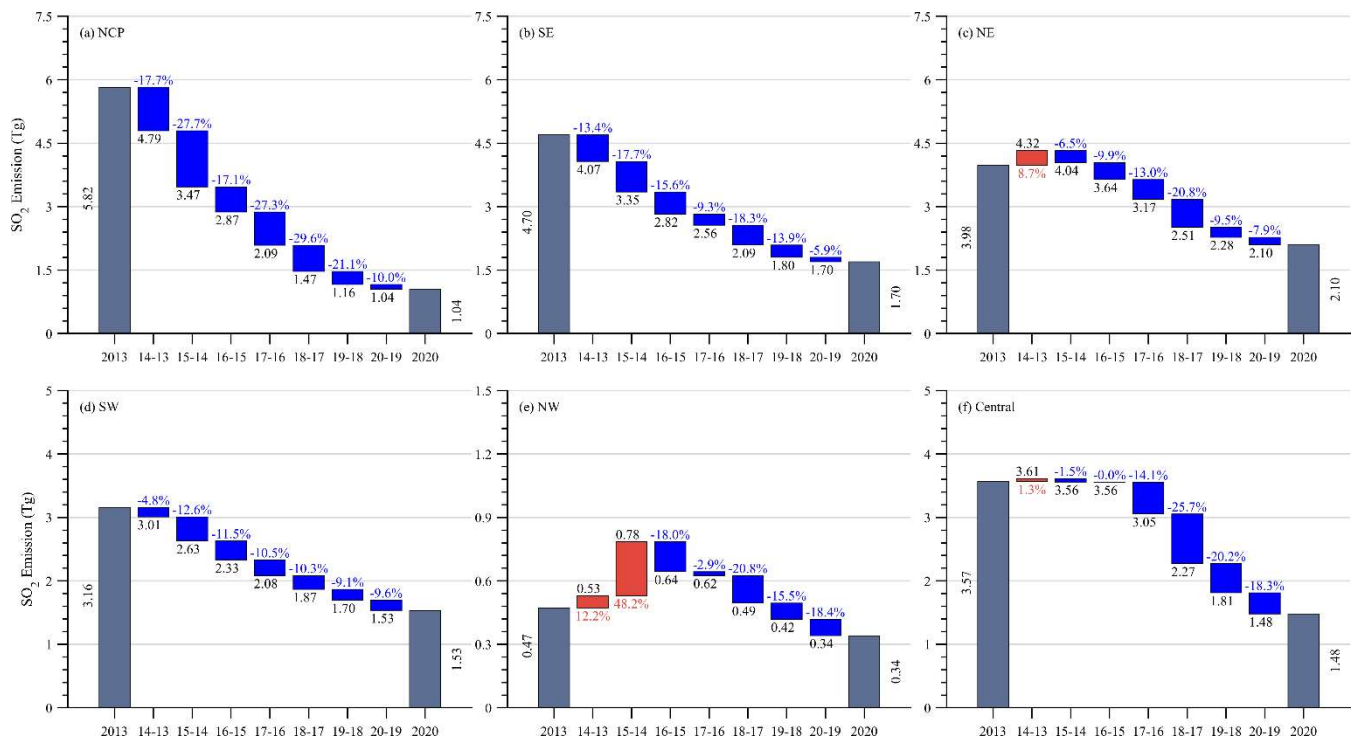


Figure S53: Same as Fig. S31 but for SO₂.

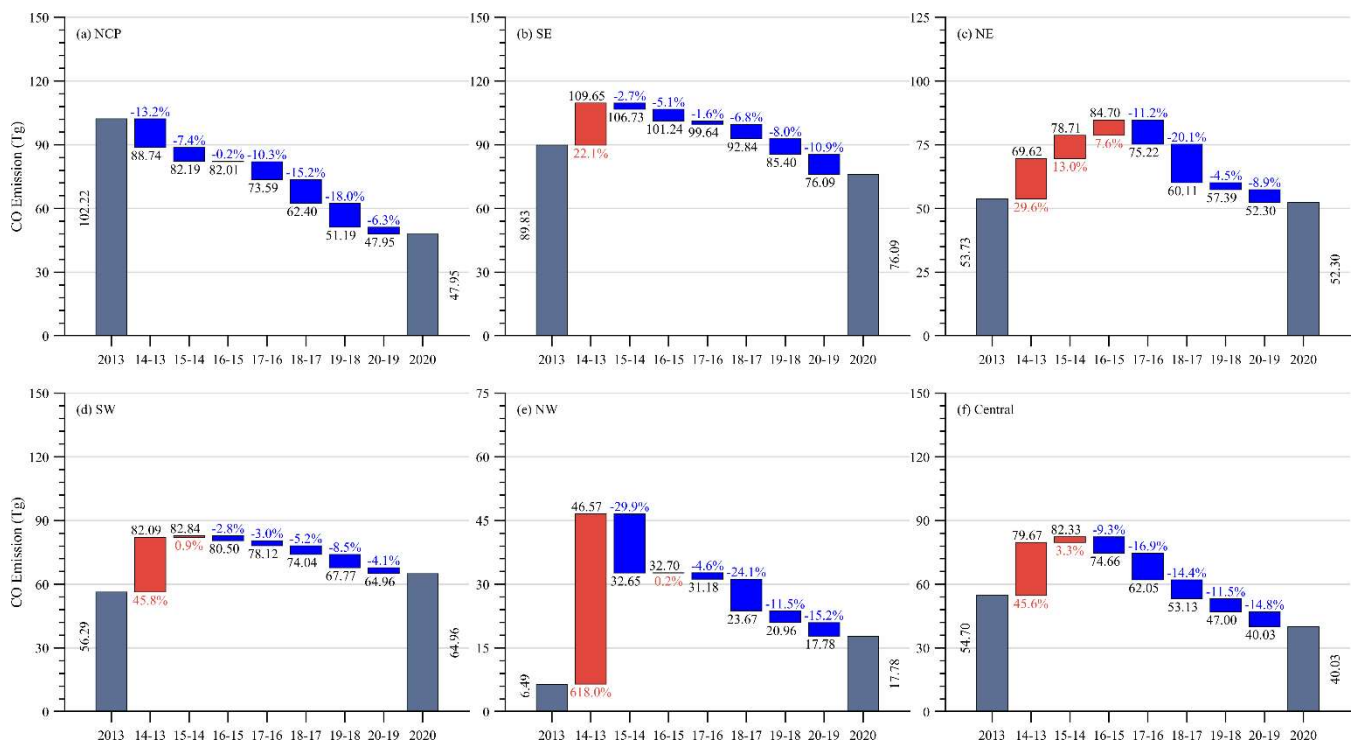


Figure S64: Same as Fig. S31 but for CO.

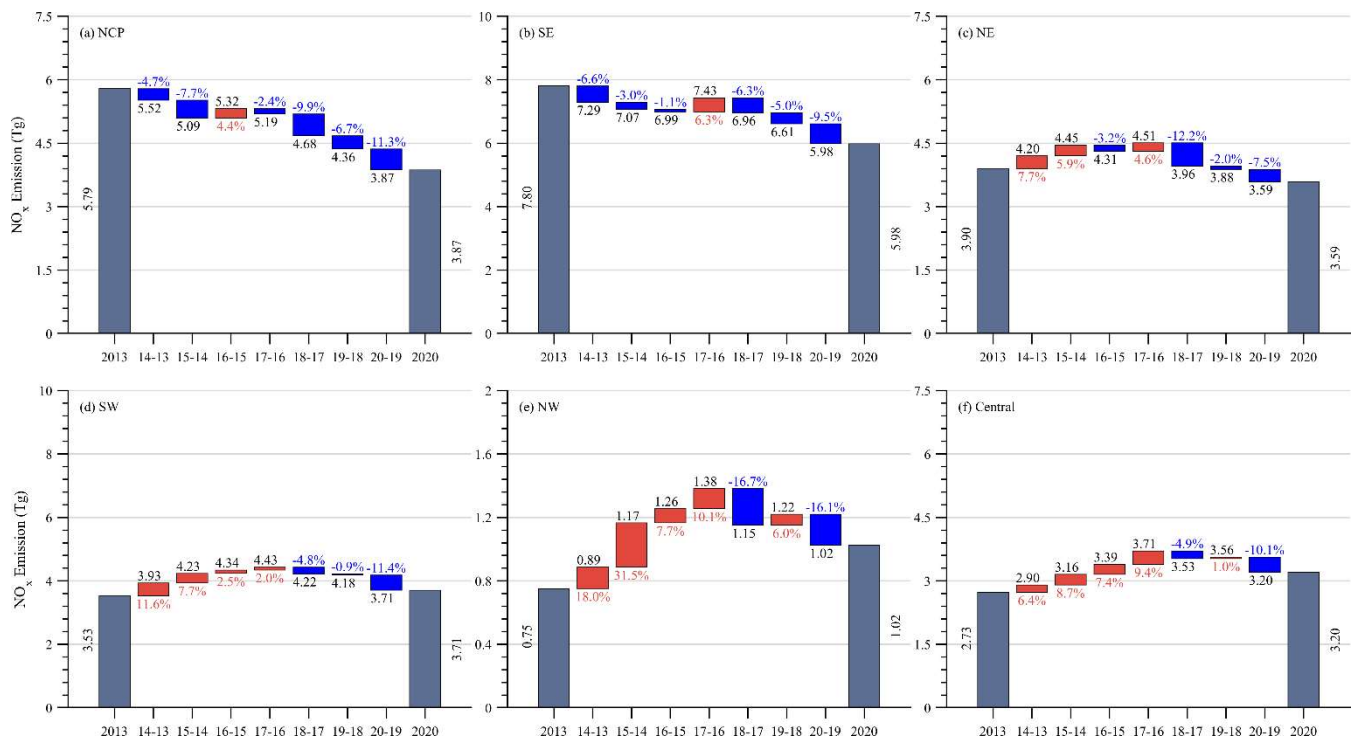


Figure S75: Same as Fig. S31 but for NO_x.

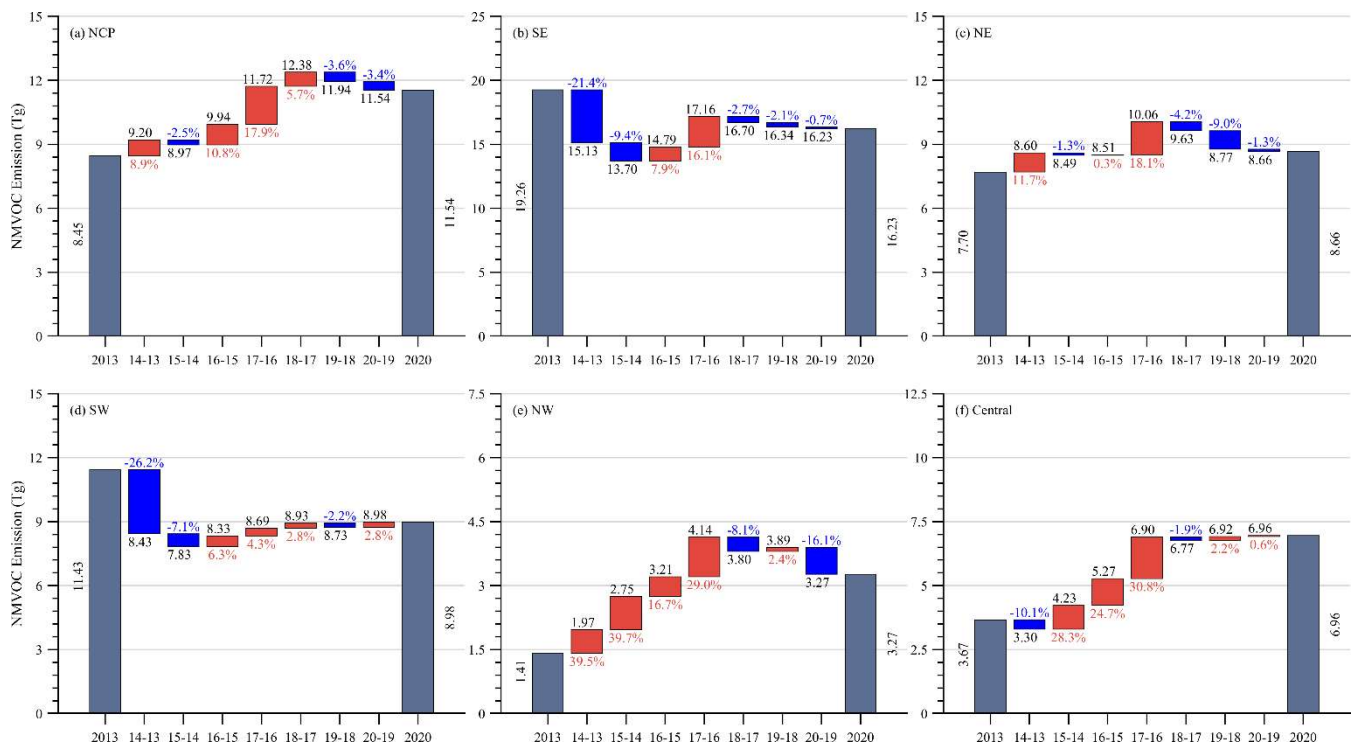


Figure S86: Same as Fig. S31 but for NMVOC.

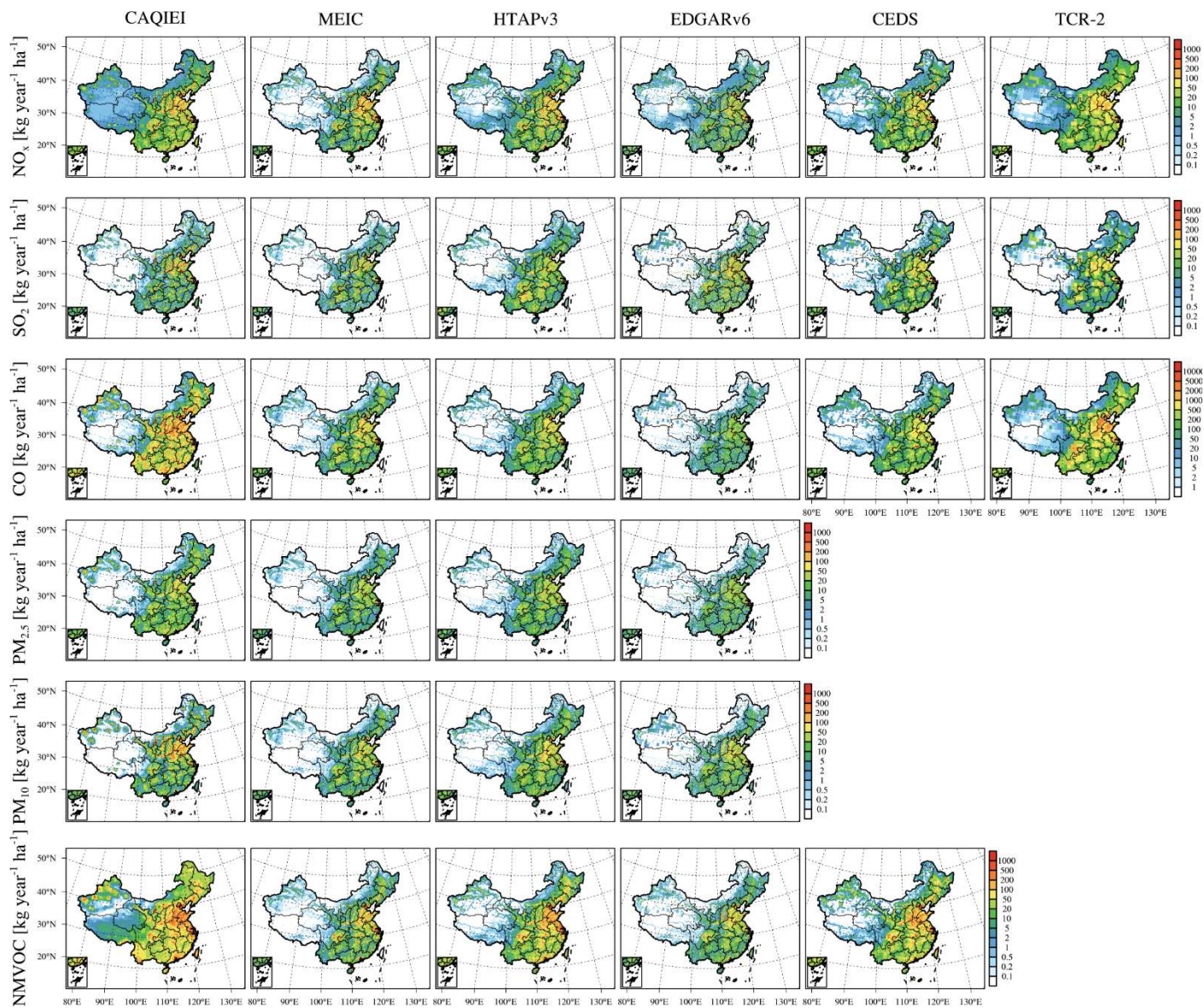


Figure S9: Spatial distributions of the averaged emissions of different air pollutants in China during 2015–2018 obtained from CAQIEI, MEIC, HTAPv3, EDGARv6, CEDS and TCR-2. Note the due to absence of gridded products of the ABaCAS inventory, we did not provide its spatial distributions. Also, the natural sources were not added to the previous emission inventories in this figure because of the different spatial resolutions among these inventories.

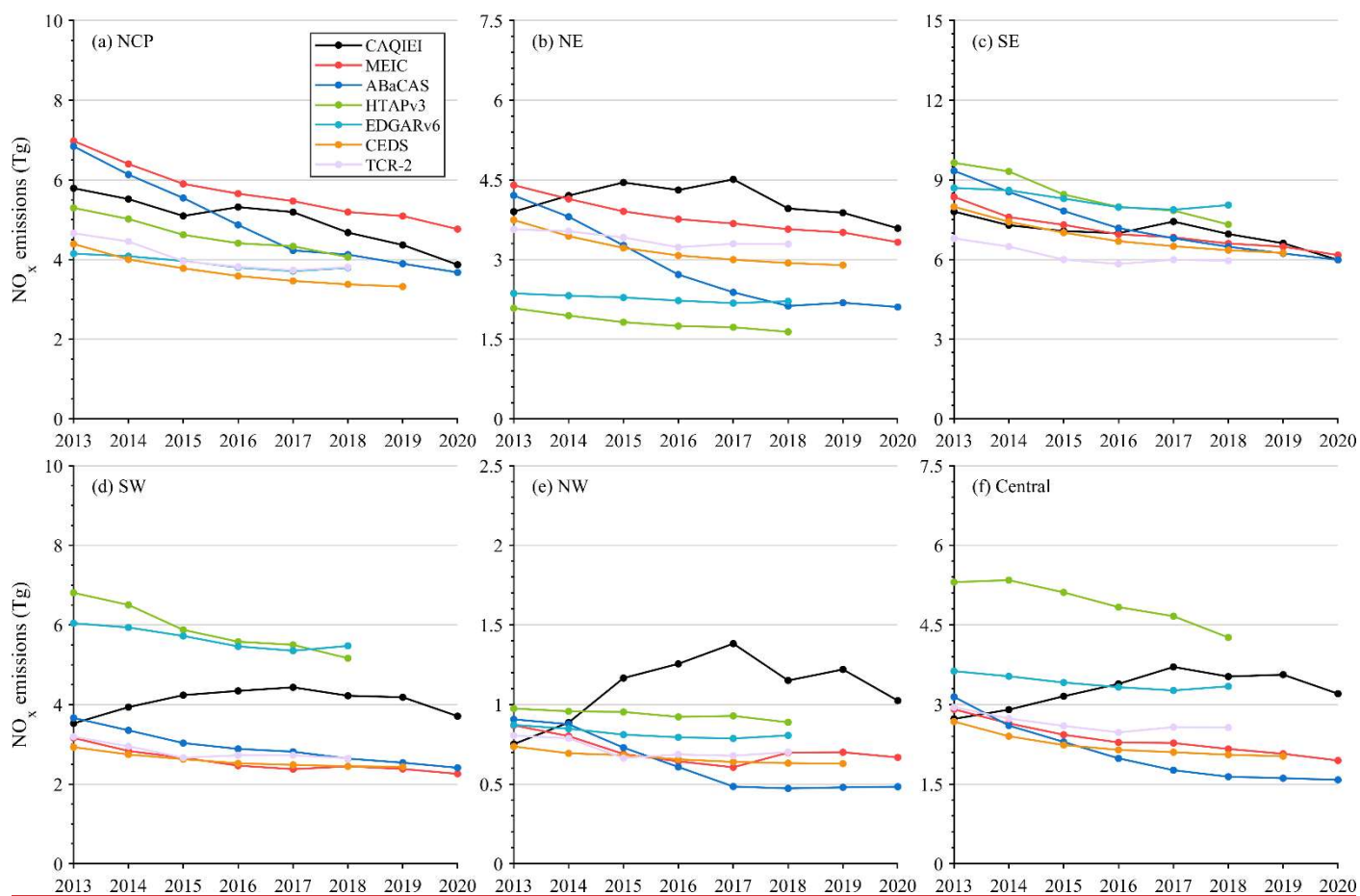


Figure S10: Time series of annual NO_x emissions over of different regions of China: (a) NCP, (b) NE, (c) SE, (d) SW, (e) NW and (f) Central from 2013 to 2020 obtained from CAQIEI and previous inventories. Note that the natural sources were not included in the previous inventories in this figure.

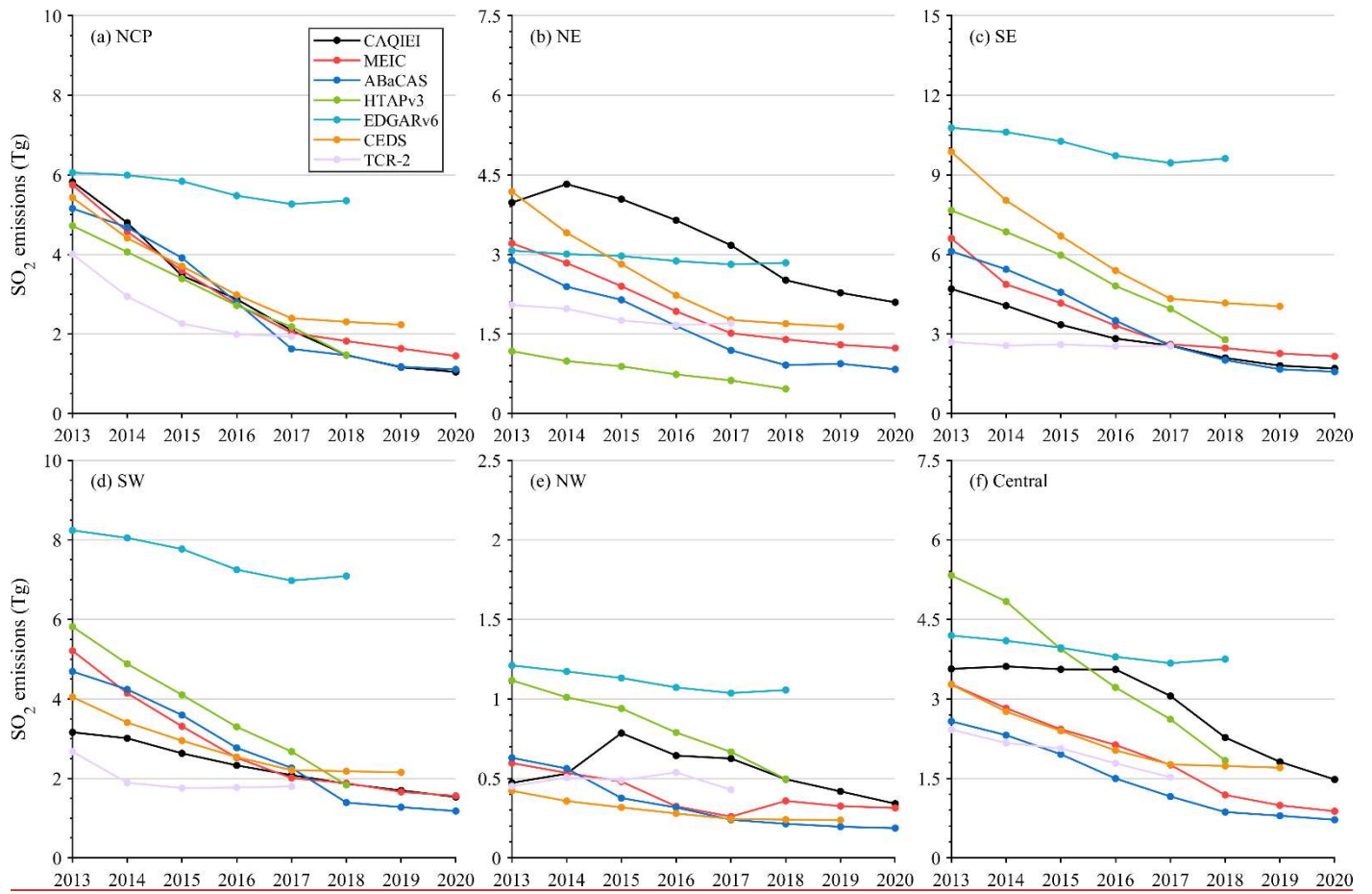


Figure S11: Same as Fig. S10 but for SO₂.

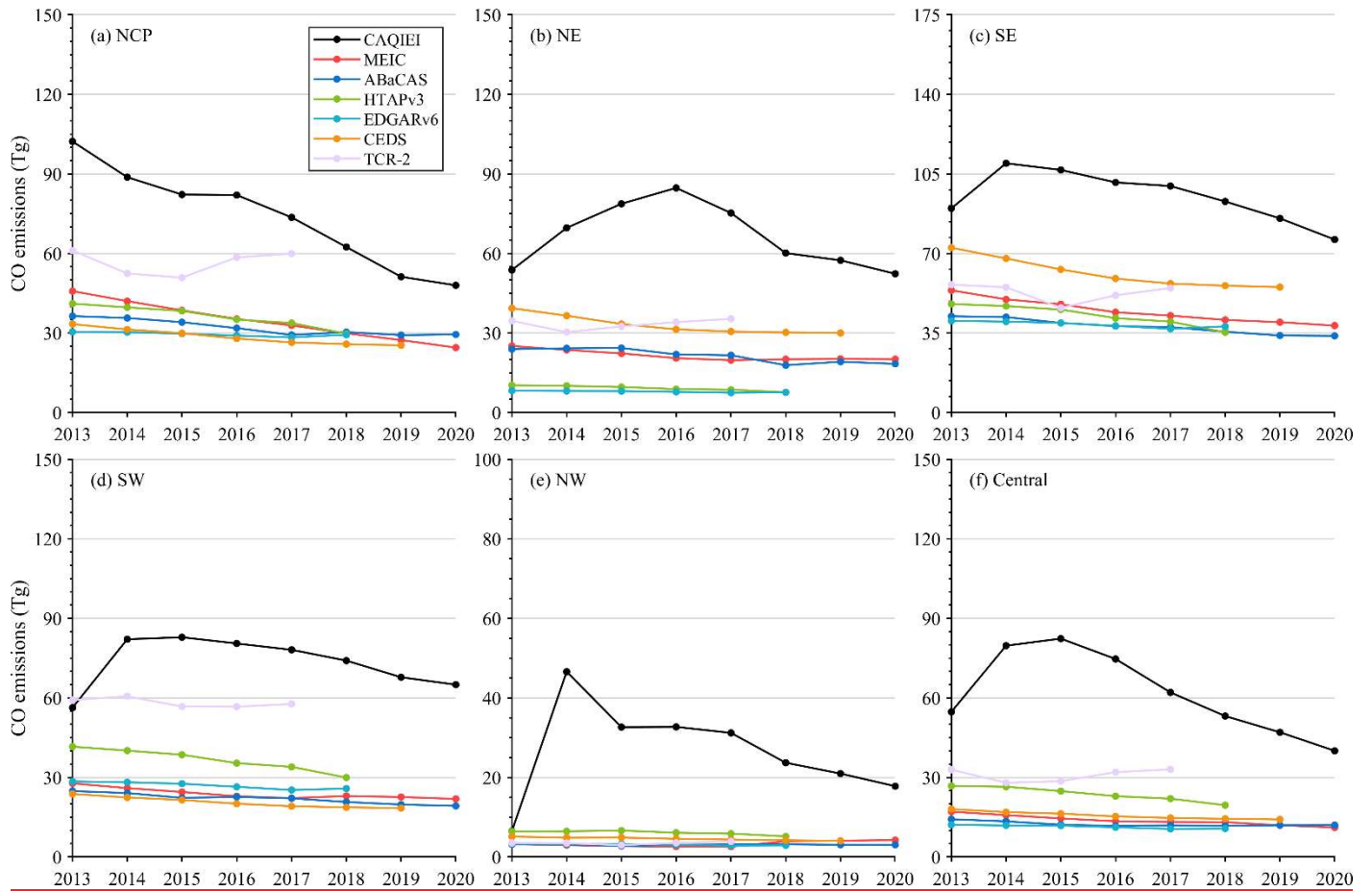


Figure S12: Same as Fig. S10 but for CO.

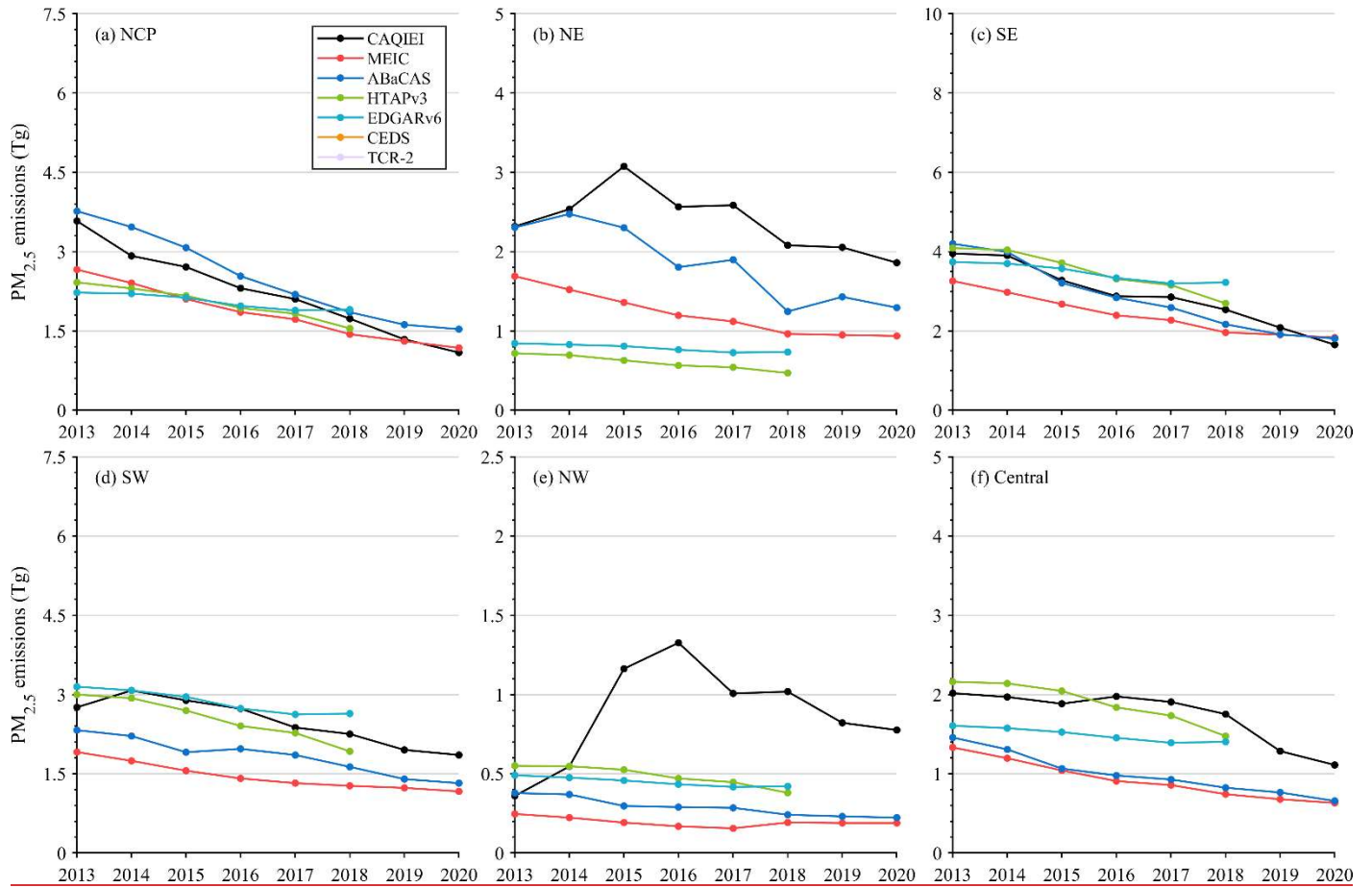


Figure S13: Same as Fig. S10 but for PM_{2.5}.

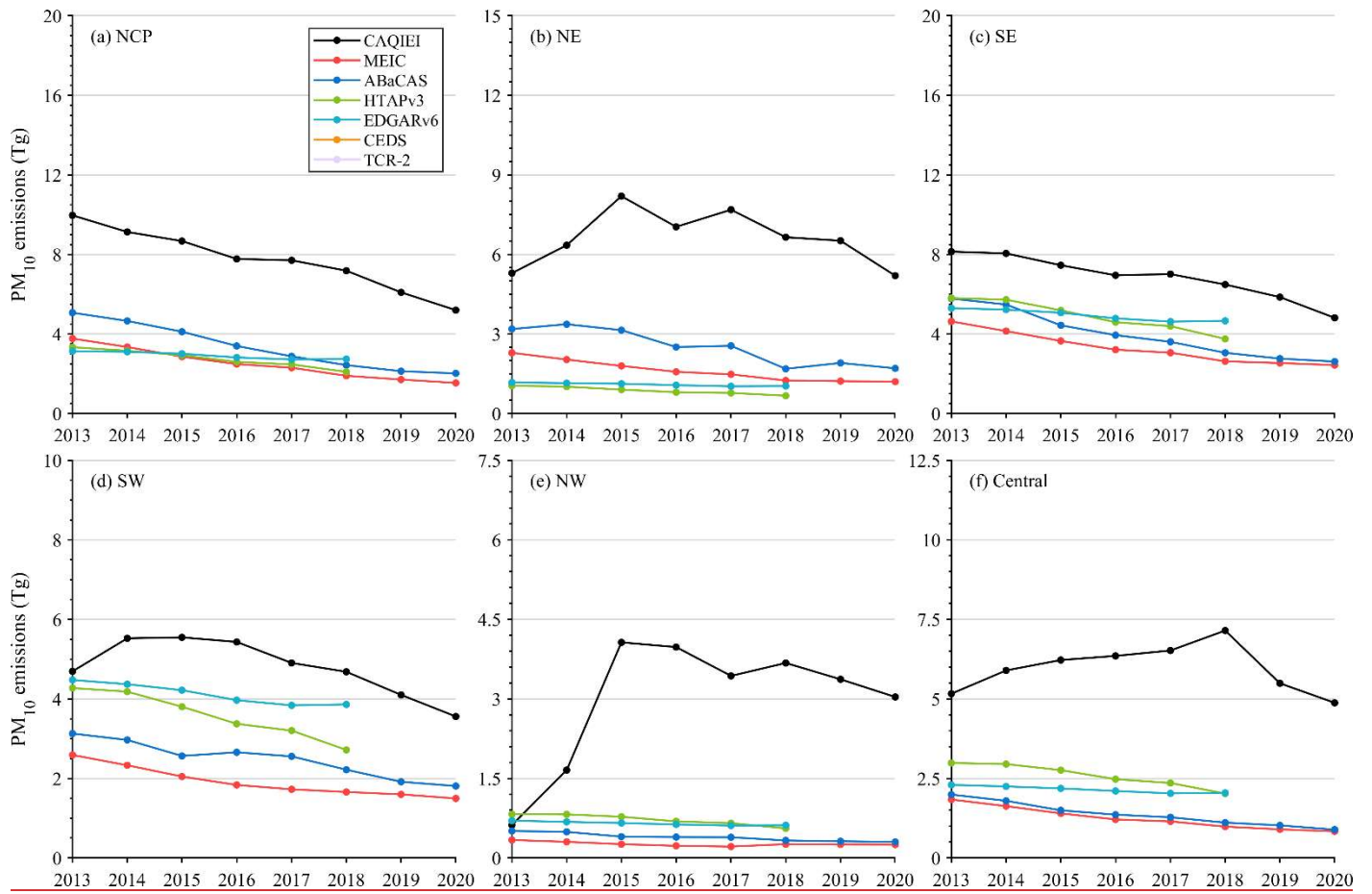


Figure S14: Same as Fig. S10 but for PM₁₀

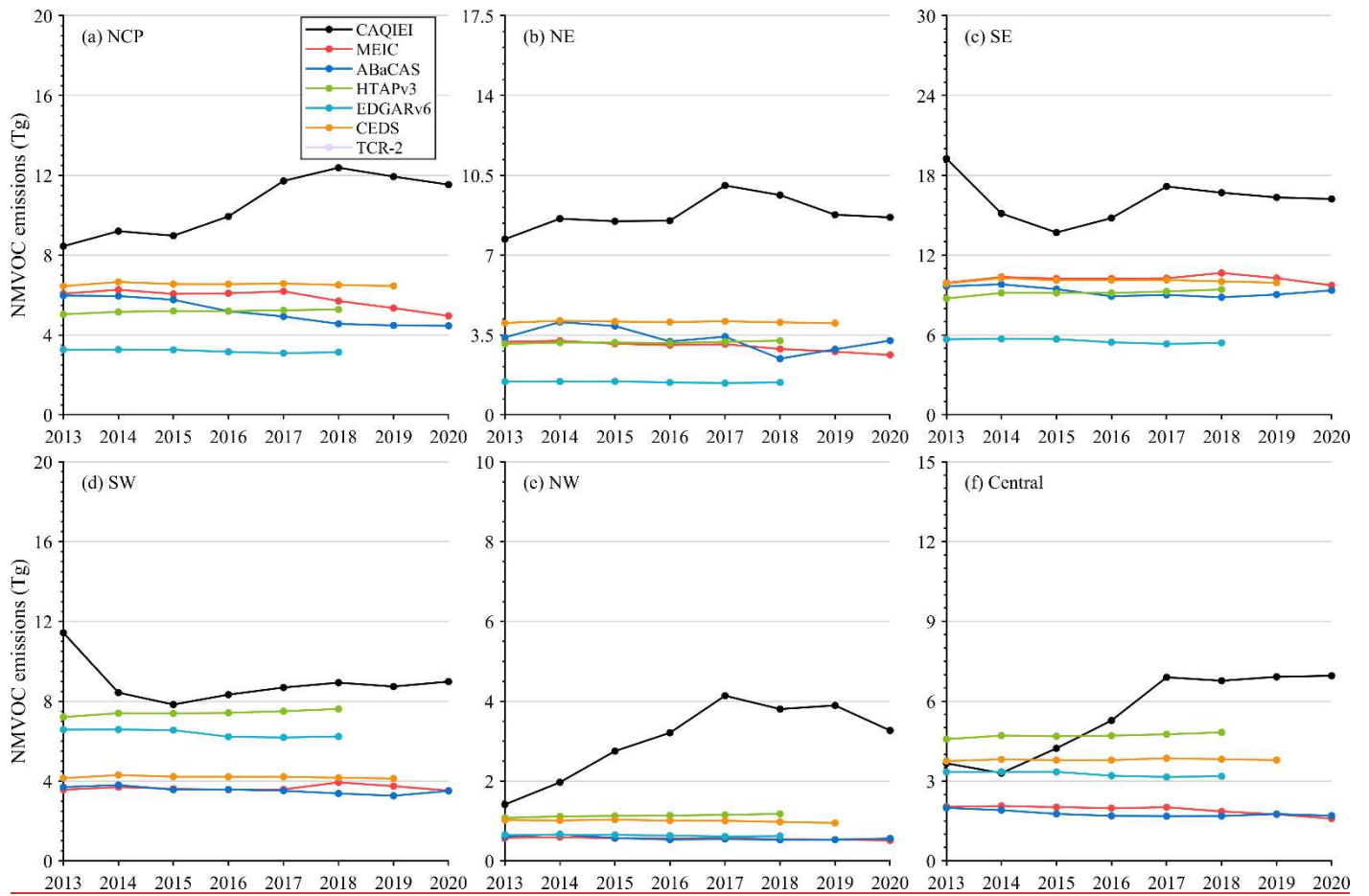


Figure S15: Same as Fig. S10 but for NMVOC.

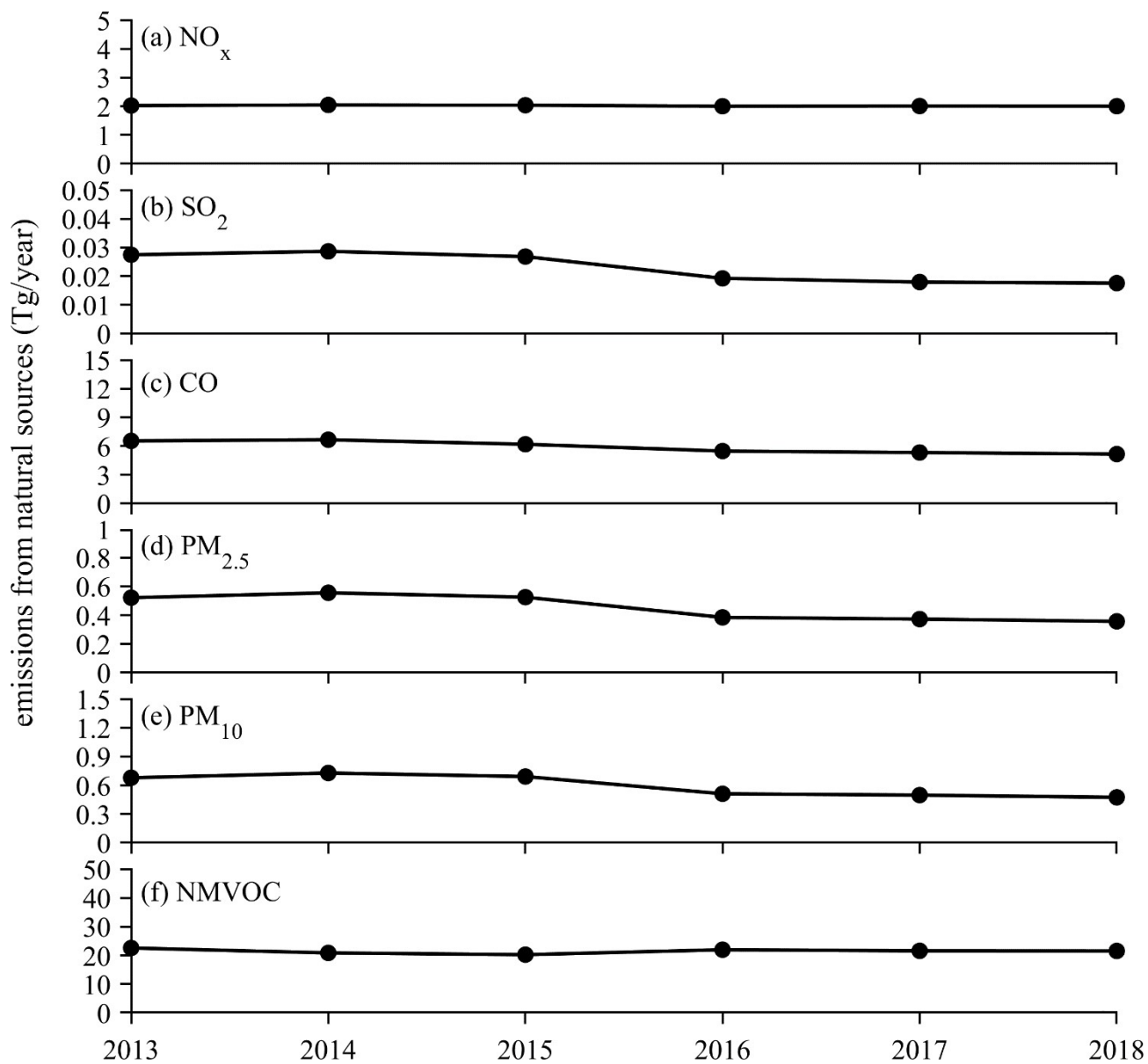


Figure S167: Time series of annual natural emissions of (a) NO_x, (b) SO₂, (c) CO, (d) PM_{2.5}, (e) PM₁₀ and (f) NMVOC in China from 2013 to 2018. The considered natural sources includes the biogenic, biomass burning and soil emissions.

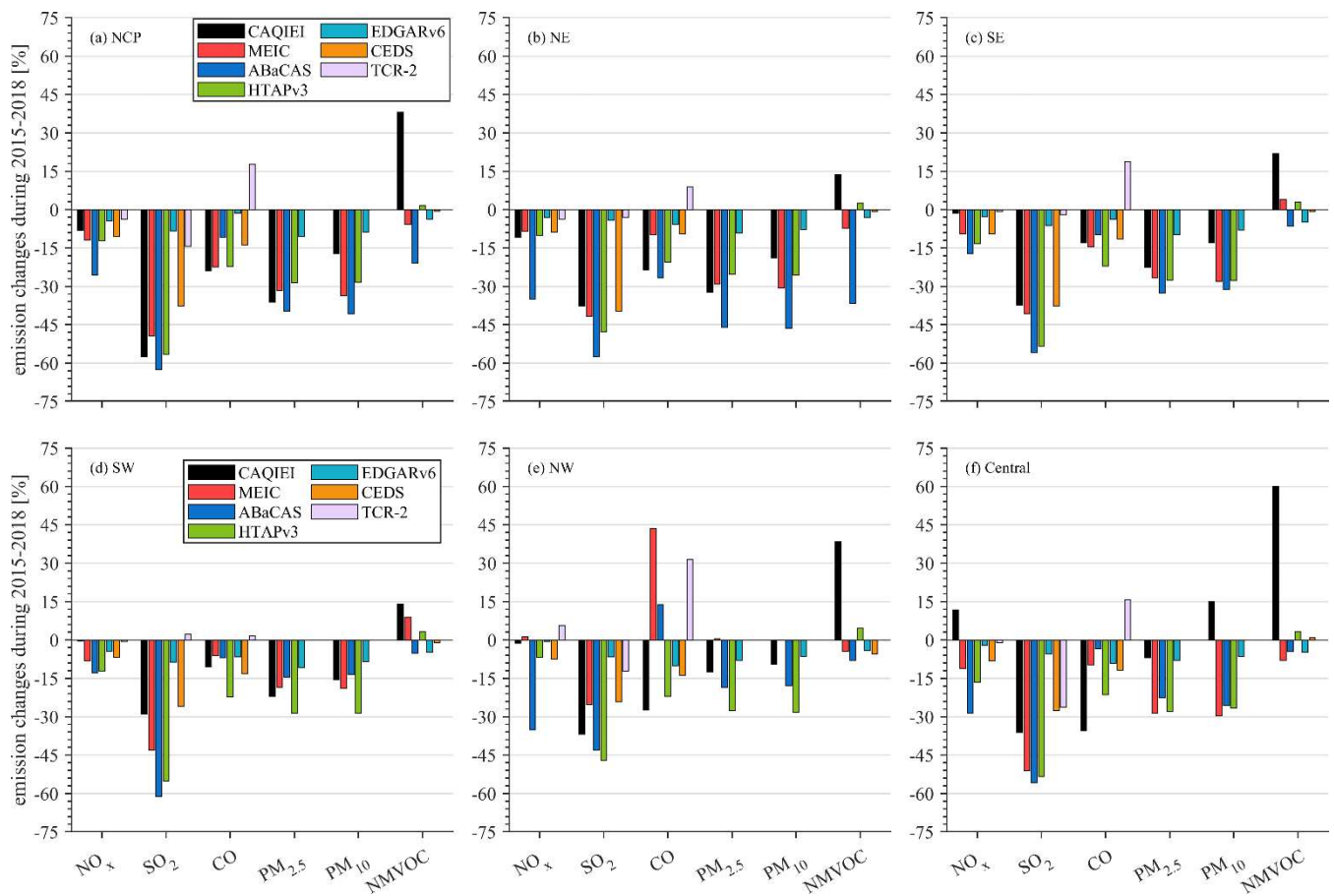


Figure S178: Comparisons of the calculated emission changes of (a) NO_x, (b) SO₂, (c) CO, (d) PM_{2.5}, (e) PM₁₀, and (f) NMVOCs over different regions of China from 2015 to 2018 between CAQIEI and previous inventories.